UNIVERSITY OF CALIFORNIA SAN DIEGO

# The Effects of Cell-Cycle on Interferon Pathway in Single Cells

A dissertation submitted in partial satisfaction of the
requirements for the degree Doctor of Philosophy

in

Biology

by

Anusorn Mudla

Committee in charge:

Professor Nan Hao, Chair
Professor Gen-Sheng Feng
Professor Wenxian Fu
Professor Jeff Hasty
Professor Jin Zhang

2020

The dissertation of Anusorn Mudla is approved, and it is acceptable in quality and form for publication on microfilm and electronically:

_____

_____

_____

_____

_____

Chair

University of California San Diego

2020

# DEDICATION

I would like to dedicate this thesis to my parents, Aek Madla and Aminah Madla, for believing in my potential and supporting my dream of becoming a scientist. I am from a poor farmer family living in a countryside of Thailand where education is a privilege. Despite very little money we had, my parents made certain I always went to school every day. Thank you for never giving up on my education.

## EPIGRAPH

Science is converging on an all-encompassing dogma,
which says that organisms are algorithms and life is data processing.

Yuval Harari

TABLE OF CONTENTS

LIST OF FIGURES

LIST OF TABLES

ACKNOWLEDGEMENTS

I am sincerely thankful to my wonderful mentor, Nan Hao, for being the most supportive PI I have ever known. I started my project with not even a single mammalian cell in our lab, not knowing how to code and never touched a microfluidic device. Yet, Nan was always encouraging and never lost patience in my gradual progress. I thank Nan a million times for guiding me through this difficult and often insecure path. I am grateful for opportunities to explore multiple projects and different areas of my interest. I could not become a better scientist and more importantly a better person without him.

I appreciate the support and insight from my committee members: Dr. Gen-Sheng Feng, Dr. Jeff Hasty, Dr. Jin Zhang and Dr. Wenxian Fu, throughout the years. My projects could not be in better shapes without your feedbacks. It was not easy to gather annually especially in the summer when you were all travel. Your commitment and time have been impactful to my progress.

The past and present lab members were important factor in my success. I chose this lab 6 years ago because of the welcoming and friendly environment. I appreciate the help and support in troubleshooting experiments and thoughtful comments during lab meeting. I also want to extend my appreciation to the members of Hasty Lab who were a tremendous help with microfluidic device production and other numerous technical issues with setting up microfluidic experiments and sharing reagents.

I could not express enough gratitude to my family in Thailand who have always mentally supported me. I thank for prayers you made and heart-warming messages you sent over the years to lift my spirit. I thank my American host family, Gail and Kurt Diezel for making me feel like I have a family in the United States.

I am grateful to the Development and Promotion of Science and Technology Talents Project (DPST) for sponsoring me in this journey. I awarded the scholarship in the first year of high school and the program has have supported me financially and intellectually for the past 14 years. Without this program I cannot imagine coming the United States and let alone receiving my Ph.D. I am in debt to Thai people whose tax money was used toward my education. I also thank the Office of Educational Affairs staff who assisted and advised me during my time in the United States.

Chapter 1, in part, has been submitted for publication as it may appear as Anusorn Mudla, Yanfei Jiang, Kei-ichiro Arimoto, Bingxian Xu, Adarsh Rajesh, Andy Ryan, Wei Wang, Matthew D Daugherty, Dong-Er Zhang and Nan Hao. “Cell cycle-gated feedback control mediates desensitization to interferon stimulation.” *eLife* (2020). The dissertation author is the first author of the paper.

## VITA

2010 – 2014 Bachelor of Science, Purdue University, West Lafayette

2015 – 2018 Teaching Assistant, University of California San Diego

2018 – 2019 Teaching Associate, University of California San Diego

2020 Doctor of Philosophy, University of California San Diego

## PUBLICATIONS

Mudla, Anusorn, Yanfei Jiang, Kei-ichiro Arimoto, Bingxian Xu, Adarsh Rajesh, Andy P. Ryan, Wei Wang, Matthew D. Daugherty, Dong-Er Zhang, and Nan Hao. "Cell cycle-gated feedback control mediates desensitization to interferon stimulation." *bioRxiv*, 2020.

## FIELDS OF STUDY

Major Field: Biology

Studies in Molecular Biology
Professor Nan Hao

ABSTRACT OF THE DISSERTATION

The Effects of Cell-Cycle on Interferon Pathway in Single Cells

by

Anusorn Mudla

Doctor of Philosophy in Biology

University of California San Diego, 2020

Professor Nan Hao, Chair

Mammalian cells are surrounded by fluctuations of various cytokines, small proteins that control a broad range of cellular signaling. In order to survive, cells must respond appropriately to these different dynamics of these signaling molecules. This thesis work presents partial answers to how human epithelial cells decode information encoded in the dynamics of the external stimuli and successfully execute proper responses. We focus on interferon (IFN) pathway which is important for viral infection as well as tumorigenesis. We employed CRISPR/Cas9 technology to generate reporter cell lines, time-lapse microscopy,

microfluidics, single cell analysis and computational modeling to dissect the molecular mechanism governing the cytokine responses. In chapter 1, we studied how IFN-α pretreatment could lead to two contradictive effects: priming and desensitization. We discovered that short pretreatment duration produced priming effect while prolonged IFN treatment caused activation of delayed negative feedback, USP18, responsible for desensitization. Intriguingly, USP18 induction was duration and cell-cycle dependent. Understanding this regulation paves ways to improve the usage of IFN in virus infection such as SARS-CoV-2 and cancer therapy.

In chapter 2, we systemically studied the cellular response to different type of IFN. We found that three types of IFN process distinct dynamic responses. Type I IFN (IFN-I) was a potent *IRF9* inducer than type III but succumbs to desensitization. Single cells analysis revealed unique heterogenous subpopulation of cell in response to IFN-III stimulation. Type II was strong STAT1 activator but was unable to induce IRF9 and USP18. Interestingly, combination of IFN-II and -III generated a synergy effect mimicking IFN-I response but without USP18 induction and therefore no desensitization. Short pulses of low IFN-II dose were sufficient to maintain the synergy. We believe that this will provide alternative methods to deliver IFN to patients especially against virus infection.

## Introduction

A key survival property of living organisms is to efficiently response and adapt to changes in the environment. Reactions to the changes have to be tuned specifically to both time and duration of unique stimuli. Throughout the evolution, organisms have developed sophisticated mechanisms embedded in the genetic codes to enable appropriate reactions to external cues precisely down to the single cell level. Since there are countless number of stimuli with various combinations of concentrations and durations but limited number of cellular components, cells must consist of intricate signaling networks to efficiently process the multiple inputs. For example, three different types of interferons (IFNs), cytokines responsible for responding to pathogen infection, act through the same transcription factor signal transducer and activator of transcription (STAT) but generate various distinct responses. For example, STAT3 can be activated by different upstream signals including cytokines, growth factor, and pathogen [1], yet yield appropriate corresponding outcomes (Fig I.1). How the cells can encode and decode many different signals through the same downstream pathways cannot be explained exclusively through formation of different complexes of pathway components, which begs the question of whether a more dynamic view of the system should be undertaken to understand these signaling pathways.

Many transcription factors (TF) such as mammalian p53, MAP kinase and NF-κB have been shown to encode information about the environment in their temporal dynamics in response to different signals (Fig I.2). For example, in response to γ-radiation, p53 shows oscillatory nuclear translocation dynamics of which results in cell cycle arrest. In contrary, UV radiation causes a prolong p53 nuclear translocation of which leads to apoptosis. The two distinct dynamic patterns allow cells to appropriately activate certain groups of genes responsible for the designated outcomes. Moreover, frequency of nuclear translocation

pulses and duration encode information about the doses of the stimuli. In addition, combination of stimuli generates dynamic patterns of which can be interpreted from the sum of individual stimulus [2]. Therefore, understanding how individual stimulus affect transcription factor dynamics provides a powerful predictive tool and eliminates unnecessary experimental testing.

Traditional drug discovery has been focusing on targeting a molecular component of dysregulated pathway. As previously mentioned, several pathways are highly interconnected and important for cell survival. Therefore, inhibition of a common molecule, especially a signaling hub, can result in broad and undesired effects. A new emerging pharmacological approach is to perturb the dynamic of the signaling hub to steer toward desired outcome [3]. It is early in the development of such approach but accumulation of knowledge in the field will soon produce fruitful results.

Single cells study has rapidly become a powerful tool to unveil numerous mysterious biological phenomena. Genetically identical cells behave heterogeneously to identical stimulus depending on internal cellular state or temporal fluctuation of the external environment. Variation in transcriptomic and proteomic in individual cells contribute to the heterogeneity [4]. Unlike population study, single cell study captures rare events that are hidden in population analysis, for example, fractional killing of cancer cells upon chemotherapy or graded response to hormones [5,6]. The term “single cell” is often referred to single cell RNA sequencing (RNA-seq) due to popular trend in single cell resolution of mRNA measurement. However, single cell study is not only limited to RNA-seq or other types of sequencing-based methods but also to methods used to study single cell behaviors. One of such examples is single cell dynamics. This approach can not only

capture disparity between cells over time but also provides rich information on how cells make decision upon changing environment.

To study the dynamics of a transcription factors, a major challenge is to be able to monitor the proteins over a long period of time in lived single cells. Several technical obstacles need to be overcome to obtain reliable and accurate data. First, protein of interest needs to be fluorescently labeled [7]. Over several decades this was achieved by exogenously expressing the coding sequences of proteins of interest along with the fluorescent proteins. It was relatively easy in bacteria and yeast but very difficult in mammalian cells. The caveat of this method is difficulty in obtaining endogenous level of the protein and its regulation in the native cellular context [8]. The advance in molecular biology in the past decades has allowed more efficient endogenous gene tagging via tools such as zing finger nuclease, TALEN, and CRISPR/Cas9 [9]. In addition, development of new biosensors, protein engineering and fluorescent conjugated small molecule increases alternative ways to monitor proteins of interest [10,11] Second, time-lapse imaging needs to be performed on lived cells [12]. Advance in high-resolution microscope technology [13], more affordable highly sensitive CCD camera [14,15] and cheaper storage units permit collection of high quality and large quantity of single cell data. Furthermore, the microfluidic device allows precise manipulation of the cellular environment such as doses and duration of the stimuli [16]. Third, due to large number of images, the process of quantifying fluorescent signal requires high accuracy and automation [17]. More affordable computer prices and several easy to use programming software have enhance the image analysis tools both read-to-use and customized versions [18,19]. In addition, the methods designed for single cell studies are widely adopted in recent years facilitating sharing of data and in-house tools. Lastly, discovery in one system must be able to generalize to other systems

and provide useful prediction [20]. Applying mathematical modeling approach with the use of computational modeling and simulation helps biologists to design experiments more efficiently and reduces resources.

In this work, we used time-lapse lived-cell imaging technique in combination with microfluidic and computational modeling to decipher the information encoded in the dynamics of STAT1. In chapter 1, we focus on the role of STAT1 in type I interferon pathway and its regulation. In chapter 2, we study how STAT1, as a signal hub, behaves in responses to different types of interferon.

STAT1 is a one out of seven members of STAT family of TF all of which are activated by cytokines, hormones and growth factors. STAT proteins share considerable homology despite unique yet overlapping functions [21]. STAT1 plays critical roles in viral infection, development and tumorigenesis [22]. Two splice isoforms of STAT1 has been reported. A shorter isoform, STAT1$\beta$ (84kD), lacks the 38 amino acid at the C-terminus of which functions as transactivation domain and has long been thought to be a dominant negative form of STAT1$\alpha$ (91kD) isoform [23]. However, several studies have shown that STAT1$\beta$ can function as antiviral protein in innate immunity and can boost STAT1$\alpha$ activity [24].

The main upstream activator of STAT is interferon (IFN), a cytokine produced and secreted in response to virus infection to interfere with viral replication. However, STAT1 can be activated by other cytokines such as interleukin-21 (IL-21), IL-27 and IL-35 [25]. IFN is a widely expressed cytokine involved not only in viral infection but growth-inhibition and immune-surveillance of malignant cells [26]. Over several decades, a family of IFN has been discovered, purified and characterized into three distinct types based on their receptors. Type I interferon (IFN-I) consists of several subtypes, but all transduce signal through type I IFN receptors comprised of IFN-α receptor (IFNAR1) and IFNAR2. In humans, IFN-I

includes IFN- α, IFN-β, IFN-ε, IFN-κ and IFN-ω that are all clustered on chromosome 9 [27]. Almost all cell types can secrete and respond to IFN-I although immune cells are major IFN-I producers [25]. Type II interferon (IFN-II) only has one member, IFN-γ, located on chromosome 12. IFN-γ binds to IFN-γ receptor 1 (IFNGR1) and IFNGR2 known as IFN type II receptors [28]. Type III interferon (IFN-III) has been recently discovered comprised of IFN-λ1, IFN-λ2 and IFN-λ3 which are also known as interleukin-29 (IL-29), IL-28α and IL-28β respectively. IFN-λ acts through type III IFN receptors composed of two chains: IFNLR1 (IL-28 receptor-α) and IL-10Rβ [29]. Very recently, IFN-λ4 was identified [30] and showed to function similar to IFN-λ3 with much weaker expression level [31]. Although IFN-I and IFN-III use different receptors, they share the common downstream signal transduction pathway [32].

In IFN-I and IFN-III signaling, binding of the ligands to the receptors causes receptor dimerization led to tran- and auto-phosphorylation of Janus kinase 1 (JAK1), tyrosine kinase 2 (Tyk2) and the receptors, creating a binding for STAT1 and STAT2 proteins. STAT1 is phosphorylated at tyrosine 701 (Y701) and STAT2 is phosphorylated at Y689 [33]. Serine 727 of STAT1 is required for the full transcriptional activation but not for the nuclear translocation [34]. Phosphorylated STAT1 and STAT2 form heterodimers and bind to interferon regulatory factor 9 (IRF9) to form interferon-stimulated gene factor 3 (ISGF3). ISGF3 translocates into the nucleus where it binds and activates genes containing interferon stimulated response element (ISRE) in their promoters. Similarly, a dimer of IFN-γ binds to IFNGR1/2 caused phosphorylation of pre-associated JAK1 and JAK2, transphosphorylation of the receptor and recruitment of STAT1. Unlike in type I and III signaling pathway, Tyr701-phosphorylated STAT1 molecules form homodimer, also known as IFN- γ activation factor (GAF), which translocates into the nucleus, binds and activates

genes containing gamma-activated sequence (GAS). A schematic of IFN pathway is showed in Figure I.4.

Genes induced by IFNs, termed IFN-stimulated genes (ISGs), covers broad range of antiviral effector functions. Hundreds of ISGs are activated during viral infection or IFN stimulation with different temporal patterns [25]. Several of ISGs expressions are induced rapidly but transiently while others are induced slowly but in a sustained manner. For example, MX1 protein is induced within 4 hour of stimulation and decreased within 24 hours while IFI27 takes 16 hours to be fully induced but can last up to 5 days [35]. We suspect that ISG promoters have different activation kinetics which allow them to be tuned by different upstream IFN dynamics. It is beneficial to understand how cells couple upstream signal dynamics (encoding) with downstream gene expression (decoding) because this would enable us to specifically control the outcomes of IFN treatments.

IFN signaling is terminated by various mechanisms. Endocytosis and turnover of IFN receptors are common mechanisms to reduce JAK-STAT signaling [36]. Negative regulators such as suppressor of cytokine signaling 1 (SOCS1), SOCS3 and protein inhibitor of activated STAT (PIAS) are induced during STAT1 activation and provide negative feedback to the pathway [37]. SOCS1 can bind directly to IFN receptors blocking further activation of STAT1 [38]. PIAS binds to phosphorylated STAT1 and inhibits dimer formation as well as prevents binding of STAT1 to ISG promoters [39]. The most potent sustained negative regulator of IFN-I is USP18 (or UBP43) which binds selectively to IFNAR2; therefore, not affecting type II and III signaling [40]. Additionally, Src-homology region 2 domain-containing phosphatase 2 (SHP2) can inhibit STAT1 signaling by reducing STAT1 tyrosine phosphorylation in the cells [41]. TCP45 and HAT acetylation were also reported to participate in turning off STAT1 activation [42]. These mechanisms of IFN signal

termination cause desensitization to further IFN stimulation. This is a great challenge in viral infection and cancer therapy because patients respond ineffectively to the multiple rounds of treatments.

Dysregulation of interferon pathway can lead to several diseases, a term called interferonopathy [43]. ISG expression leads to an inflammatory phenotype resulting in recruitment of immune cells to clear out infection. This inflammation should normally be transient to prevent tissue damage and autoimmune disease. Rheumatoid arthritis (RA) is an example of a pathology caused by dysregulated IFN response in which too much inflammation caused by IFN-$\alpha$ and IFN-$\lambda$ signaling leads to synovial tissue destruction [44]. Another example of pro-inflammatory phenotypes in IFN signaling is overactive IFN-I signaling in bacterial infection, which can result in sepsis and tissue damage [45]. Interestingly, IFN- $\beta$ shows anti-inflammatory phenotype in treating RA, but the mechanism of treatment remains unknown [46]. This begs the question of how these different IFNs sharing an identical downstream signaling pathway cause heterogeneous phenotypic outcomes. Furthermore, several studies showed evidence of contradictory roles of IFN-$\gamma$ in cancer progression [47] where IFN-$\gamma$ possesses both antitumor and protumor functions. This indicates that different dynamics of the same IFN could contribute to the opposite phenotypes. Studying these phenomena will yield useful information about STAT1 signaling as a pharmacological target.

In chapter 1, we intensively studied the regulation of IFN-I in particular IFN-$\alpha$. IFN-$\alpha$ is routinely used clinically in viral infection and cancer treatment. Generally, IFN-$\alpha$ is produced by leukocytes but response to IFN-$\alpha$ is ubiquitous. Pretreatment cells with IFN-$\alpha$ results in two contradictive effects: priming and desensitization. Priming is a phenomenon when cells respond stronger to the second round of stimulation [48]. In contrary,

desensitization is reduction in response to the repeat stimulation in comparison the no pretreatment condition. Priming is considered a beneficial effect to the cells. IFN-I priming can change naïve cells into a potent responder [49] and prepare cells for severe infection. However, exposure to a stimulus can cause cell to become less responsive [50], resulting in loss of effectiveness in treatment of drug required multiple administration like IFN-$\alpha$ [51]. Understand the mechanism underlie these opposite effects can potentially improve efficacy of IFN-$\alpha$.

To investigate the underlying mechanism, we hypothesized that the durations of pretreatment determine the priming and desensitization outcomes. To test this hypothesis, we generate HeLa reporter cell line using CRISPR/Cas9 to monitor STAT1 activation and transcription of a downstream ISG gene, *IRF9.* Using microfluidic device customized for long-term mammalian cell culture, we could precisely control the duration of the pretreatment, breaktime and the duration of the second treatment while were able to track dynamics of reporter proteins in single cells. As expected, shorter pretreatment duration of 2 or 10 hours resulted in priming effect while 24-hour pretreatment caused desensitization both in STAT1 activation and the rate of IRF9 induction. We then identified USP18 as a delayed negative feedback molecule responsible for the desensitization. We investigated further into the mechanism of USP18 activation and found that induction of USP18 was duration and cell-cycle dependent. The methylation of USP18 promoter caused longer gene activation time compared to IRF9. Taken together, we discovered molecular mechanism of priming and desensitization in type I IFN pathway.

In chapter 2, we broadened our study to investigate the crosstalk between three types of IFN. Although IFN-I is a potent activator of ISG, its omnipresent expression of receptors can lead to detrimental adverse effect such as cytokine storm [52]. IFN-III, even

though using the same signaling cascade, its receptors are restricted to epithelial cells, we aimed to better understand the STAT1 dynamic in response to different IFNs and potentially improve the use of IFN-III in alternative to IFN-I. We used IFN-α, IFN-γ and IFN-λ1 to represent IFN-I, -II and -III respectively. Using previously develop reporter cell line we discovered very intriguing different kinetics of downstream induction. IFN-α showed modest STAT1 activation and induced strong *IRF9* and *USP18* expression. On the other hand, IFN-γ showed very fast and strong STAT1 activation but no induction of IRF9 and USP18. More surprisingly, IFN-λ1 showed undetectable STAT1 nuclear translocation and after 72 hours showed minimal IRF9 and USP18 induction. We also observed heterogeneity in IRF9 and USP18 induction among IFN-λ treated-cells as we later classified as responder and non-responder cells. We are currently investigating the origin of the heterogeneity focusing on receptor expression level, epigenetic regulation and crosstalk with NF-κB pathway.

In attempt to increase IFN-III response, we combined IFN-λ with IFN-γ. We observed a strong synergy between them and the IRF9 induction was significantly increased. However, the kinetics of IRF9 induction was still difference from IFN-I. We hypothesized that the mechanism of synergy relies on phosphorylation of STAT1 of which provided by IFN-γ stimulation. Based on the rapid STAT1 activation by IFN-γ, we tested the hypothesize by treating cells with pulses of IFN-γ in the presence of sustained IFN-λ. Indeed, the pulses of IFN-γ was sufficient to maintain the synergy. The results can lead to new intervention in IFN delivery to increase efficacy and reduce undesired adverse effects.

This thesis dissertation presents studies aiming to understand the regulatory mechanism of STAT transcription factor in response to cytokines. Deciphering how cells encode stimulus information and decode to produce appropriate responses will pave way to develop interventions effectively targeting specific dysfunctional pathways. The novel

tools used in the studies can be applied to other biological problems and advance our knowledge in the realm of cell signaling.

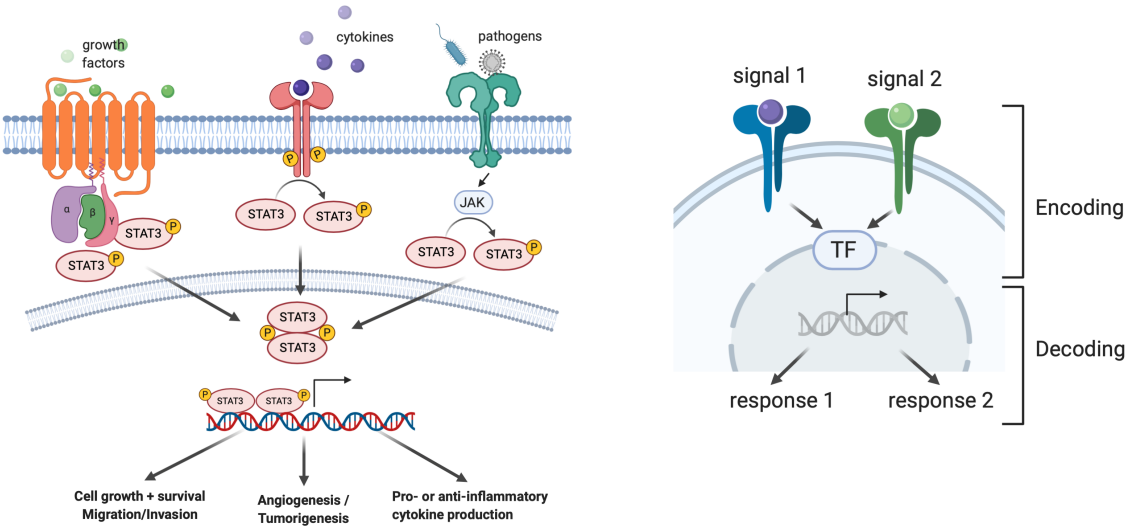


**Figure I.1 Transcription factor serves as signaling hub in multiple pathways.**
(A) Growth factor, cytokines and pathogens signal through different receptors but relay information via STAT3 which translocates to the nucleus and activate different corresponding downstream genes. (B) Schematic of general signaling pathway with common TF. Signal 1 and 2 represents different type of stimuli of which bind to different receptors and lead to different dynamics of TF which in turn "encode" unique information about the stimuli. Dynamics of TF nuclear translocation carries information which can be "decoded", resulting in different gene expression and responses.

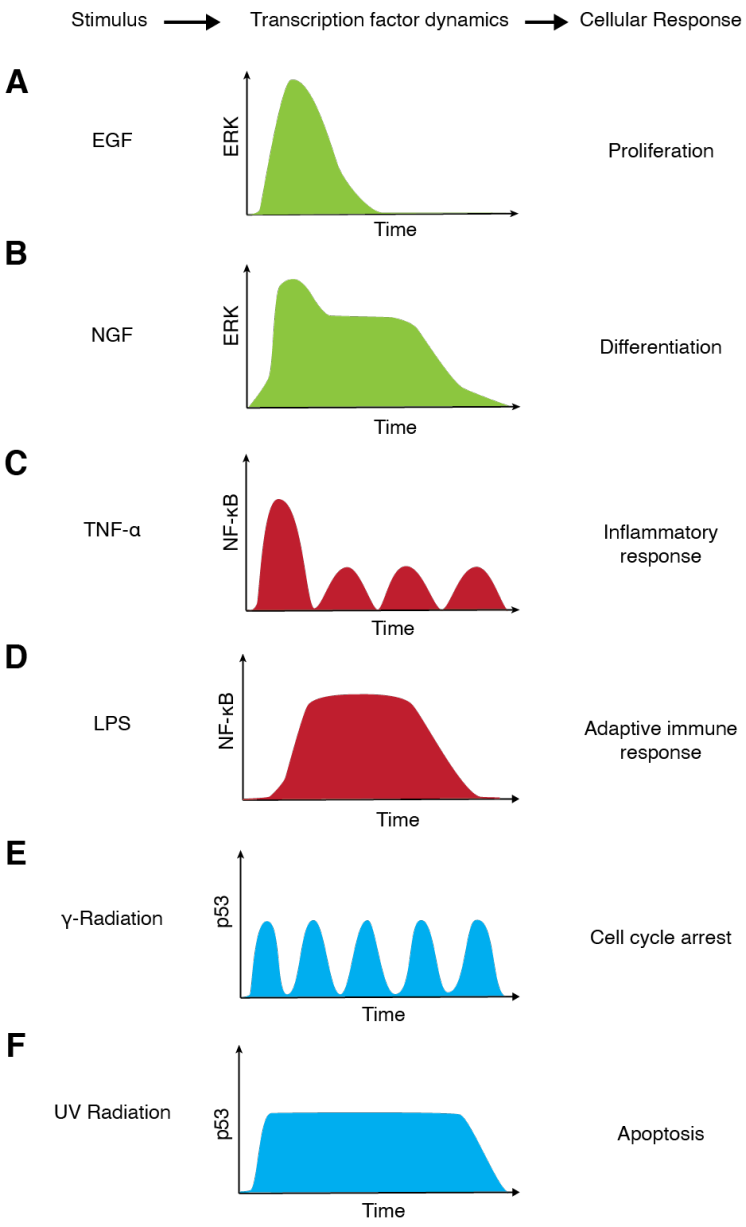


**Figure I.2 Dynamics of transcription factor encode upstream signal identity and produce different phenotypic outcomes.**
(A-B) EGF causes transient nuclear translocation of ERK leading to proliferation while NGF causes sustained ERK nuclear translocation of which lead to cell differentiation. (C-D) In response to TFN-α, NF-κB shows pulsatile nuclear oscillation and triggers inflammatory response. On the contrary, prolong nuclear NF-κB accumulation in response to LPS activates adaptive immune response. (E-F) p53 exhibits different nuclear accumulation in response to γ-radiation and UV radiation determine cell fate commitment to either cell cycle arrest or apoptosis.
Note: Adapted from Purvis and Lahav, 2013.

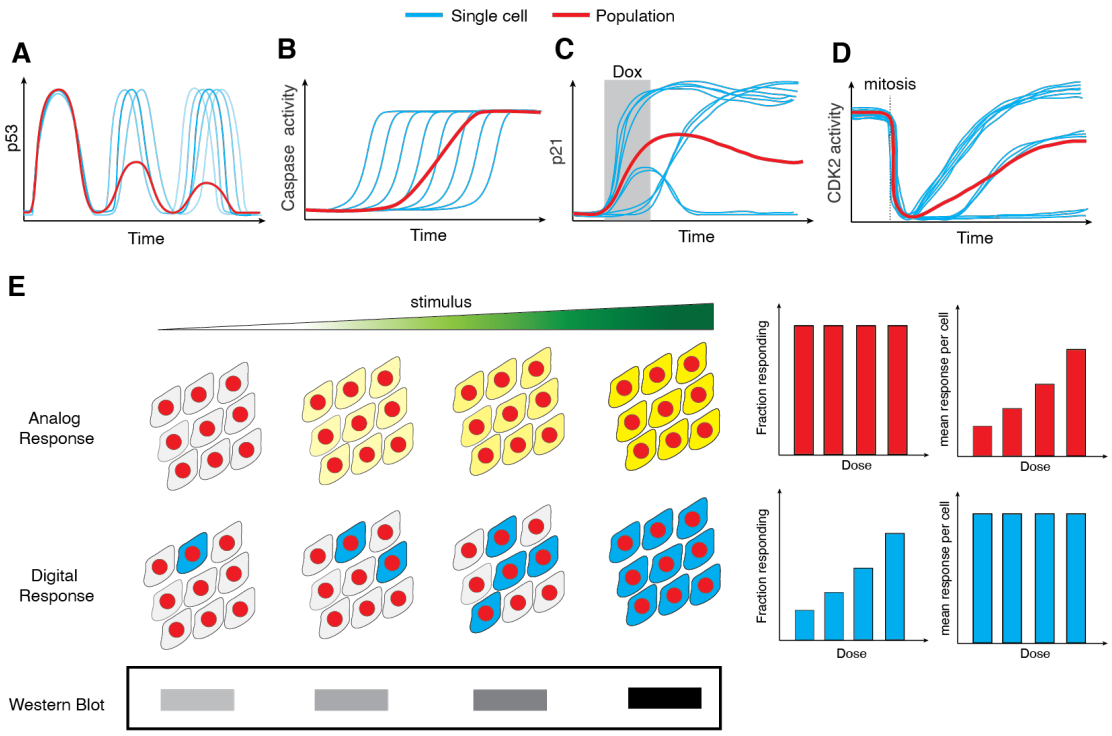


**Figure I.3 Single cell analysis reveals meaningful biological phenomena hidden in population analysis.**
Different protein dynamics quantified in single cells (blue lines) are very different from the population average (red line). (A) Averaged measurement of p53 in response to DNA damage shows damped oscillation; however, single cell analysis exhibits homogenous oscillation with consistent amplitude but different frequency [53]. (B) Caspase cleaves proteins to induce apoptosis at different time in individual cells, but average measurement fails to capture this heterogeneity [53]. (C) Short treatment with doxorubicin (Dox) leads to differential p21 nuclear level causing cells to undergo different cell fates. Population measurement is unable to distinguish different cell types [54]. (D) CDK2 activity measured in single cells shows three distinct cell types which undergo either proliferation, delayed proliferation or quiescence. Average measurement cannot illustrate these 3 groups of cells. (E) In response to increasing concentration of a stimulus, cell response can be classified as analog or digital response of which produces similar western blot patterns. Population level studies fail to capture heterogeneity in single cells and hide non-responsive cells [55].

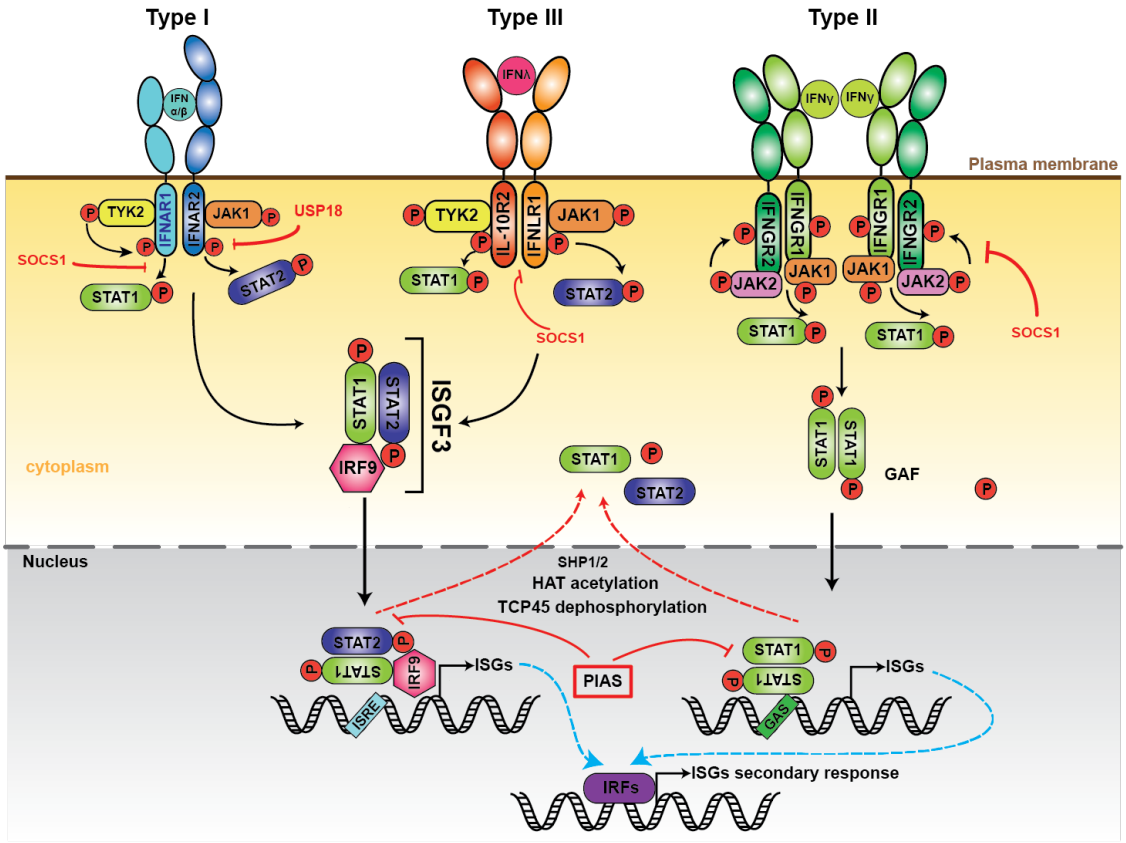


**Figure I.4 The interferon signaling cascade**. Three types of IFNs bind to different receptors leading to STAT1 phosphorylation. Phosphorylated STAT1 form two classes of complexes: heterodimer of STAT1-STAT2 or homodimer, translocate into the nucleus and activate two classes of promoters. Multiple negative regulators inhibit the pathway at multiple steps both in the nucleus and the cytoplasm.

**Reference:**


[1] H. Yu, H. Lee, A. Herrmann, R. Buettner, and R. Jove, “Revisiting STAT3 signalling in cancer: New and unexpected biological functions,” *Nature Reviews Cancer*. 2014.

[2] N. Geva-Zatorsky, E. Dekel, A. A. Cohen, T. Danon, L. Cohen, and U. Alon, “Protein Dynamics in Drug Combinations: a Linear Superposition of Individual-Drug Responses,” *Cell*, 2010.

[3] M. Behar, D. Barken, S. L. Werner, and A. Hoffmann, “The dynamics of signaling as a pharmacological target,” *Cell*, vol. 155, no. 2, p. 448, 2013.

[4] S. K. Bhayvani, B. Dang, G. Bellala, R. Divekar, S. Visweswaran, A. R. Brasier, and A. Kurosky, “Unlocking proteomic heterogeneity in complex diseases through visual analytics,” *Proteomics*. 2015.

[5] J. Roux, M. Hafner, S. Bandara, J. J. Sims, H. Hudson. D. Chai, and P. K. Sorger, “Fractional killing arises from cell-to-cell variability in overcoming a caspase activity threshold,” *Mol. Syst. Biol.*, 2015.

[6] B. Qiu, J. Zhang, and T. Zhou, “Dynamic variability in apoptotic threshold as a strategy for combating fractional killing,” *bioRxiv*, 2018.

[7] G. Crivat and J. W. Taraska, “Imaging proteins inside cells with fluorescent tags,” *Trends in Biotechnology*. 2012.

[8] K. H. Khan, “Gene expression in mammalian cells and its applications,” *Adv. Pharm. Bull.*, 2013.

[9] R. M. Gupta and K. Musunuru, “Expanding the genetic editing tool kit: ZFNs, TALENs, and CRISPR-Cas9,” *Journal of Clinical Investigation*. 2014.

[10] K. Thorn, “Genetically encoded fluorescent tags,” *Molecular Biology of the Cell*. 2017.

[11] M. A. Plamont, E. Billon-Dennis, S. Maurin, C. Gauron, F. M. Pimenta, C. G. Specht, J. Shi, “Small fluorescence-activating and absorption-shifting tag for tunable protein imaging in vivo,” *Proc. Natl. Acad. Sci. U. S. A.*, 2016.

[12] K. M. Piltti, B. J. Cummings, K. Carta, A. Manughian-Peter, C. L. Worne, K. Singh, D. Ong, Y. Maksymyuk, M. Khine and A. J. Anderson, “Live-cell time-lapse imaging and single-cell tracking of in vitro cultured neural stem cells – Tools for analyzing dynamics of cell cycle, migration, and lineage selection,” *Methods*, 2018.

[13] B. Huang, M. Bates, and X. Zhuang, “Super-Resolution Fluorescence Microscopy,” *Annu. Rev. Biochem.*, 2009.

[14] H. T. Beier and B. L. Ibey, “Experimental comparison of the high-speed imaging performance of an EM-CCD and sCMOS camera in a dynamic live-cell imaging test case,” *PLoS One*, 2014.

[15] B. Mandracchia, X. Hua, C. Guo, J. Son, T. Urner, and S. Jia, “Fast and accurate sCMOS noise correction for fluorescence microscopy,” *Nat. Commun.*, 2020.

[16] T. A. Duncombe, A. M. Tentori, and A. E. Herr, “Microfluidics: Reframing biological enquiry,” *Nature Reviews Molecular Cell Biology*. 2015.

[17] E. Moen, E. Borna, G. Miller, M. Schwartz, D. Bannon, N. Koe, I. Camplisson, K. Kyme, C. Pavelchek, T. Price, and T. Kudo, “Accurate cell tracking and lineage construction in live-cell imaging experiments with deep learning,” *bioRxiv*, 2019.

[18] S. Uchida, “Image processing and recognition for biological images,” *Development Growth and Differentiation*. 2013.

[19] J. Rittscher, “Characterization of Biological Processes through Automated Image Analysis,” *Annu. Rev. Biomed. Eng.*, 2010.

[20] S. Motta and F. Pappalardo, “Mathematical modeling of biological systems,” *Brief. Bioinform.*, 2013.

[21] K. A. Dorritie, J. A. McCubrey, and D. E. Johnson, “STAT transcription factors in hematopoiesis and leukemogenesis: Opportunities for therapeutic intervention,” *Leukemia*. 2014.

[22] K. Meissl, S. Macho-Maschler, M. Müller, and B. Strobl, “The good and the bad faces of STAT1 in solid tumours,” *Cytokine*. 2017.

[23] N. Zakharova, e. S. Lymar, E. Yang, S. Malik, J. J. Xhang, R. G. Roeder, and J. E. Darnell, “Distinct Transcriptional Activation Functions of STAT1α and STAT1β on DNA and Chromatin Templates,” *J. Biol. Chem.*, 2003.

[24] C. Semper, N. R. Leitner, C. Lassnig., M. Parrini, T. Mahlakõiv, M. Rammerstorfer, K. Lorenz, K. Rigler, S. Müller, T. Kolber, C. Vogl, “STAT1β Is Not Dominant Negative and Is Capable of Contributing to Gamma Interferon-Dependent Innate Immunity,” *Mol. Cell. Biol.*, 2014.

[25] W. M. Schneider, M. D. Chevillotte, and C. M. Rice, “Interferon-Stimulated Genes: A Complex Web of Host Defenses,” *Annu. Rev. Immunol.*, 2014.

[26] L. Avalle, S. Pensa, G. Regis, F. Novelli, and V. Poli, “STAT1 and STAT3 in tumorigenesis,” *JAK-STAT*, 2012.

[27] G. Trinchieri, “Type I interferon: Friend or foe?,” *J. Exp. Med.*, vol. 207, no. 10, pp. 2053–2063, 2010.

[28] K. Schroder, P. J. Hertzog, T. Ravasi, and D. A. Hume, “Interferon-γ: an overview of signals, mechanisms and functions,” *J. Leukoc. Biol.*, 2004.

[29] C. Sommereyns, S. Paul, P. Staeheli, and T. Michiels, “IFN-lambda (IFN-λ) is expressed in a tissue-dependent fashion and primarily acts on epithelial cells in vivo,” *PLoS Pathog.*, 2008.

[30] L. Prokunina-Olsson, B. Muchmore, W. Tang, R. M. Pfeiffer, H. Park, H. Dickensheets, D. Hergott, P. Porter-Gill, A. Mumy, I. Kohaar and S. Chen, “A variant upstream of IFNL3 (IL28B) creating a new interferon gene IFNL4 is associated with impaired clearance of hepatitis C virus,” *Nat. Genet.*, 2013.

[31] P. S. Sung, S. Hong, J. Chung, S. Kim, S. Park, H. M. Kim, S. K. Yoon and E. Shin “IFN-λ4 potently blocks IFN-α signalling by ISG15 and USP18 in hepatitis C virus infection,” *Sci. Rep.*, 2017.

[32] D. E. Levy, I. J. Marié, and J. E. Durbin, “Induction and function of type i and III interferon in response to viral infection,” *Current Opinion in Virology*. 2011.

[33] K. Fink and N. Grandvaux, “STAT2 and IRF9: Beyond ISGF3,” *JAK-STAT*, 2013.

[34] T. Decker and P. Kovarik, “Serine phosphorylation of STATs,” *Oncogene*. 2000.

[35] M. T. Dill, Z. Makowsda, G. Trincucci, A.J. Gruber., J.E. Vogt, M. Filipowicz, D. Calabrese, I. Krol, D.T. Lau, L. Terracciano and E. van Nimwegen, “Pegylated IFN-α regulates hepatic gene expression through transient Jak/STAT activation,” *J. Clin. Invest.*, 2014.

[36] M. Marchetti, M.N. Monier, A. Fradagrada, K. Mitchell, F. Baychelier, P. Eid, L. Johannes and C. Lamaze, “Stat-mediated signaling induced by type I and type II interferons (IFNs) is differentially controlled through lipid microdomain association and clathrin-dependent endocytosis of IFN receptors,” *Mol. Biol. Cell*, 2006.

[37] L. B. Ivashkiv and L. T. Donlin, “Regulation of type i interferon responses,” *Nature Reviews Immunology*. 2014.

[38] N. P. D. Liau, A. Laktyushin, I. S. Lucet, J. M. Murphy, S. Yao, E. Whitlock, K. Callaghan, N. A. Nicola, N. J. Kershaw and J. J. Babon, “The molecular basis of JAK/STAT inhibition by SOCS1,” *Nat. Commun.*, 2018.

[39] B. Liu, J. Liao, X. Rao, S. A. Kushner, C. D. Chung, D. D. Chang, and Ke Shuai, “Inhibition of Stat1-mediated gene activation by PIAS1,” *Proc. Natl. Acad. Sci. U. S. A.*, 1998.

[40] V. François-Newton, G. M. de F. Almeida, B. Payelle-Brogard, D. Monneron, L. Pichard-Garcia, J. Piehler, S. Pellegrini, and G. Uzé, “USP18-based negative feedback control is induced by type I and type III interferons and specifically inactivates interferon α response,” *PLoS One*, 2011.

[41] M. Baron and J.-L. Davignon, “Inhibition of IFN-γ-Induced STAT1 Tyrosine Phosphorylation by Human CMV Is Mediated by SHP2,” *J. Immunol.*, 2008.

[42] O. H. Krämer Krämer, S. K. Knauer, G. Greiner, E. Jandt, S. Reichardt, K. H. Gührs, R. H. Stauber, F. D. Böhmer, and T. Heinzel, “A phosphorylation-acetylation switch regulates STAT1 signaling,” *Genes Dev.*, 2009.

[43] M. P. Rodero and Y. J. Crow, “Type I interferonâ-mediated monogenic autoinflammation: The type i interferonopathies, a conceptual overview,” *J. Exp. Med.*, 2016.

[44] J. J. Goronzy and C. M. Weyand, “Developments in the scientific understanding of rheumatoid arthritis,” *Arthritis Research and Therapy*. 2009.

[45] L. Dejager, S. Vandevyver, M. Ballegeer, E. V. Wonterghem, L. L. An, J. Riggs, R. Kolbeck, and C. Libert, “Pharmacological inhibition of type i interferon signaling protects mice against lethal sepsis,” *J. Infect. Dis.*, 2014.

[46] P. P. Tak, “IFN-beta in rheumatoid arthritis.,” *Frontiers in bioscience : a journal and virtual library*. 2004.

[47] J. Zhang, “Yin and yang interplay of IFN-γ in inflammation and autoimmune disease,” *Journal of Clinical Investigation*. 2007.

[48] L. S. Davis, “The yin and yang of cytokine priming on the macrophage epigenome,” *Science immunology*. 2017.

[49] H. Phipps-Yonas, J. Seto, S. C. Sealfon, T. M. Moran, and A. Fernandez-Sesma, “Interferon-β pretreatment of conventional and plasmacytoid human dendritic cells enhances their activation by influenza virus,” *PLoS Pathog.*, 2008.

[50] S. Sakamoto, J. Qin, A. Navarro, A. Gamero, R. Potla, T. Yi, W. Zhu, D. P. Baker, G. Feldman, and Andrew C. Larner, “Cells Previously Desensitized to Type 1 Interferons Display Different Mechanisms of Activation of Stat-dependent Gene Expression from Naïve Cells,” *J. Biol. Chem.*, 2004.

[51] S. A. Taghavi and A. Eshraghian, “Successful interferon desensitization in a patient with chronic hepatitis C infection,” *World J. Gastroenterol.*, 2009.

[52] S. H. Nile, A. Nile, J. Qiu, L. Li, X. Jia, and G. Kai, “COVID-19: Pathogenesis, cytokine storm and therapeutic potential of interferons,” *Cytokine and Growth Factor Reviews*. 2020.

[53] J. E. Purvis and G. Lahav, “Encoding and decoding cellular information through signaling dynamics,” *Cell*. 2013.

[54] C. H. Hsu, S. J. Altschuler, and L. F. Wu, “Patterns of Early p21 Dynamics Determine Proliferation-Senescence Cell Fate after Chemotherapy,” *Cell*, 2019.

[55] S. Jeknić, T. Kudo, and M. W. Covert, “Techniques for studying decoding of single cell dynamics,” *Frontiers in Immunology*. 2019.

# Chapter 1

# Cell Cycle-Gated Feedback Control Mediates Desensitization to Interferon Stimulation


## Abstract

Cells use sophisticated molecular circuits to interpret and respond to extracellular signal factors, such as hormones and cytokines, which are often released in a temporally varying fashion. In this study, we focus on type I interferon (IFN) signaling in human epithelial cells and combine microfluidics, time-lapse microscopy, and computational modeling to investigate how the IFN-responsive regulatory network operates in single cells to process repetitive IFN stimulation. We found that IFN-$\alpha$ pretreatments lead to opposite effects, priming versus desensitization, depending on the input durations. These effects are governed by a regulatory network composed of a fast-acting positive feedback loop and a delayed negative feedback loop, mediated by upregulation of ubiquitin-specific peptidase 18 (USP18). We further revealed that USP18 upregulation can only be initiated at the G1 and early S phases of cell cycle upon the treatment onset, resulting in heterogeneous and delayed induction kinetics in single cells. This cell cycle gating provides a temporal compartmentalization of feedback control processes, enabling duration-dependent desensitization to repetitive stimulations. Moreover, our results, highlighting the importance of IFN dynamics, may suggest time-based strategies for enhancing the effectiveness of IFN pretreatment in clinical applications against viruses, such as SARS-CoV-2.


## Introduction

Under physiological conditions, cells often encounter environmental cues that change over time. Many hormones, cytokines, and signal factors are released in a temporally varying fashion. Increasing evidence demonstrated that cells can use complex

signaling networks to interpret the dynamic patterns of these inputs and initiate appropriate cellular responses [1, 2]. For example, the mitogen-activated protein kinase Hog1 pathway in the yeast *S. cerevisiae* responds to the various frequencies of oscillating osmotic stress and differentially control the growth rate under stress [3-5]. Moreover, the gene regulatory program mediated by the yeast general stress responsive transcription factors (TFs) Msn2 and Msn4 can decode various input pulses and induce differential gene expression [6-9]. In mammalian systems, it has been shown that the nuclear factor κB (NFκB) pathway can process the pulsatile stimulation of tumor necrosis factor-α (TNF-α) to determine the timing and specificity of downstream gene expression [10-12]. Similarly, the p53 tumor suppressor differentially regulates target genes and cell fates by processing temporal patterns of DNA damage cues [13-15]. Intriguingly, many of these studies observed that individual cells exhibit widely different behaviors even to the same stimuli, and, as a result, population-based measurements may obscure the actual response dynamics of individual cells, leading to inaccurate interpretation of the data. Furthermore, these observed cell-to-cell variabilities play important roles in enhancing the diversity of physiological behaviors and biological functions [16-20]. In this study, we focus on interferon (IFN)-α signaling in human epithelial cells and investigate how the IFN-driven gene regulatory network operates in single cells to decode various signal dynamics.

IFN-α is a member of the type I IFN family of cytokines, which are synthesized and secreted in mammals upon pathogen infection and initiate innate immune responses to limit pathogen spread via reducing protein production, upregulating antiproliferative and antiviral genes, and programmed cell death [21, 22]. IFN-α has also been clinically used in treatments of a variety of diseases, such as hepatitis B and C infection, HIV infection, melanoma, kidney cancer, leukemia and lymphoma [23, 24]. IFN-α exerts its anti-

pathogenic and anti-proliferative effects by activating the Janus kinase (JAK)-signal transducer and activator of transcription (STAT) pathway, leading to the expression of over 300 IFN-stimulated genes (ISGs) [21, 25]. IFN-$\alpha$ binds to a heterodimeric transmembrane receptor, the IFN-$\alpha$ receptor (IFNAR), triggering the activation of receptor-associated kinases Janus kinase 1 (JAK1) and tyrosine kinase 2 (TYK2), which in turn phosphorylate transcription factors signal transducer and activator of transcription 1 (STAT1) and STAT2. The phosphorylated STAT1 and STAT2 dimerize and associate with IFN-regulatory factor 9 (IRF9) to form IFN-stimulated gene factor 3 (ISGF3) complex. ISGF3 then translocates to the nucleus and binds to the DNA consensus sequences, known as IFN-stimulated response element (ISRE), activating the transcription of ISGs [26, 27]. The duration and strength of the IFN-mediated inflammatory responses are tightly controlled in mammals. A response that is too short or too weak will fail to limit pathogen spread, whereas a response that is too prolonged or too strong will result in tissue damage, organ failure, and carcinogenesis [28-30]. In many epidemics, uncontrolled inflammatory responses to infection have led to the cytokine storm and high mortality [31, 32].

Although the molecular components of the JAK-STAT pathway have been well characterized, how they are regulated to generate appropriate responses to dynamic IFN-$\alpha$ inputs remains largely elusive. In particular, during chronic inflammation, cells receive varying IFN signals from neighboring cells [33-35]. However, previous studies have reported opposing results regarding the effect of IFN-$\alpha$ pretreatment. In some studies, a prior exposure to IFN-$\alpha$ accelerates cells' responses to the second IFN input, enabling a "priming" effect [36-39]. In other studies, however, a pretreatment with IFN-$\alpha$ diminishes the responses to the following stimulation, resulting in a "desensitization" effect [40-42]. To resolve this paradox, we combined time-lapse imaging, microfluidics, and computational

modeling to track and quantify JAK-STAT signaling and downstream gene expression in single human epithelial cells. We revealed that a cell cycle-gated negative feedback loop functions to decode IFN pretreatments with different durations and induce differential single-cell responses, reconciling the opposing results from previous studies. A number of recent studies have shown that type I IFN pretreatment could be an effective preventive strategy against severe acute respiratory syndrome coronavirus 2 (SARS-CoV-2) infection [43-45], which causes the pandemic COVID-19. Our findings unravel the important role of the dynamics of IFN pretreatments on modulating cellular responses, suggesting that optimizing administration timing may help boosting the effectiveness of IFN treatment against SARS-CoV-2.

## Results

### IFN-α pretreatments confer opposite effects depending on their durations

IFN-α activates the JAK-STAT pathway and upregulates the expression of IFN-stimulated genes (ISGs), initiating an acute inflammatory response to limit pathogen spread. Recent studies found that individual cells respond to IFNs in a highly heterogeneous manner, both *in vitro* [46-48] and *in vivo* [49, 50]. Therefore, traditional assays that measure averaged responses across populations at static time points may not be able to accurately characterize cells' responses to IFNs. To monitor the dynamics of JAK-STAT signaling at the single cell level, we constructed a reporter cell line in HeLa cells, in which *STAT1* was C-terminally tagged with mCherry at its native locus using CRISPR/Cas9. In addition, to monitor downstream gene expression, we inserted a yellow fluorescent protein (YFP) under the endogenous promoter of a representative ISG *IRF9* ($P_{IRF9}$), with a translational skip spacer (P2A) between the reporter and the *IRF9* coding region (Figure 1.1A; Figure 1.6, A-C). Using this reporter cell line and time-lapse microscopy, we were able to simultaneously

track nuclear translocation of STAT1 and downstream gene expression of in a large number of single cells (Figure 1.1B). We observed a rapid nuclear translocation (within ~0.5 hours) of STAT1 followed by a gradual increase in $P_{IRF9}$-driven gene expression in response to IFN-$\alpha$ stimulation (Figure 1.1B and 1.1C), consistent with traditional western blotting results (Figure 1.6D). For each single cell, we quantified the nuclear to cytoplasmic ratio of STAT1, which resembles STAT1 activation, and the rate of increase in YFP fluorescence (dYFP/dt) to reflect the $P_{IRF9}$-driven transcriptional activity. STAT1 nuclear translocation correlated temporally with the increase in downstream transcriptional activity (Figure 1.1C). We examined single-cell responses to various doses of IFN-$\alpha$ (Figure 1.7) and chose 100 ng/ml (10000 IU/ml), a sub-saturating and clinically relevant [51] concentration, for the following analyses.

To examine the responses to repetitive IFN-$\alpha$ stimulation, we employed a previously reported microfluidic device designed for mammalian cell culturing [52]. The device features rapid cell loading by on-chip vacuum and long-term cell culturing in chambers that are isolated from shear stress. In this study, we modified the device to enable constant flows for medium refreshing and computer-programmed dynamic control of IFN inputs (Figure 1.1D). Using this device, we first performed a single pulse experiment to determine the duration of a breaktime. To do so, we treated the cells with different durations of IFN-$\alpha$, removed the stimulus and continued the experiment with normal media for at least another 24 hours. We found that $P_{IRF9}$-YFP fluorescence continued to increase for about 8 hours after IFN-$\alpha$ was removed then declined (Figure 1.4). Therefore, we decided to use 8 hours as the break time duration.

Next we performed a two-pulses experiment by exposing the cells to a pulse of IFN-$\alpha$ pretreatment with different durations, followed by an 8-hour break time with the normal

medium. We then imposed a second 10-hour IFN-α treatment and evaluated single-cell responses. The device was integrated with time-lapse microscopy to allow tracking of a large number of single cells throughout the experiments (Figure 1.1D and Figure 1.5B). We found that a 2- or 10-hour pretreatment accelerated and enhanced the transcriptional response to the second IFN-α input, as indicated by increased induction rates and levels of the $P_{IRF9}$-driven reporter, compared to the control without pretreatment (Figure 1.1, E and F; compare green and blue curves/bars with black ones, a full time traces are shown in Figure 1.5A). Intriguingly, a 24-hour pretreatment, however, dramatically decreased the transcriptional response to the second input (Figure 1.1, E and F; compare red curves/bars with black ones). Therefore, a pretreatment of IFN-α, depending on its duration, could lead to opposite effects on the responses to the subsequent input. A short pretreatment induces a priming effect, whereas a prolonged pretreatment triggers desensitization. We also examined how changing the dose of 24-hour IFN pretreatment impacts the effect on the response to the second input and found that a dose higher than 10 ng/ml is required for desensitization (Figure 1.6, A-C).

Additionally, we investigated the duration of the desensitization. The reporter cells were pretreated with IFN-α for 24 hours followed by different break-time durations. We compared the level of STAT1 nuclear translocation and $P_{IRF9}$-YFP induction to cells without pretreatment. We found that percentage of STAT1 nuclear translocation increased with longer break time and fully restored after 48 hours (Figure 1.7A). However, the $P_{IRF9}$-YFP induction was not fully restored until 72 hours later (Figure 1.7B).

**USP18 is responsible for desensitization induced by the prolonged IFN-α pretreatment**

We next considered the mechanisms underlying the opposite effects induced by IFN pretreatments. Previous studies have demonstrated that the priming effect can be attributed to the expression induction of IRF9, STAT1 and STAT2, which are components of ISGF3 transcriptional complex that mediates IFN-driven gene expression [53], and IFN-induced chromatin modifications [54]. To determine the mechanism of desensitization caused by the prolonged pretreatment, we use a short hairpin RNA (shRNA) to knock-down the expression of ubiquitin-specific peptidase 18 (USP18), a major negative regulator of JAK-STAT signaling that we identified previously [55-58], in the reporter cell line (Figure 1.7, *USP18-KD*). *USP18* is transcriptionally upregulated by IFN treatment and exerts inhibition of IFN-α signaling at the receptor level, forming a negative feedback loop [41, 59-61]. Without pretreatment, USP18-KD cells showed no STAT1 nuclear translocation difference to WT cells (Figure 1.7B). However, the induction of $P_{IRF9}$-YFP started to be distinctively different after 24 hours (Figure 1.7C) suggesting that USP18 expression might be delayed. In addition, knocking down USP18 did not affect cell growth as the cell cycle length remained similar to the WT cells (Figure 1.7D).

We found that a 24-hour IFN-α pretreatment substantially diminished STAT1 nuclear translocation in WT cells upon the second IFN input, whereas 2-hour or 10-hour pretreatment shows a modest effect (Figure 1.8A and 1.9, “WT”). However, this desensitization effect was abolished when USP18 expression was knocked down (Figure 1.8A, “*USP18-KD*”). Furthermore, in accord with STAT1 nuclear translocation, IFN-α pretreatments boosted the transcriptional responses in *USP18*-KD cells upon the second input, exhibiting priming effects independent of their durations (Figure 1.8, B and C; Figure

1.6, D-F). These results indicate that desensitization is primarily mediated by USP18. We also examined the role of suppressors of cytokine signaling 1 (SOCS1), another negative regulator of JAK-STAT signaling [62]. In contrast to *USP18-KD*, knocking down *SOCS1* (*SOCS1-KD*) did not affect the desensitization of STAT1 nuclear translocation by the prolonged IFN pretreatment (Figure 1.10). Moreover, to determine how USP18-mediated desensitization influences the antiviral effect of IFN-$\alpha$ treatment, we examined viral replication upon IFN-$\alpha$ pretreatments with different durations. While a 10-hour pretreatment to WT cells resulted in a substantial repression of viral replication, extending the pretreatment to 24 hours only furthered the repression modestly. In contrast, the 24-hour pretreatment, in *USP18-KD*, induced a much more dramatic repression of viral replication (Figure 1.11). These results indicated that USP18-mediated desensitization attenuates the antiviral effect of prolonged IFN-$\alpha$ pretreatment. In addition, USP18-KD cells and longer IFN-$\alpha$ pretreatment showed increase apoptosis upon doxorubicin treatment (Figure 1.12). Doxorubicin is a chemotherapy drug and its effects rely on STAT1 activation [63]. Therefore, obliteration of USP18 enhanced and prolonged STAT1 activity resulting in faster apoptosis rate.

**Computational modeling suggests a delayed negative feedback loop through USP18**

Based on our experimental results, we postulated that the opposite effects induced by short versus prolonged pretreatment inputs might be caused by different expression kinetics of ISGF3 components and USP18: a short input is sufficient to trigger ISGF3 expression and thereby the priming effect, whereas a prolonged input is required to induce USP18 expression and hence desensitization. To test this hypothesis *in silico*, we devised a simple computational model, which is composed of two ordinary differential equations that govern the expression of *IRF9*, an ISGF3 component, and *USP18*. In this model, IRF9 and

USP18 act as the positive and the negative feedback regulators of the JAK-STAT pathway, respectively. Another major difference is that, as we proposed above, the upregulation of *USP18* expression features a delayed kinetics and hence requires a continuous IFN stimulation that lasts longer than the delay time $\tau$, whereas the upregulation of *IRF9* initiates immediately upon the IFN treatment (Figure 1.14; see Materials and Methods for details).

This model was able to reproduce the results from pretreatment experiments, where the priming effect dominates for the short pretreatments (2 and 10-hour pretreatments) and the desensitization effect dominates when the pretreatment duration increases to 24 hours (Figure 1.1, E and F). To investigate the effect of the delay in *USP18* upregulation, we altered the delay time from 1 to 20 hours while keeping all the other parameters free. By fitting the model to the data for each assigned delay time, we found that the fitting error (between simulations and data) reaches the minimum when the delay time is 8 hours (Figure 1.14, B and C). Based on this 8-hour delay time in *USP18* upregulation, the model further predicted that repetitive IFN input pulses, with the duration less than 8 hours, could not trigger the USP18-mediated negative feedback loop and hence could lead to a higher transcriptional response than that induced by a prolonged input with the same total treatment time. For example, pulsatile inputs with 5 x 8-hour pulses could produce a higher transcriptional response than that induced by a 40-hour sustained input, and the difference should be USP18-dependent (Figure 1.14, D and E). This prediction was tested experimentally and a higher transcriptional response, indicated by the $P_{IRF9}$-driven reporter, was observed when 5 x 8-hour IFN pulses were given, compared to that induced by a single 40-hour treatment. Furthermore, this difference caused by different input dynamics was abolished in *USP18-KD* cells (Figure 1.14F and Figure 1.15). Similarly, in microfluidic

device experiment, we confirmed that 3 x 8-hour IFN pulses induced higher transcriptional response with faster kinetic than a 24-hour pulse (Figure 1.16).

In summary, our modeling results suggest that a prolonged input is required to initiate *USP18* upregulation. Therefore, when the input duration is short, the ISGF3-mediated positive feedback loop dominates the regulation of JAK-STAT pathway, conferring the priming effect to subsequent stimulation. Once the input duration is prolonged enough to induce USP18 upregulation, the negative regulation by USP18 overrides the positive regulation by ISGF3, resulting in desensitization.

**The kinetics of *USP18* upregulation by IFN is heterogeneous in single cells**

To test our model directly, we set out to compare the expression kinetics of *IRF9* and *USP18* in living cells. To this end, we built upon the dual reporter cell line constructed in Figure 1.17A and inserted a cyan fluorescent protein (CFP) with a nuclear localization signal (NLS) under the endogenous *USP18* promoter ($P_{USP18}$) with a P2A spacer between the reporter and the *USP18* coding region (Figure 1.17A; Figure 1.18). This cell line enabled us to simultaneously track the kinetics of $P_{IRF9}$ and $P_{USP18}$ -driven gene expression in the same cells.

To evaluate the temporal difference in *IRF9* and *USP18* upregulation, we measured and quantified, in each individual cell, the induction kinetics of $P_{IRF9}$ and $P_{USP18}$ -driven gene expression upon IFN stimulation. We defined the time needed for induction to initiate as “activation time” and the difference between the activation times of *IRF9* and *USP18* as “delay time” (Figure 1.17B). We found that, consistent with our model results, *IRF9* and *USP18*, although induced by the same upstream JAK-STAT signaling, exhibited strikingly different activation times. $P_{IRF9}$-driven expression was induced with a fast and relatively uniform kinetics among cells; in contrast, $P_{USP18}$-driven expression exhibited a slow and

heterogeneous kinetics (Figure 1.17C). Intriguingly, we quantified the delay times of *UPS18* induction, relative to that of *IRF9*, in single cells and observed a bimodal distribution: about 83.3% of cells showed modest delays in induction (< 10 hours), whereas the other 16.7% cells exhibited more prolonged delays (> 10 hours). We classified these two subpopulations as “Group 1” and “Group 2”, respectively (Figure 1.17D).

To determine the source of this clonal heterogeneity in *USP18* induction, we considered the contribution of the cell cycle stage at IFN treatment onset, as the cell cycle progression has been shown as a major factor that coordinates gene expression [63]. To this end, we quantified the extent of cell cycle progression in each single cell at IFN treatment onset (“% of cell cycle progression”) and examined its relationship with the *USP18* delay time in the same cell. We found that cells showed modest delays if the treatment was added at the early phase of their cell cycles (0 – 35% of the cell cycle). In contrast, in those cells that progressed beyond this phase, the IFN treatment could not initiate USP18 induction until the next cell cycle, resulting in sharply extended delay times (Fig. 4E). These results suggest that the cell-to-cell variability in USP18 delay times may stem from different cell cycle stages among cells at the treatment onset.

**Cell cycle phases differentially regulate *USP18* expression**

Our results in Figure 1.17E suggest that the early phase of cell cycle (0 – 35% of the cell cycle time), likely the G1 and early S stages, may provide a time window that allows immediate *USP18* induction without significant delays. To directly test that, we imposed chemical perturbations to arrest cells in G1 or G1/S stage and monitored the delay times of *USP18* induction, relative to that of *IRF9*. Specifically, we treated cells with serum starvation [64], lovastatin [65, 66], and roscovitine [67], all of which arrested cells in G1 or G1/S stage, prior to the IFN-$\alpha$ treatment. As expected, we observed that cell cycle synchronization

substantially reduced the fraction of cells with prolonged delays of *USP18* induction (Figure 1.19).

Furthermore, to explicitly determine the cell cycle stages of individual cells at the treatment onset and their relationships with *USP18* induction delays, we generated another reporter cell line in which we stably integrated a cyclin-dependent kinase 2 (CDK2) activity reporter [68], allowing us to infer the cell cycle stages based on the dynamics of DNA helicase B (DHB) nuclear translocation (Figure 1.19B). In the same cell line, $P_{USP18}$-driven fluorescent reporter was introduced as described in Figure 1.17A. Using this cell line, we classified cells into three groups, G1, S, and G2 cells, based on their cell cycle stages at the IFN treatment onset (Figure 1.19C, left). We found that G1 and S cells showed relatively fast USP18 activation times, whereas a large fraction of G2 cells exhibited a substantial delay in USP18 induction (Figure 1.19C, right). We also employed another cell cycle reporter system called fluorescent ubiquitination-based cell cycle indicator (FUCCI) [69] and observed similar patterns to those obtained using the CDK2 activity reporter (Figure 1.20). These results, together with the cell cycle inhibitor data in Figure 1.19A, confirmed the influence of cell cycle stages on *USP18* induction. The G1/S stages allow rapid induction of expression induction, but the G2 stage restrains the initiation of gene induction, resulting in a prolonged delay in USP18 expression.

What is the mechanism underlying the effects of cell cycle stages on *USP18* expression? Previous studies revealed global variations of epigenetic modifications during cell cycle. For instance, DNA methylation decreases in G1 and increases during S and G2 phases [70-72]. We postulated that cell cycle progression might influence USP18 expression through variations in DNA methylation. To test this possibility, we first searched the genome-wide DNA methylation profiles of various human cell types. Intriguingly, the

promoter of *USP18* contains a large number of CpG sites, which are highly methylated in all the cell types examined. In contrast, the *IRF9* promoter contains less CpG sites and is less methylated [73] (Figure 1.21). To determine whether the promoter methylation influences *USP18* expression, we treated cells with decitabine (also known as 5-Aza-2'deoxycytidine), a commonly-used DNA methyltransferase inhibitor [74, 75]. We observed that the fraction of cells with prolonged delay times in *USP18* induction were dramatically reduced, indicating that the promoter methylation inhibits *USP18* induction (Figure 1.19D). This result is consistent with a previous study showing that a decreased promoter methylation leads to increased *USP18* expression in breast cancer [76]. We note that decitabine also leads to cell cycle arrest in G2 stage [77]. Since *USP18* induction is largely delayed in G2 (Figure 1.19C), the accelerating effect of decitabine on *USP18* expression should be via inhibition of methylation rather than cell cycle arrest. In summary, our results suggested that the cell cycle stages may impact the initiation of USP18 upregulation through modulating the promoter methylation level.

**Cell cycle-gated feedback control shapes single-cell responses to repetitive IFN inputs**

Finally, we incorporated the cell cycle-gated regulation into our model, in replace of the arbitrary delay time, to test whether it is sufficient to account for the experimentally-observed delays in *USP18* induction and, consequently, desensitization, at the single cell level. Based on our experimental results (Figs. 4 and 5), we assumed that *USP18* can be induced immediately if the IFN input starts within a fixed time window (G1 and early S phases) of a cell cycle. However, if the input starts outside of the window, cells will have to wait until the open window of the next cell cycle with the delay time equals to the waiting time. We also assumed that the IFN input onset time is uniformly distributed within a cell

cycle. The length of a full cell cycle was estimated to be 21.82 hours based on the single-cell time trace measurements (Figure 1.8D). The model was fit to the experimentally-determined distribution of USP18 delay times within a cell cycle (Figure 1.22B; the data from Figure 1.17E) and we obtained an estimate of the open window length to be 7.3 hours (~33% of 21.82 hours). Using these experimentally-constrained parameters, we then performed stochastic simulations of single-cell responses to different pretreatment experiments, by introducing noise to gene expression reactions. We observed that the 24-hour pretreatment effectively induced *UPS18* upregulation, to a much higher extent than those upon 2-hour and 10-hour pretreatments. Importantly, as shown in Figure 1.22C, the higher levels of USP18 expression by the prolonged pretreatment lead to reduced IRF9 induction upon the second stimulation at the single-cell level, consistent with our experimental data (Figure 1.22D). Nonetheless, cells in the 24-hour pretreatment could be sensitive to the second IFN input if the first stimulation was added outside the activation window and/or the duration was less than the required activation threshold. The heterogeneity in USP18 activation resulted in the heterogeneity in the desensitization of STAT1 nuclear translocation (Figure 1.23).

Taken together, our experimental and modeling results suggest that the cell cycle gating can give rise to the delay in *USP18* upregulation and USP18-mediated negative feedback loop, wherein the delay time is largely determined by the length of the open window in the cell cycle (a longer open window results in a shorter delay time). When the duration of pretreatment is shorter than or close to the delay time (e.g. 2 or 10-hour pretreatment), *USP18* can only be partially induced in some cells so that the fast-acting positive feedback loop and the priming effect dominate. In contrast, the 24-hour pretreatment, with a duration longer than the entire length of a cell cycle, can fully induce

USP18-mediated negative feedback in most cells regardless of their cell cycle stages at treatment onset, resulting in desensitization to subsequent stimulation. In this way, key regulatory processes can be compartmentalized temporally by the cell cycle to decode dynamically-varying signals.

**Discussion**

IFN signaling is vital in initiating the innate immune response and providing the first line of cellular defense against infection. Although much progress has been made in identifying molecular components that mediate the IFN responses, what remains missing is an understanding about how these components interact and operate dynamically to process varying signals and fine-tune the extent and duration of responses. For example, how cells respond to repetitive IFN stimulation remains puzzling, as previous studies led to opposing conclusions [37, 38, 41, 42]. In this study, we used microfluidics and time-lapse imaging to track the responses to repetitive IFN inputs in single human epithelial cells. We found that the effects of IFN pretreatments are governed by a gene regulatory network comprised of a fast-acting positive feedback loop, in part through upregulation of ISGF3, and a delayed negative feedback loop mediated by upregulation of USP18. A short pretreatment input can only induce the positive feedback loop, leading to the priming effect to following stimulation, whereas a prolonged pretreatment activates the negative feedback loop that desensitizes the pathway. Our study reconciled the opposing results from previous studies and revealed that the effects of IFN pretreatments depend on their input durations. This dynamics-based regulation stems from coupled feedback loops that act with different kinetics. Regulatory circuits with coupled negative and positive feedback loops have been discovered in many biological processes, and, depending on the specific mechanisms and kinetics, can give rise to various dynamic behaviors, such as sustained oscillations [78, 79] and excitable

gene expression [80-82]. In this study, the coupled feedback system in the JAK-STAT pathway enables a new function of this well-studied network architecture: it serves as a timer that measures the initial input duration and coordinate the temporal order of regulatory processes with opposing effects, leading to differential cellular responses to subsequent stimuli.

Moreover, through a closer investigation of the delayed negative feedback, we found that cell cycle phases at IFN treatment onset differentially influence USP18 upregulation, resulting in heterogeneous delays in the induction of this signaling suppressor. More specifically, the G1/S phases enable an open window for immediate USP18 upregulation upon the IFN treatment. If cells are exposed to IFN when they pass the G1/S phases, the IFN treatment cannot initiate USP18 induction until the G1 phase of the next cell cycle, causing a dramatic delay in the induction kinetics. In this way, individual cells exhibit substantial cell-to-cell variability in their USP18 induction delay times, as observed experimentally (Fig. 4D), which arises from their different cell cycle phases at IFN treatment onset. Delays in the expression of key regulatory factors have been widely observed in signal-dependent transcriptional responses and have been found important for ensuring proper execution of biological functions [83-85]. Common mechanisms underlying these delays include extensive nucleosome occupancy at the promoter regions [86, 87] and cascades in gene expression programs [88]. The cell cycle gating revealed in this study represents a new mechanism that leads to delayed induction of specific genes upon stimulation. Distinct from other mechanisms, in this scenario, the cell cycle serves as a control hub that connects the expression of key pathway regulators with extracellular and intracellular conditions, enabling potential cross-regulation of IFN signaling by various factors. For example, external serum or nutrient conditions, which influence cell cycle

progression, could thereby modulate USP18 expression and impact IFN responsiveness. This mode of regulation may also provide a link between cell cycle stages and the effects of IFNs on cancer cells. For instance, the resistance of cancer stem cells to IFN treatments may be attributed partially to the fact that they spend the majority of time in G0/G1 [89], resulting in high USP18 expression and low IFN responsiveness. Along the same line, a recent report showed that IFN in combination with an G2/M inhibitor increased necroptosis in cancer cells [90], possibly due to delayed USP18 induction.

We acknowledge that our study only considered the control of specific ISGs, *STAT1*, *IRF9*, and *USP18*, which play crucial regulatory roles in IFN-driven signaling. There are other mechanisms that also contribute to priming or desensitization of the JAK-STAT pathway. For instance, it has been recently shown that acquisition of histone H3 methylation upon IFN pretreatment accelerates the recruitment of RNA polymerase II and transcription factors, leading to primed transcriptional responses to re-stimulation [54]. For desensitization, the family of SOCS proteins represses JAK-STAT signaling at multiple layers via various mechanisms [91], constituting negative feedback loops in addition to that mediated by USP18. The coupled ISGF3-USP18 feedback system revealed in this study may function together with all the other mechanisms to maintain homeostasis in the responses to varying IFN signals. Further work will be needed to evaluate the relative contributions of different mechanisms and how they coordinate to fine-tune the IFN responsiveness.

Future studies will also be needed to determine the detailed mechanisms underlying the cell cycle-gated regulation of USP18. Our results suggest that DNA methylation at the promoter region may be involved in mediating the effects of cell cycle on gene expression (Fig. 5D). However, more experiments will be required to directly monitor DNA methylation

level over time and measure its effects on chromatin modifications and the recruitments of transcription factors and RNA polymerase II. Intriguingly, ISGs have a wide range of CpG site numbers, and potentially methylation levels, in their promoters. Among the 278 ISGs examined, 114 genes, besides USP18, have more than 100 CpG sites in their promoters (Fig. S10A). It would be interesting to perform a genome-wide analysis to see whether the cell cycle-gated regulation can be more generally observed in other ISGs and how this regulatory scheme contributes to the innate immune response at a global level. Furthermore, IFN-$\alpha$ induces proinflammatory and antiviral responses in many types of cells. As our current study has focused only on epithelial cells, it would be interesting for future studies to examine and compare the dynamics and regulation of IFN-driven signaling and gene expression responses in other cell types, such as macrophages, dendritic cells, natural killer cells, and T cells, all of which are important players in mounting innate and adaptive immune responses. With specialized physiologies and functions, these cells may exhibit largely distinct response dynamics and modes of regulation. A careful investigation along this direction will advance our understanding about how various types of cells utilize the same set of molecular pathways with different kinetics to communicate with one another and coordinate their responses to infection. In addition, our study, and many recent single-cell analyses from other groups [92], highlight the presence of substantial clonal heterogeneity in cellular responses to signals. An open question that deserves extensive further exploration is how these cell-to-cell variabilities contribute to biological functions, *in vitro*, and more importantly, *in vivo*, under physiological contexts. Ongoing and future technological advances will enable us to tackle the emerging questions and challenges in single-cell biology, providing a more comprehensive, quantitative, and dynamic view of biological systems.

Finally, due to the pandemic COVID-19 caused by SARS-CoV-2, there is an urgency in understanding the basic biology of host response to viral infection, which may help the development of clinical strategies against the disease. Latest research revealed that SARS-CoV-2 is especially sensitive to type I IFNs, compared to other coronaviruses, making IFN pretreatment a potential strategy to prevent SARS-CoV-2 infection [43-45]. Our findings suggested possible ways to enhance the effectiveness of IFNs for future clinical use. For example, repetitive short-term administrations of IFN may lead to less desensitization and a more dramatic effect than prolonged treatments. Alternatively, the combined use of USP18 inhibitors with type I IFNs may substantially boost the effectiveness of IFNs against SARS-CoV-2. Further studies in animal models will be needed to test these strategies and to direct clinical applications for treating the disease.

**Figure 1.1 IFN-α pretreatments with different durations lead to opposite effects to the second stimulation.** (A) Schematic of HeLa reporter cell line engineered using CRISPR/Cas9 (top). *STAT1* was tagged with mCherry at C-terminus to monitor the translocation and expression. The coding sequence for P2A-YFP was inserted at the C-terminus of *IRF9* coding sequence to generate a transcription reporter ($P_{IRF9}$). A simplified diagram of the IFN-α pathway components that can be monitored using the reporter cell line (bottom). (B) Time lapse images of a representative cell treated with 100 ng/ml IFN-α for 48 hours. Scale bar: 20 μm. The time traces of nuclear/cytoplasmic STAT1-mCherry and $P_{IRF9}$-YFP signals of the cell are shown on the right. Vertical dashed lines represent cell divisions. (C) Averaged time traces of nuclear/cytoplasmic STAT1-mCherry, $P_{IRF9}$-YFP, and the time derivative of $P_{IRF9}$-YFP (dYFP/dt) (n = 257 cells). Data are represented as the mean (solid lines) and ± standard deviation (SD) (shaded areas). (D) Schematic of IFN-α pretreatment experiments (top). Cells were pretreated with 100 ng/ml IFN-α for 0, 2, 10 and 24 hours followed by 8 hours of break time and re-stimulated with 100 ng/ml IFN-α for an additional 10 hours. Bottom: A diagram of the microfluidic set-up. Two syringes filled with culture medium with or without IFN-α were connected to programmable Arduino-controlled valves that control the duration of IFN-α treatments. Images were captured every 5 min throughout the entire experiment that lasted for a total of 52 hours. (E) Averaged time traces of $P_{IRF9}$-driven YFP induction (left) and the rate of induction (dYFP/dt, right) in response to the second IFN-α treatment under different pretreatment conditions. For $P_{IRF9}$-YFP induction, the baselines at the beginning of the second stimulation were normalized to the same level for the comparison of induction levels under different pretreatment conditions. Results were from at least three independent experiments. (F) Amounts of $P_{IRF9}$-YFP induction by the second IFN-α stimulation under different pretreatment conditions were shown in bar graph (left) and violin plot (right). The bar showed the averages from three independent experiments, represented as mean ± standard deviation of the mean (SEM). The violin plot showed the distributions of single-cell responses under different pretreatment conditions.

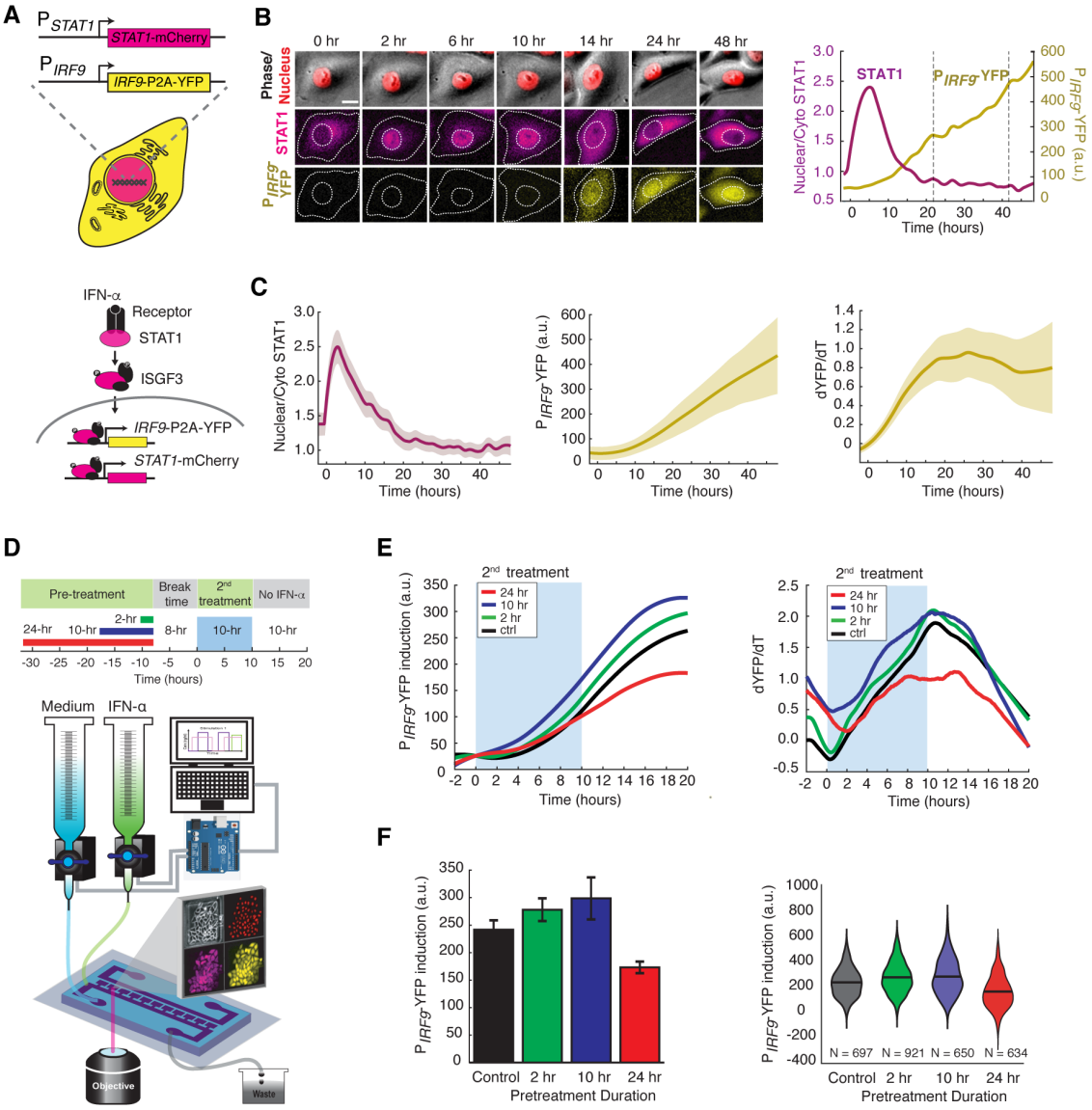
A
P STAT1
STAT1-mCherry
P IRF9
IRF9-P2A-YFP
IFN-α
Receptor
STAT1
ISGF3
IRF9-P2A-YFP
STAT1-mCherry
B
0 hr
2 hr
6 hr
10 hr
14 hr
24 hr
48 hr
Phase/ Nucleus
STAT1
P IRF9 YFP
Nuclear/Cyto STAT1
P IRF9-YFP (a.u.)
Time (hours)
C
Nuclear/Cyto STAT1
P IRF9-YFP (a.u.)
dYFP/dT
Time (hours)
D
Pre-treatment
Break time
2nd treatment
No IFN-α
24-hr
10-hr
2-hr
8-hr
Time (hours)
Medium
IFN-α
Objective
Waste
E
2nd treatment
24 hr
10 hr
2 hr
ctrl
P IRF9-YFP induction (a.u.)
dYFP/dT
Time (hours)
F
P IRF9-YFP induction (a.u.)
Control
2 hr
10 hr
24 hr
Pretreatment Duration
N = 697
N = 921
N = 650
N = 634

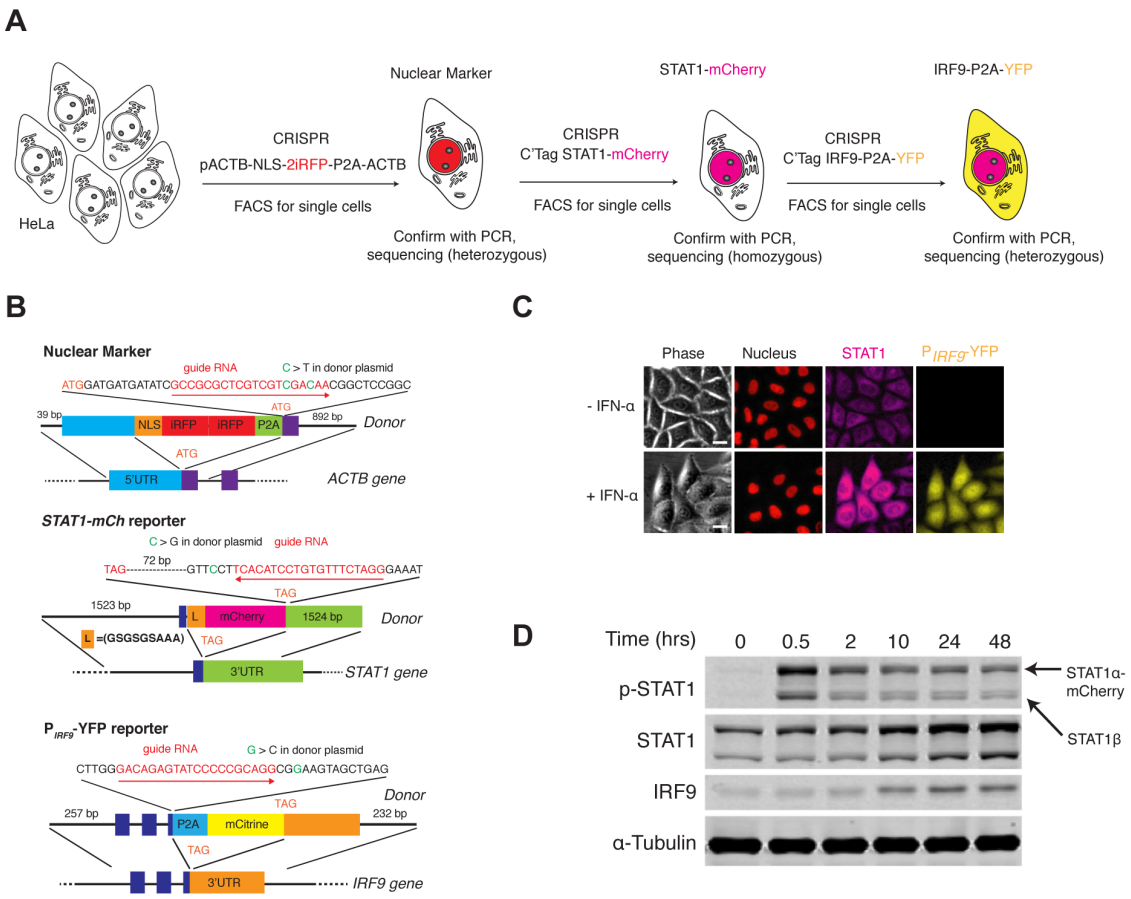


**Figure 1.2 Cell line construction and validation.** (A) Illustration of cell line construction steps. Full detail was described in Materials and Methods. Fluorescent reporters introduced and the targeted genes are shown. In each step, homogenous clones grew from single cells were carefully validated with PCR and sequencing to determine correct integration and homozygosity. Only one positive clone was selected to proceed with the next step. (B) Schematics of the *ACTB* (top), *STAT1* (middle) and *IRF9* (bottom) tagged loci. Sequences of the gRNA along with the recognition direction and the synonymous substitutions to avoid Cas9 recognition are shown. Targeted integration loci and the design of the donor DNA with indicated homology arms along with the inserts are also shown. (C) Representative images of the reporter cell line in response to IFN-α. Cells were treated without or with 100 ng/ml IFN-α for 48 hours. Scale bar: 20 μm. (D) Time course western blots showing the dynamics of phosphorylation (pY701) and expression of STAT1, and the dynamics of IRF9 expression in the reporter cell line. Cells were treated with 100 ng/ml IFN-α for indicated times, harvested and lysed for immunoblotting with indicated antibodies. The dynamics of the endogenous protein phosphorylation and expression, measured using immunoblotting, are similar to those measured using fluorescence microscopy (compare with Fig. 1C).

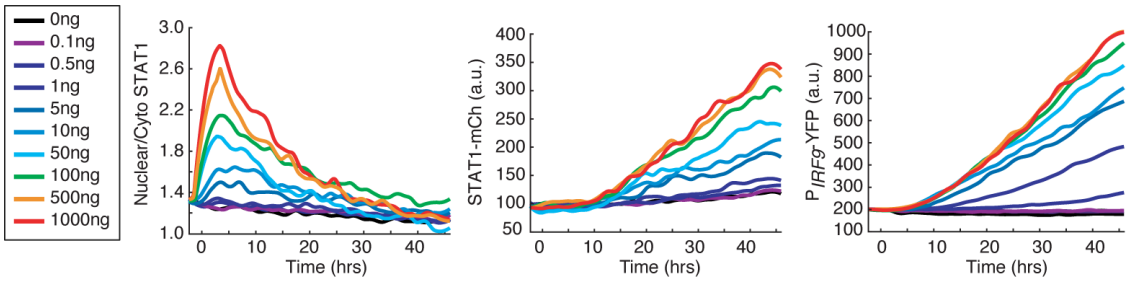


**Figure 1.3 Dose-dependent responses to IFN-α treatment.** Time traces of nuclear to cytoplasmic ratio for STAT1-mCherry, STAT1-mCherry fluorescence, and $P_{IRF9}$-YFP fluorescence in response to different concentrations (ng/ml) of IFN-α, as indicated. Averages of single cell traces were shown.

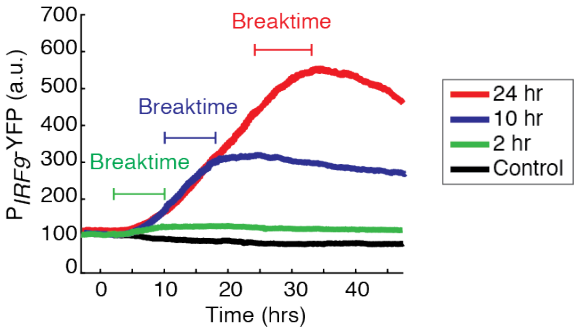


**Figure 1.4 Determination of breaktime duration.** Averaged time traces of $P_{IRF9}$-driven YFP fluorescence in response to different durations of 100 ng/ml IFN-α treatment. Results were from three independent experiments. Cells were treated with IFN-α for 0, 2, 10 or 24 hours followed by normal media for the total time of 48 hours using microfluidic devices. The breaktime is defined as the duration required for $P_{IRF9}$-YFP fluorescence to reach maximum after IFN-α was remove.

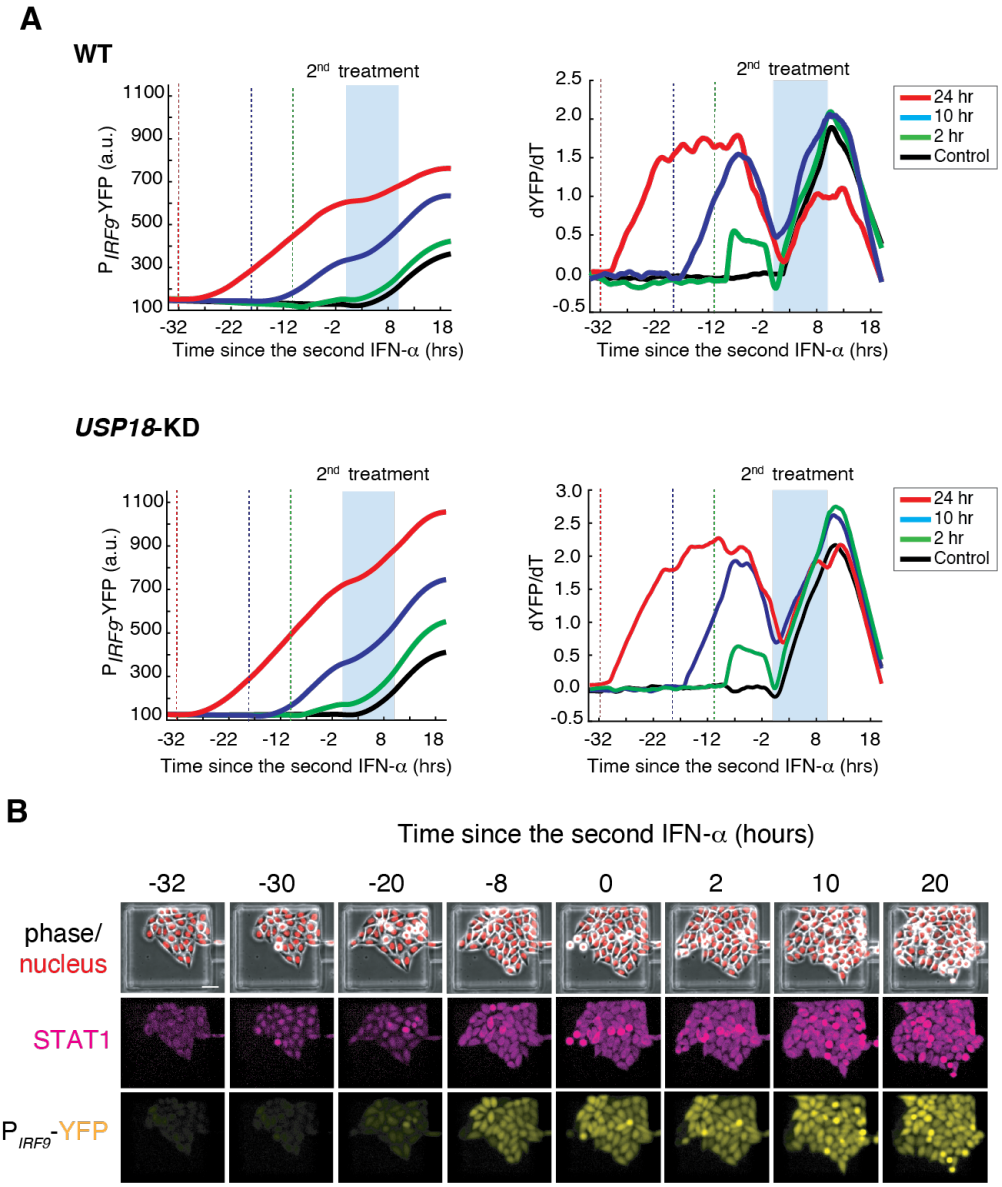


**Figure 1.5 The entire time trace quantification of fluorescent reporter in the pretreatment experiment.** (A) Averaged time traces of $P_{IRF9}$-driven YFP induction (left) and the rate of induction (dYFP/dt, right) in response to repetitive IFN-α treatment in WT (top) and *USP18*-KD cells (bottom). Results were from at least three independent experiments. The vertical dash lines represent the time when the first IFN-α was added for each pretreatment condition: 24-hr (red), 10-hr (blue) and 2-hr (green). The second treatment was added at the same time (time = 0) and lasted for 10 hours (shaded blue area). (B) Representative time-lapse images of WT reporter cells in a microfluidic cell chamber illustrating cell morphology and fluorescent signal induction under 24-hr pretreatment condition. Scale bar: 50 μm.

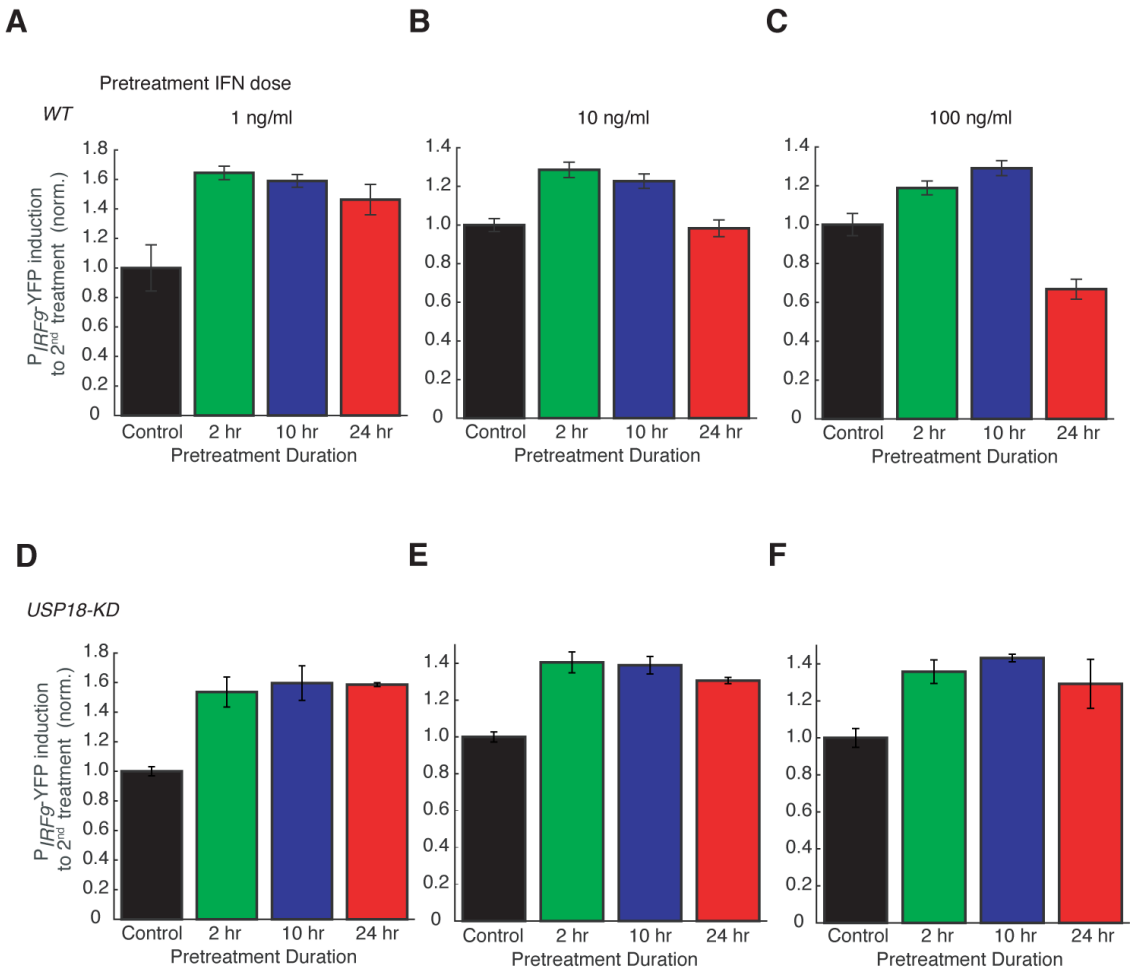


**Figure 1.6 Dose dependence of desensitization to IFN-α treatment.** Bar graphs showing the amounts of $P_{IRF9}$-YFP induction to the second IFN input (100 ng/ml) in WT (A - C) and USP18-KD (D – F), pretreated with different concentrations of IFN-α for different durations, as indicated. The results were normalized to the non-pretreatment condition (control).

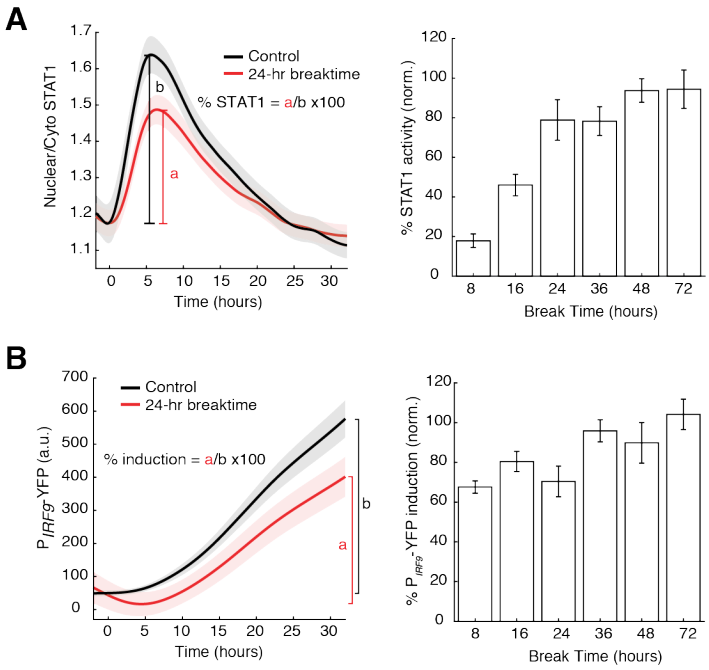


**Figure 1.7 Break time dependence of desensitization to IFN-α treatment.** Dual reporter cells were treated with 100 ng/ml IFN-α for 24 hours, washed with PBS 3 times and replaced with the normal medium. IFN-α was added 8,16, 24, 36, 48 and 72 hours later. Left: average time traces of nuclear to cytoplasmic ratio of STAT1-mCherry (A) and $P_{IRF9}$-YFP fluorescence (B) in the control (no pretreatment) and 24-hour pretreatment. The shaded area represents ± SD. The % STAT1 nuclear translocation and % IRF9 induction were calculated as relative to the control. Right: bar graphs showing percent STAT1 activity and % $P_{IRF9}$-YFP induction given different break time durations. Error bars represent ±SD.

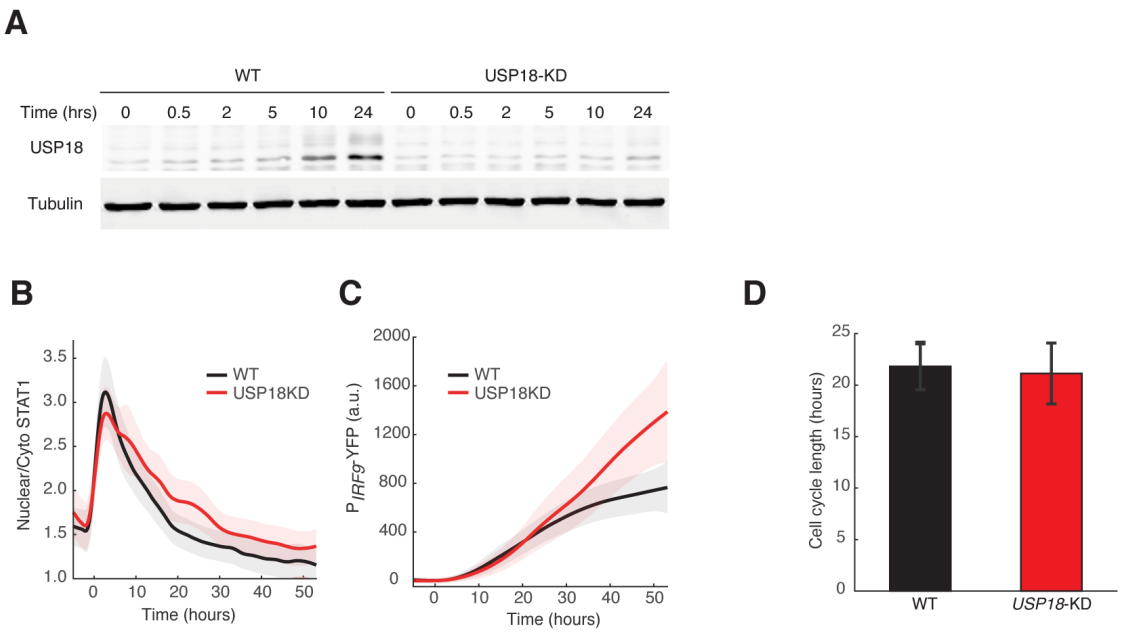


**Figure 1.8 Validation of the *USP18*-KD cell line.** (A) Western blots of USP18 expression in WT and *USP18*-KD cells. Cells were treated with 100 ng/ml IFN-α for indicated times, harvested and lysed for immunoblotting with the USP18 antibody. Time traces of nuclear to cytoplasmic ratio for STAT1-mCherry (B) and $P_{IRF9}$-YFP fluorescence (C) in WT (black) and *USP18*-KD (red) in response to IFN-α. Averages of single cell traces were shown. The shaded area represents ±SD. (D) Averaged cell cycle lengths of WT and *USP18*-KD. Cell divisions were identified in individual cells and the lengths between cell divisions were quantified. Error bars represent ±SD.

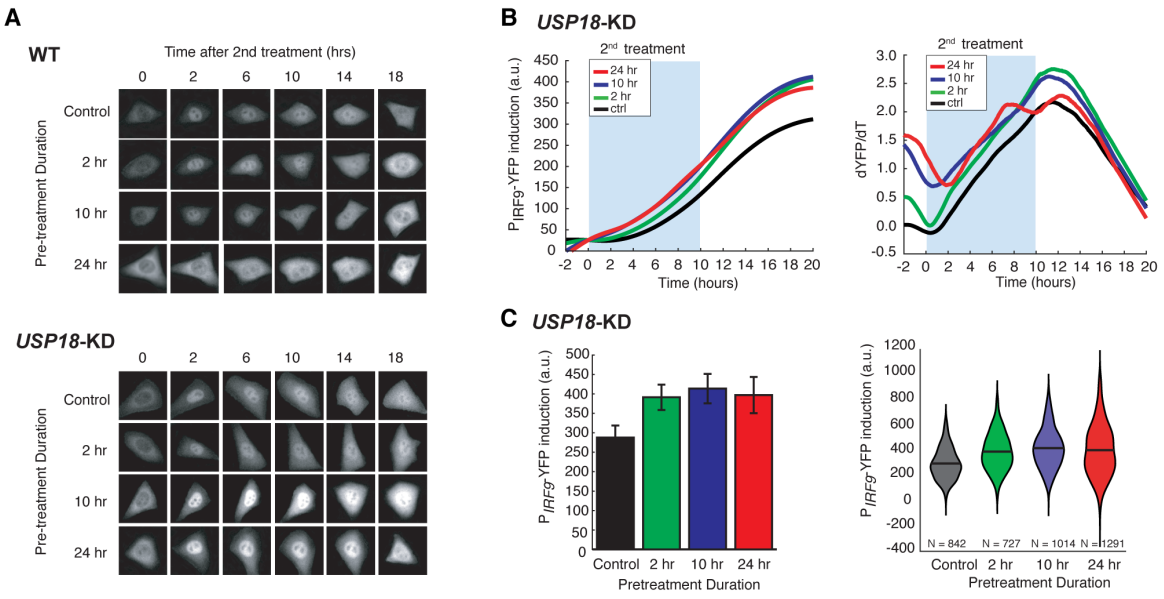


**Figure 1.9 USP18 mediates desensitization induced by the prolonged IFN-α pretreatment.** (A) Representative time-lapse images of STAT1 nuclear translocation in response to the second IFN-α treatment under different pretreatment conditions in WT cells (top) and *USP18*-KD (bottom). (B) Averaged time traces of $P_{IRF9}$-driven YFP induction (left) and the rate of induction (dYFP/dt, right) in *USP18*-KD cells in response to the second IFN-α treatment under different pretreatment conditions. (C) Amounts of $P_{IRF9}$-YFP induction in *USP18*-KD cells by the second IFN-α stimulation under different pretreatment conditions were shown in bar graph (left) and violin plot (right).

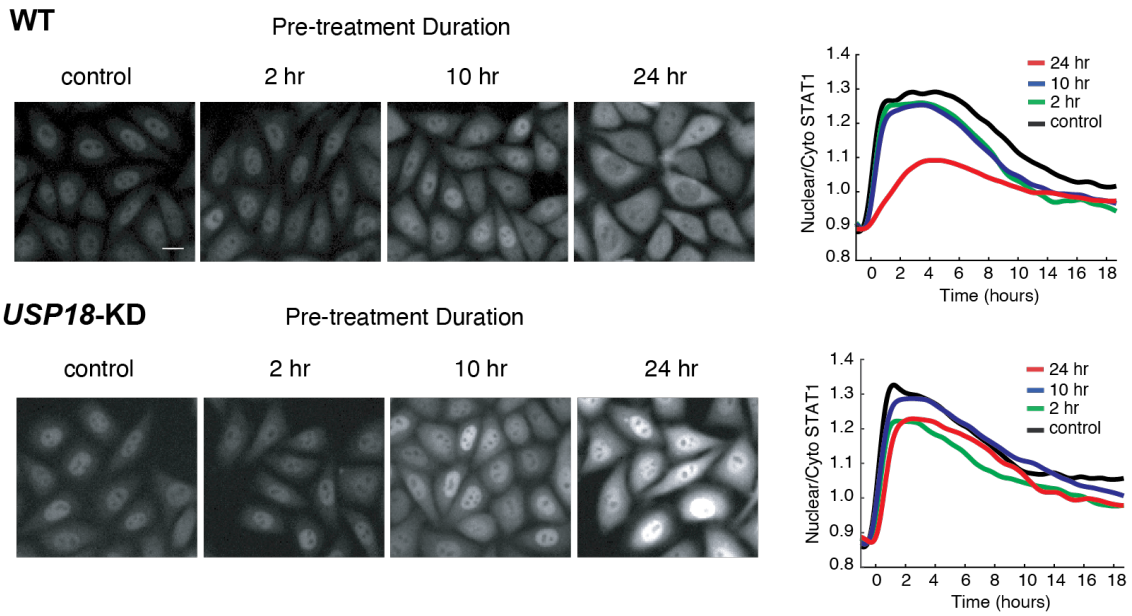


**Figure 1.10 USP18 is responsible for desensitization in STAT1 nuclear translocation.** Cells were treated with 100 ng/ml IFN-α followed by 8 hours of breaktime and re-stimulated. Representative images of STAT1 nuclear translocation at 2 hours after the second IFN-α stimulation under different pretreatment conditions in WT cells (top) and *USP18*-KD (bottom). Scale bar: 20 μm. The time traces of nuclear/cytoplasmic STAT1-mCherry ratio is shown on the right.

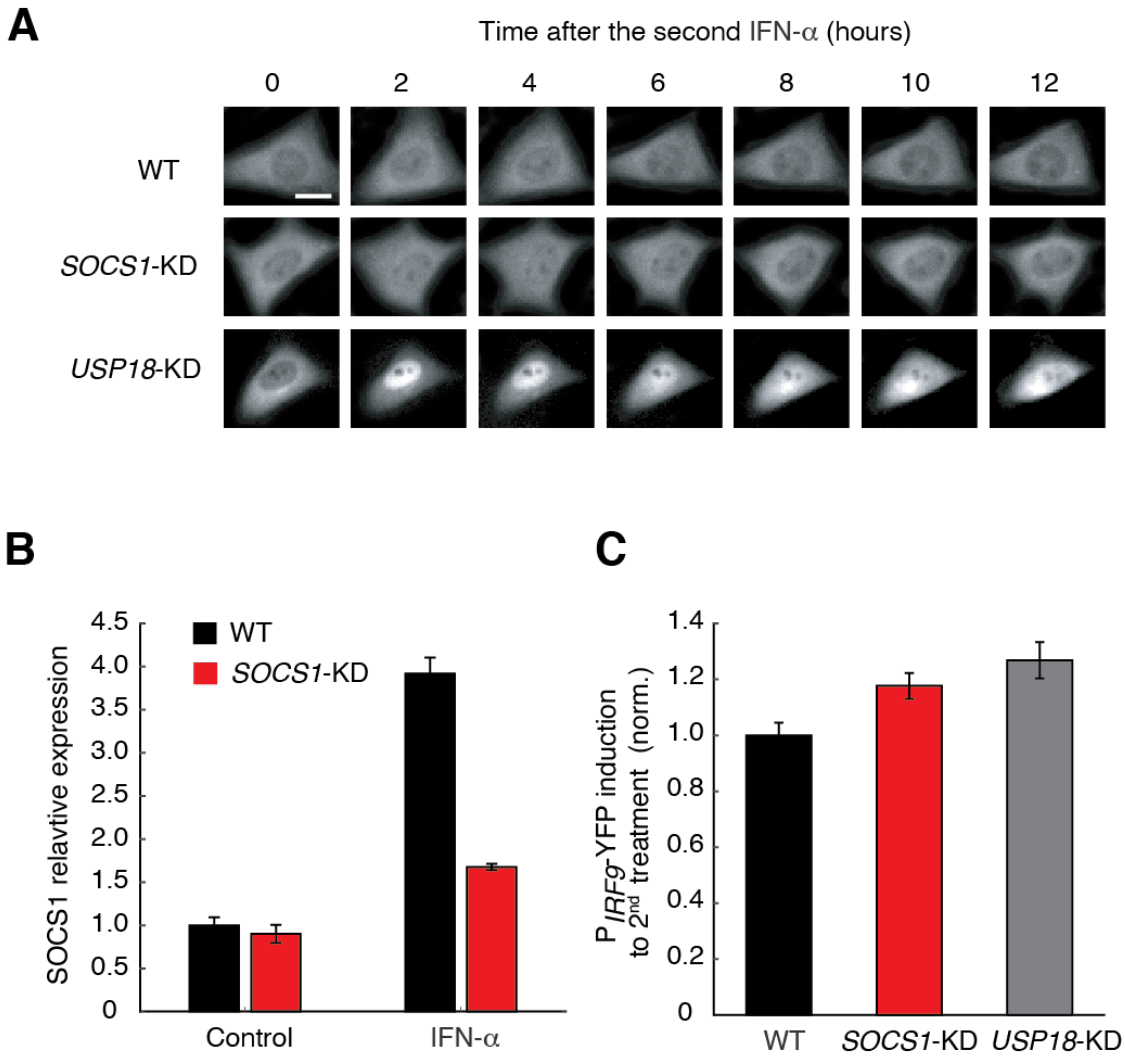


**Figure 1.11 SOCS1 does not mediate the desensitization of STAT1 nuclear translocation upon IFN stimulation.** Representative time-lapse images of STAT1 nuclear translocation upon the second IFN-α treatment in WT cells (top), *SOCS1*-KD (middle) and *USP18*-KD (bottom) cells. Cells were pretreated with 100 ng/ml IFN-α for 24 hours followed by 8 hours of break time and re-stimulated for 12 hours. Scale bar: 20 μm. (B) Quantitative PCR results showing reduced SOCS1 expression in response to IFN-α as a validation of successful knock-down. (C) Amounts of $P_{IRF9}$-YFP induction in WT, *SOCS1*-KD and *USP18*-KD cells by the second IFN-α stimulation. The error bars represent 3 replicates of the same experiment.

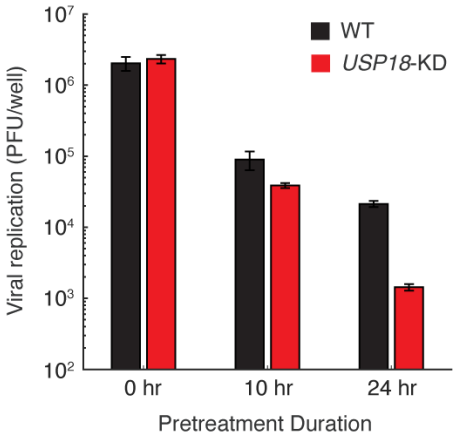


**Figure 1.12 Vesicular stomatitis virus (VSV) replication in WT and *USP18*-KD cells pretreated with different IFN-α durations.** Cell were pretreated with 100 ng/ml IFN-α for 0, 10 or 24 hours followed by 8 hours of break time and infected with 2500 PFU (plaque forming units) of VSV. After 18 hours, viral supernatant was collected and titered. Error bars represent ±SD, n=3. Note that the y-axis starts with 100 PFU/well as it is the limit of detection of our method.

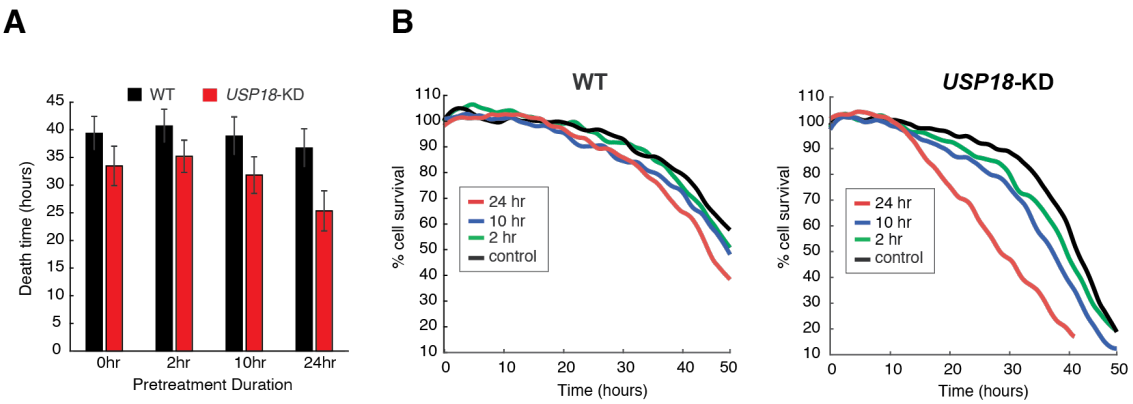


**Figure 1.13 *USP18*-KD cells is more sensitive to doxorubicin induced cell death.** Cells were pretreated with 100 ng/ml IFN-α for 0, 2, 10 or 24 hours followed by 8 hours breaktime and then treated with 1 μM doxorubicin. Time lapse images were captured for 50 hours. (A) The average cell death time after doxorubicin treatment calculated from single cells based on the morphology change. Error bars represent ±SD. (B) Percent cell survival over time upon doxorubicin treatment. Number of survival cells in the time lapse images were quantified at each time point and shown as percent cell number relative to the start of doxorubicin treatment. *USP18*-KD cells (right) showed faster rate of apoptosis induced by doxorubicin than WT cells (left).

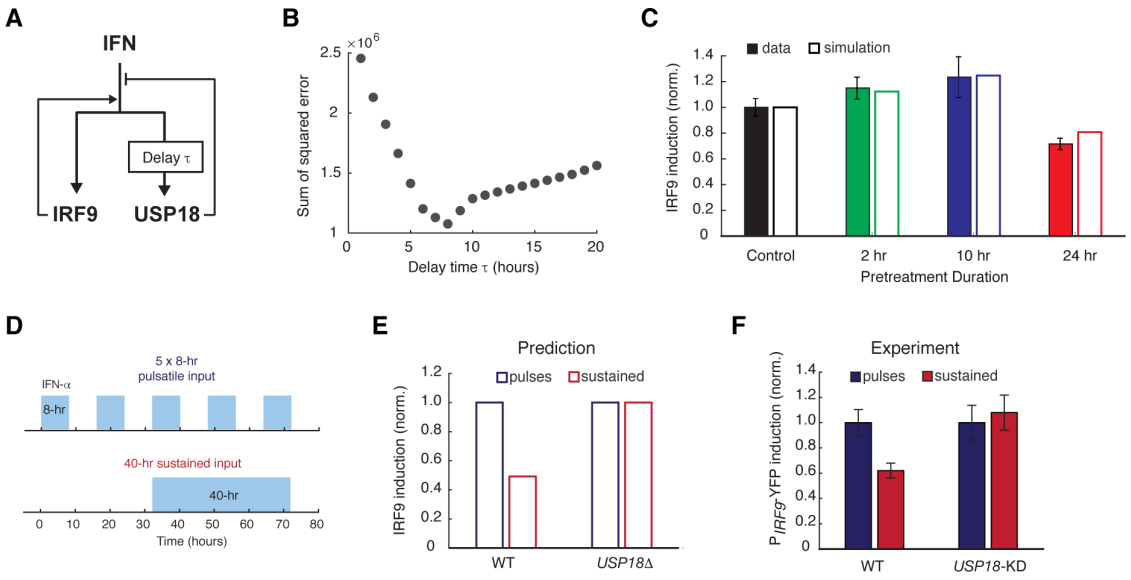


**Figure 1.14 A kinetic model suggests a delayed negative feedback loop through USP18.** (A) A diagram for the simple kinetic model of the IFN-driven gene regulatory network. (B) Fitting errors between simulations and the data with different assigned values of the delay time in USP18 upregulation. (C) Amounts of $P_{IRF9}$-YFP induction by the second IFN-$\alpha$ stimulation under different pretreatment conditions, from experimental data (solid bars) and model simulations with the best-fit parameters (open bars). Data were from Fig. 1F and were normalized to the non-pretreatment condition (control). (D) Schematic of experimental design with repetitive IFN pulses versus a sustained IFN input. (E) Model prediction of the responses to pulsatile versus sustained IFN inputs in the presence and absence of USP18. Results were normalized to the amount of induction to the pulsatile IFN input in WT. (F) Experimental data of the responses to pulsatile versus sustained IFN inputs in WT and *USP18*-KD cells.

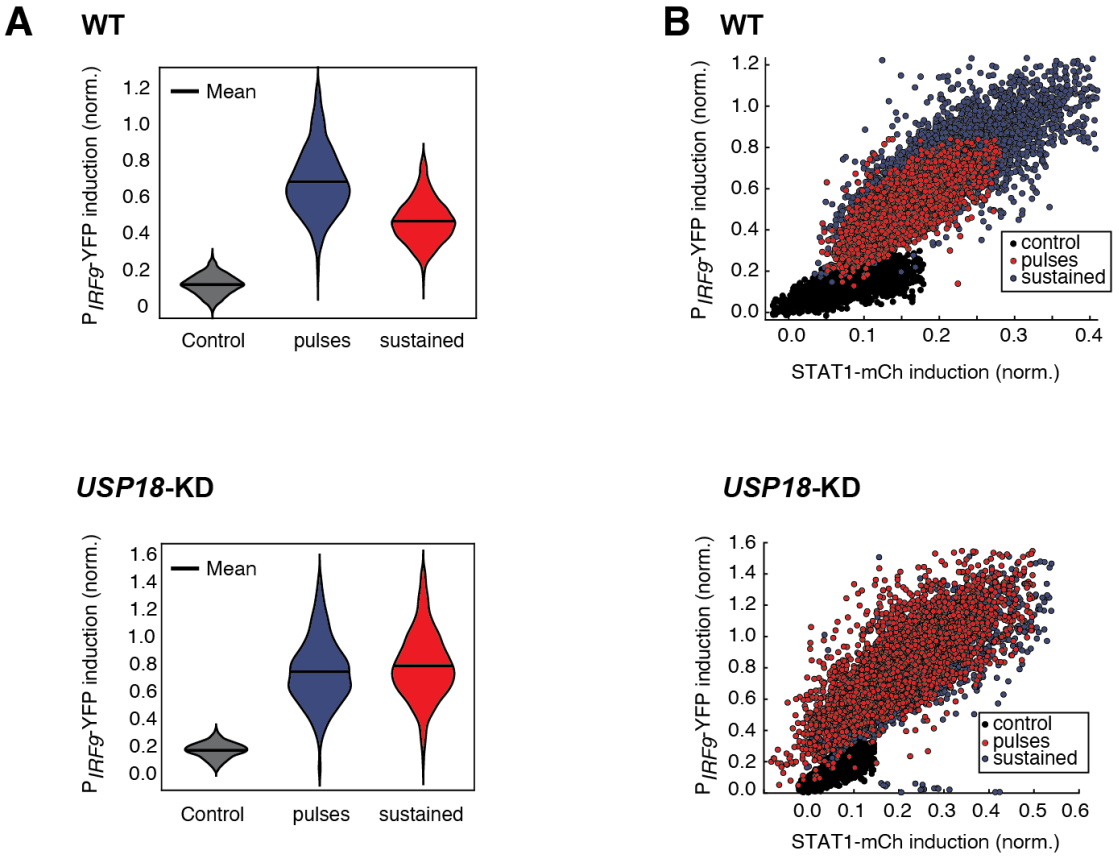


**Figure 1.15 Pulsatile IFN-α treatment induces higher ISG expression in single cells.** (A) The violin plots showing single-cell distributions of $P_{IRF9}$-YFP induction upon 5 x 8-hr pulsatile (blue) or 40-hr sustained (red) IFN-α treatments in WT (top) and *USP18*-KD (bottom) cells. (B) Scatterplots showing STAT1-mCherry versus $P_{IRF9}$-YFP induction in single cells in response to 5 x 8-hr pulsatile or 40-hr sustained IFN-α treatments in WT (top) and *USP18*-KD (bottom) cells. Fluorescent signals without IFN-α treatment were used as control.

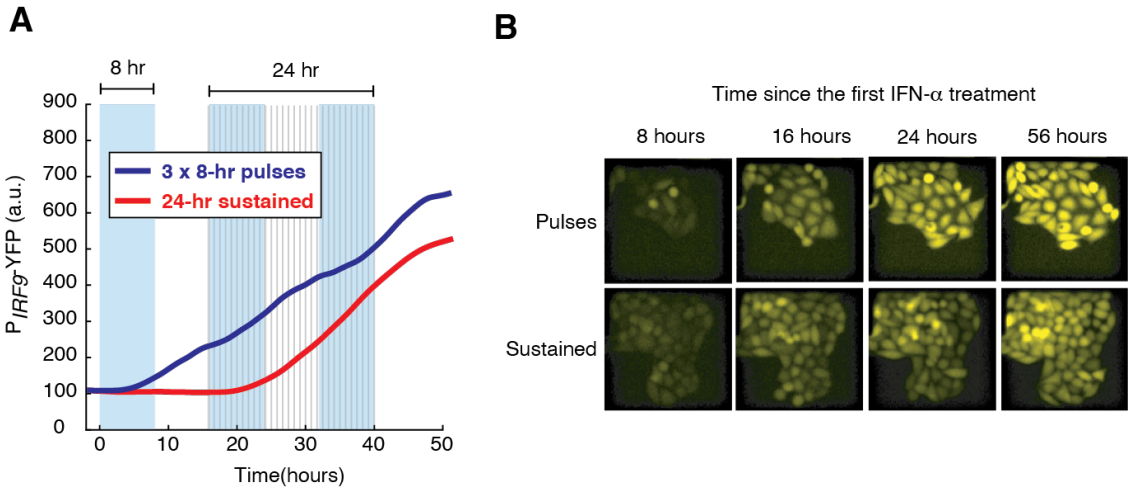


**Figure 1.16 Pulsatile IFN-α treatment induces higher ISG expression shown in microfluidic device.** (A) Averaged time traces of $P_{IRF9}$-YFP induction upon 3 x 8-hr pulsatile (blue) or 24-hr sustained (red) IFN-α treatments in WT cells. The blue and line-stripped shading indicates the presence of IFN-α in the pulses and sustained conditions respectively. (B) Representative time lapse images showing the $P_{IRF9}$-YFP induction upon the pulses or sustained treatment.

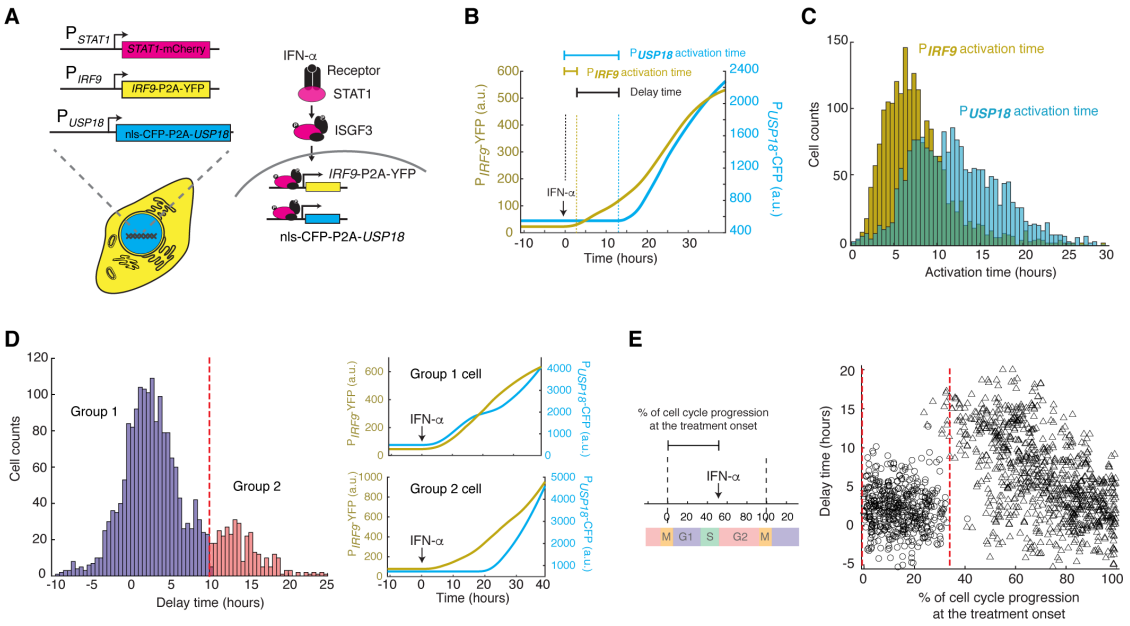


**Figure 1.17 Heterogeneous delays in *USP18* upregulation by IFN were observed in single cells.** (A) Schematic of the dual reporter cell line. A coding sequence for NLS-CFP-P2A was inserted endogenously into the N-terminus of *USP18* coding sequence of the previous cell line. IFN-α induces nuclear translocation of STAT1 and upregulation of *IRF9* ($P_{IRF9}$-YFP) and *USP18* ($P_{USP18}$-CFP). (B) Representative time traces of $P_{IRF9}$-YFP and $P_{USP18}$-CFP of a single cell in response to IFN-α. Activation time is defined as the time required to initiate the upregulation of the reporters after IFN-α treatment onset. Delay time is defined as the time difference between $P_{USP18}$ and $P_{IRF9}$ activation times. (C) Distributions of $P_{IRF9}$ and $P_{USP18}$ activation times in single cells (n = 2021 cells). (D) Distributions of delay times in single cells, quantified from the activation times in C. Cells are classified into two groups based on the delay times. Representative time traces of $P_{IRF9}$ and $P_{USP18}$ in a single cell from each group are shown (right). (E) Single-cell delay times as a function of the percentages of cell cycle progression upon IFN treatment onset. Left: Diagram illustrating the quantification of the percentage of cell cycle progression at the treatment onset in a single cell. The time between two cell divisions (dashed lines) was considered as the length of one cell cycle. % of cell cycle progression is calculated as the ratio of the time in a cell cycle before IFN-α addition versus the full cell cycle length (100%). Right: Scatterplot of delay time in each single cell versus % of cell cycle progression upon treatment onset. Open circles represent cells in which $P_{USP18}$-CFP upregulation occurred within the same cell cycle as the IFN-α addition. Open triangles represent cells in which $P_{USP18}$-CFP upregulation occurred in the next cell cycle. Red dashed lines indicate the time window for immediate $P_{USP18}$ induction.

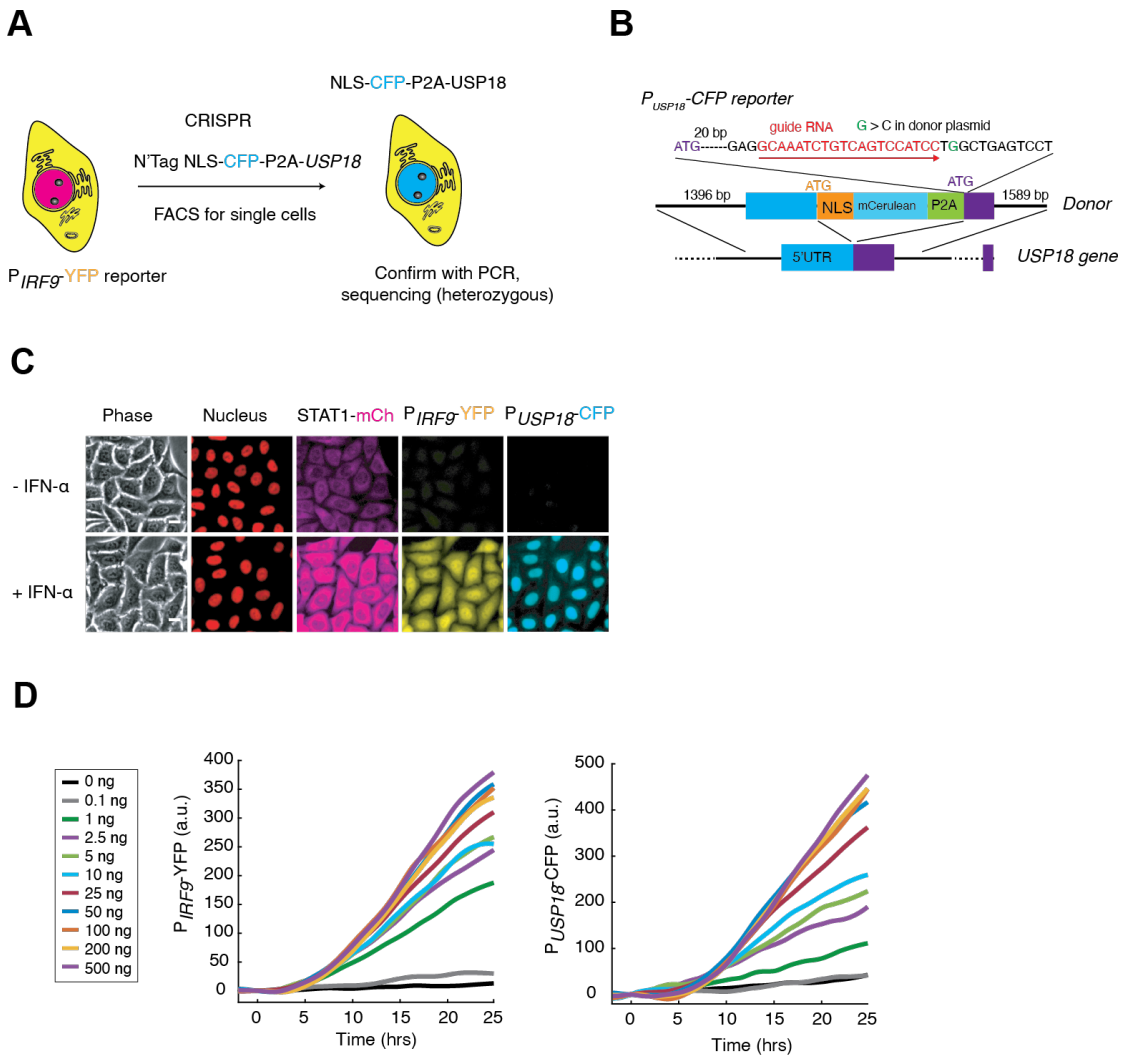


**Figure 1.18 Construction of the cell line with $P_{USP18}$-CFP reporter.** (A) Illustration showing the introduction of $P_{USP18}$-CFP into the dual reporter cell line in Fig. 1A. NLS-CFP-P2A coding sequence was inserted between the promoter and coding sequence of the *USP18* gene to generate a transcriptional reporter. (B) Schematic of *USP18* tagged locus. The sequence of the gRNA along with the recognition direction and the synonymous substitutions to avoid Cas9 recognition are shown. The design of the donor DNA with indicated homology arms along with the inserts are shown. (C) Representative images of the reporter cell line in response to IFN-α. Cells were treated without or with 100 ng/ml IFN-α for 48 hours. Scale bar: 20 μm. (D) Time traces of $P_{IRF9}$-YFP and $P_{USP18}$-CFP fluorescence in response to different concentrations (ng/ml) of IFN-α, as indicated. Averages of single cell traces were shown.

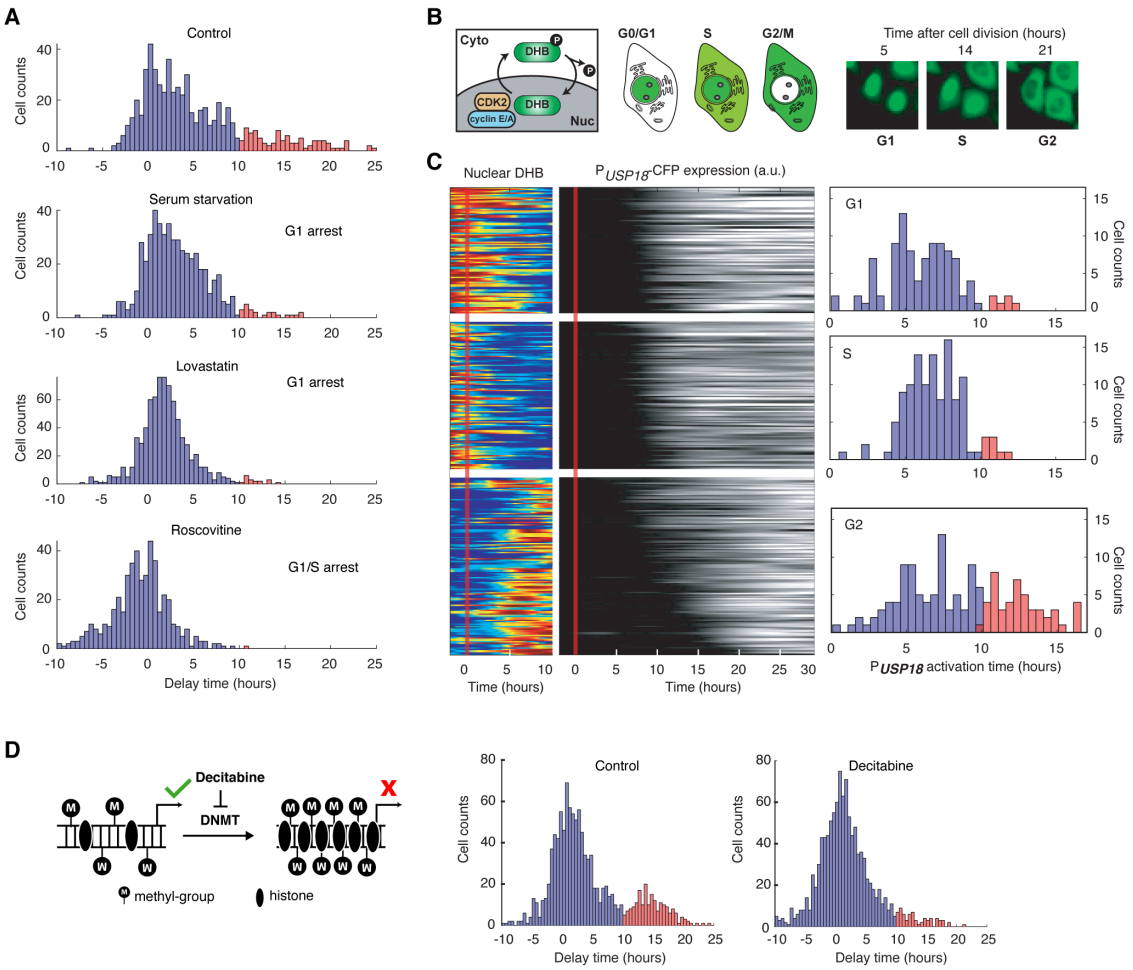


**Figure 1.19 *USP18* expression was differentially regulated by cell cycle phases.** (A) Distributions of delay times in cells treated with different cell cycle perturbations. Cells were serum-starved or treated with lovastatin (5 μM), or with roscovitine (5 μM) for 36 hours prior to IFN-α treatment. (B) Schematic of CDK2 activity reporter. Amino acids 994-1087 of human DNA helicase B (DHB) was fused with mCherry. The construct was stably integrated into $P_{USP18}$ cell line using lentivirus. The dynamics of nuclear translocation of DHB-mCherry can be used to infer the cell cycle phase. Representative time-lapse images of DHB-mCherry illustrate the inference of cell cycle phases.
(C) Color maps showing nuclear DHB and $P_{USP18}$-driven gene expression in the same single cells. Each row represents the time trace of a single cell. Cells were grouped into G1 (n = 104), S (n = 124) and G2 (n = 144) based on the nuclear DHB signals (left) at the time of IFN-α addition. For each group, cells were sorted based on $P_{USP18}$-CFP activation time (middle). Right: Distributions of $P_{USP18}$-CFP activation times for each group. (D) Distributions of delay times in cells treated with decitabine, a DNA methyltransferase (DMNT) inhibitor. Left: Schematic of the effect of decitabine on DNA methylation and nucleosome occupancy. Right: Distribution of delay times upon decitabine treatment. Cells were cultured with medium in the absence (control) or presence of 100 μM decitabine for 48 hours prior to 100 ng/ml IFN-α treatment. Cells with delay times longer than 10 hours are shown in red.

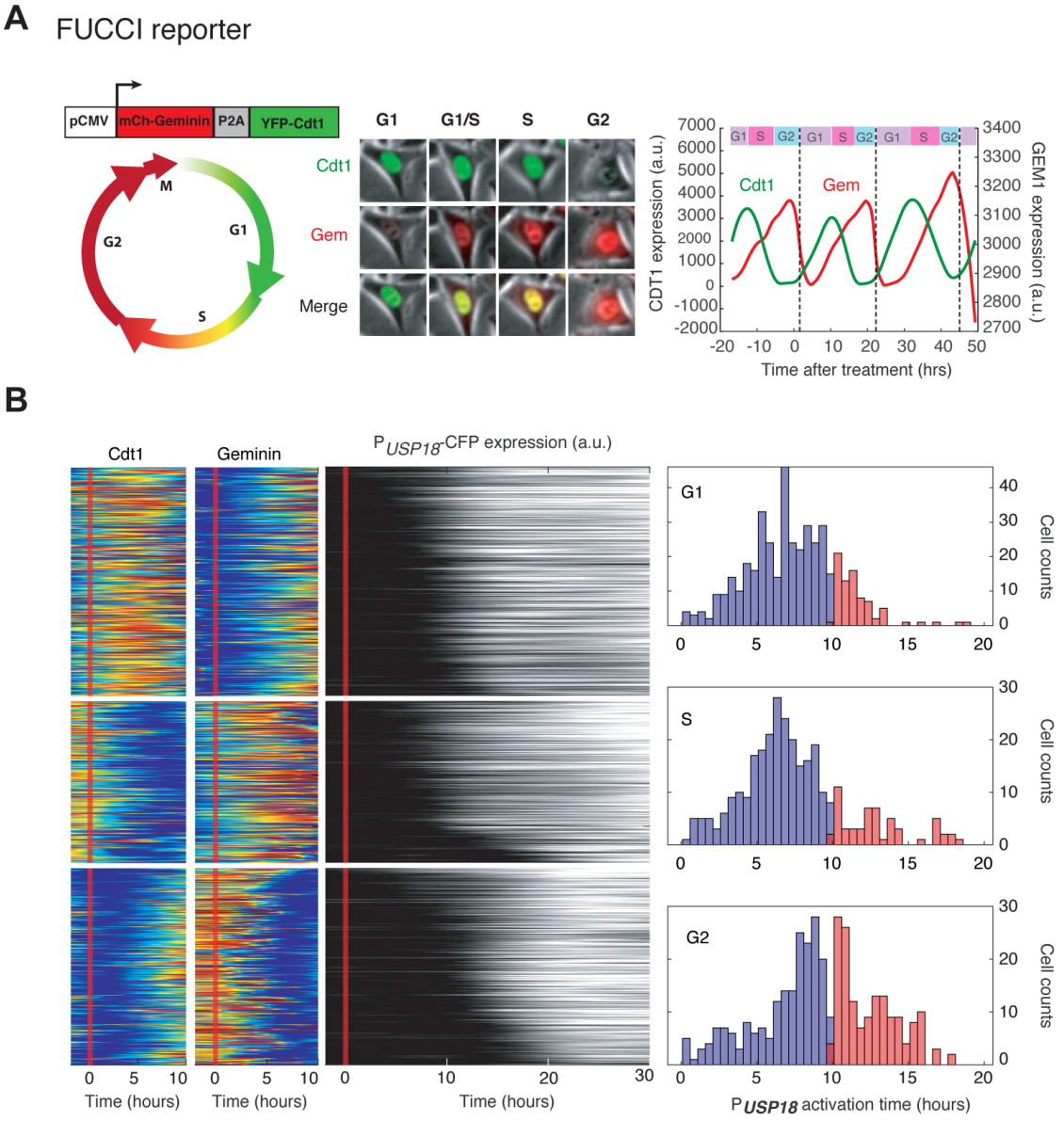


**Figure 1.20 Cell cycle-dependent *USP18* upregulation determined by the FUCCI reporter.** (A) Illustration of how the FUCCI reporter works. The fluorescent signals of chromatin licensing and DNA replication factor 1(Cdt1) and Geminin (Gem) proteins oscillate throughout a cell cycle to infer cell cycle phases. Middle: Images of a representative cell showing the Cdt1 and Gem level at different cell phases. Dynamics of Cdt1 and Gem signals in a single cell are shown along with the cell cycle phase inference. Dashed lines represent cell divisions. (B) Color maps of Cdt1, Gem and $P_{USP18}$-CFP expression in the same single cells. Each row represents the time trace of a single cell. Cells were grouped into G1 (n = 451), S (n = 388) and G2 (n = 325) based on Cdt1 and Gem signals (left) at the time of IFN-α addition. For each group, cells were sorted based on $P_{USP18}$-CFP activation time (middle). Right: Distributions of $P_{USP18}$-CFP activation times for each group.

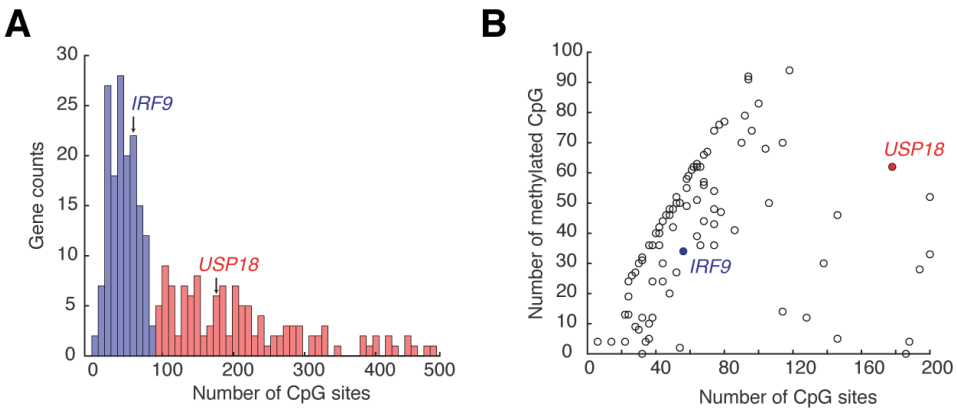


**Figure 1.21 ISG promoters contain a wide range of CpG site numbers and methylation levels.** (A) Histogram showing the numbers of CpG sites at ISG promoters. The promoter region is defined as 1000 bp upstream of the transcription start site. The data are collected from ENCODE database and the list of the 278 ISGs is from Interferome Database. (B) Scatterplot showing the numbers of methylated CpG versus of the numbers of CpG sites for ISG promoters. A CpG site is considered methylated if the methylation level is greater than 50% according to the bisulfite sequencing. Data are from ENCODE database for HeLa cells.

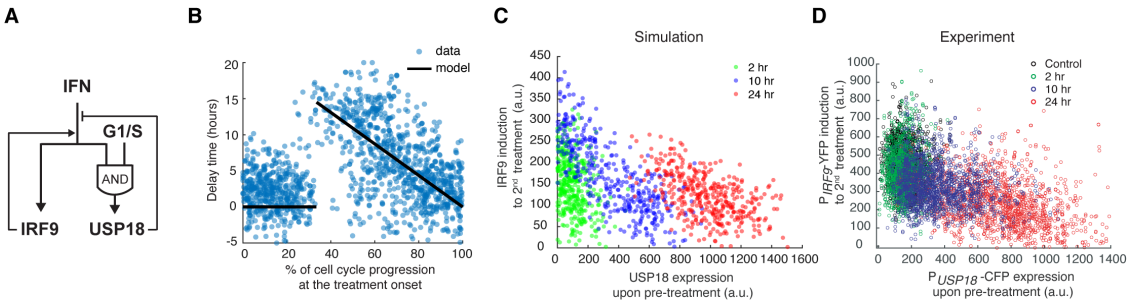


**Figure 1.22 Stochastic simulations with the cell-cycle gated feedback control reproduced single-cell responses to IFN pretreatments with different durations.** (A) A diagram for the simple model of the IFN-driven gene regulatory network that incorporates the cell cycle gating of USP18 upregulation. (B) Cell cycle-dependent delay times in the model determined by experimental data from Figure 1.17E. (C) Scatterplot showing the simulated responses under different pretreatment conditions. Stochastic simulations were performed for 400 times for each condition. In the scatterplot, each circle represents a single run with *IRF9* induction in response to the second IFN-α treatment versus *USP18* expression by the pretreatment. (D) Scatterplot showing the single-cell responses under different pretreatment conditions, from experimental data. $P_{USP18}$-CFP expression was measured at the end of the breaktime and the induction of $P_{IRF9}$-YFP was measured 34 hours after the second IFN-α input was added.

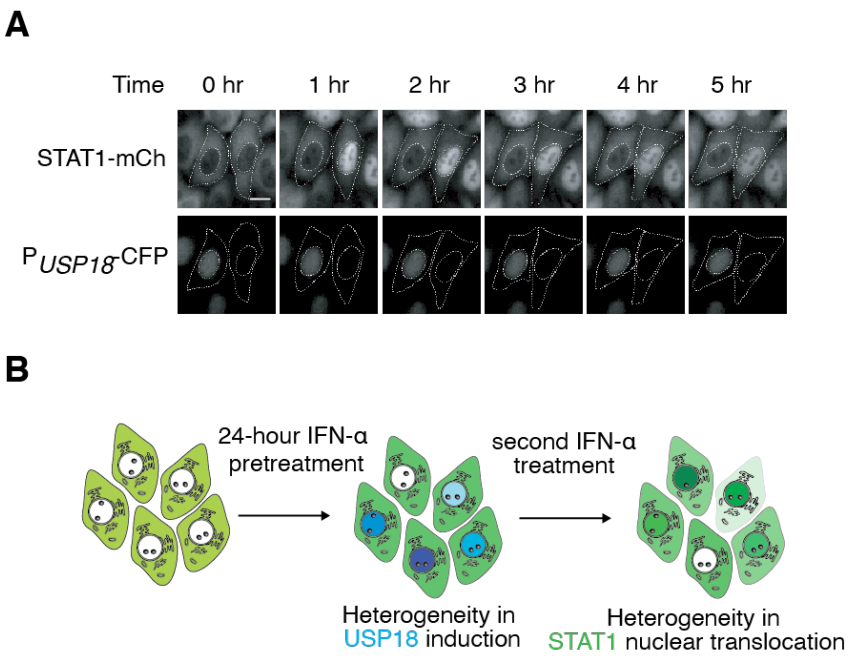


**Figure 1.23 Heterogeneity in STAT1 nuclear translocation desensitization in 24-hour IFN-α pretreatment.** (A) Representative time-lapse images of STAT1 nuclear translocation and $P_{USP18}$-CFP in response to the second IFN-α treatment. The dual reporter cell line was treated with 100 ng/ml IFN-α for 24 hours followed by 8 hours of breaktime. Scale bar: 20 μm. (B) Schematic of possible mechanism of heterogeneity in STAT1 nuclear translocation. Cells induce different level of USP18 upon the 24-hour pretreatment causing them to either be responsive or desensitized to the second stimulation.

## Materials and Methods

### Cell cultures

HeLa and HEK293T cells were cultured in Dullbecco minimal essential medium (DMEM: Thermo Scientific HyClone #SH30022FS) supplemented with 10% fetal bovine serum, 4 mM L-glutamine, 100 I.U./ml penicillin and 100 μg/ml streptomycin at 37°C, 5% $CO_2$ and 90% humidity. The imaging media is phenol red free DMEM (Life Technology-Gibco®) with identical supplements as the culture medium. The transfections were performed with 1 μg DNA: 2 μl Fugene HD (Promega E2311) ratio. Cells were seeded at 300,000 cells/well in 6-well plate for 18 hours before transfection. Two days after transfection puromycin was added to the medium at 1 μg/ml, and cells were selected for 2 days. Survival cells were grown for another 7 days before sorted with FACS into 96-well and expanded into monoclonal cell lines.

### Drug treatments

Cells were treated with 100 ng/mL recombinant human IFN-α (Prospec: cyt-520). Lovastatin (Selleck Chemicals, S2061) was used at 5 μM and Roscovitine (Sigma-Aldrich, R7772) was used at 5 μM. Decitabine (Sigma-Aldrich, A3656) was used at 100 μM.

### Cell line construction

We followed the CRISPR/Cas9 protocol [93] to construct the reporter cell line. In general, the gRNAs were designed by online CRISPR tool (http://crispr.mit.edu) and the DNA oligos were ordered from Eurofins Genomics, annealed and cloned into pSpCas9(BB)-2A-Puro (Addgene #48139) vector plasmids. gRNA plasmids were transfected into HEK293T cells and tested for gRNA efficiency using the T7 endonuclease assay. Only the most efficient gRNA was used with the donor DNA. The donor plasmids were constructed using Gibson assembly method. We used site-directed *in-vitro* mutagenesis to make

synonymous substitution in the donor plasmids to avoid gRNA recognition and Cas9 cutting of the linearized donor.

In more detail, we first developed a nuclear marker cell line by inserting the nuclear localization signal followed by two copies of infrared fluorescent protein (NLS-2xiRFP) [94] under the endogenous actin promoter followed by a P2A spacer in HeLa cells. This cell line ensured a constitutive expression without introducing exogeneous strong constitutive promoter and greatly assists cell segmentation and tracking. Briefly, the gRNA and the linearized donor DNA were transfected into HeLa cells and the transfected cells were screened with 1 μg/ml puromycin for 2 days. The cells were allowed to grow for additional 5 days before sorted by FACS. The fluorescently positive cells were sorted as single cell into 96-well plate. We collected at least 500 single cells. We grew the cells for additional 3 weeks to obtain homogenous clones. On average, about 30% of cells form colonies and all were screen for fluorescent signal with the microscope. A minimal of 10 clones were then genotyped and checked for homozygosity and correct integration using at least 3 pairs of primers and confirmed with sequencing. Positive clones were further validated with western blot to ensure correct protein expression. After construction and validation, the engineered single-clonal cell line was assigned a unique identification number, entered in our electronic database, and stored in liquid nitrogen with a cryoprotectant. The same procedure was performed for CRISPR-based tagging the additional genes, *STAT1*, *IRF9* and *USP18* sequentially.

The knockdown of *USP18* by shRNA was done using retrovirus transduction. We screened the transfected cells with 1 μg/ml puromycin for 5 days and confirmed the presence of the construct in the cells with PCR and confirmed the knock-down of USP18

with western blotting. Similarly, the knockdown of *SOCS1* by shRNA was done using lentivirus transduction, screened and validated with PCR and qPCR.

For the cell cycle reporter cell lines, we transfected *USP18* CRISPR constructs into the nuclear marker cell line and screened for a correct and homogenous monoclonal clone. We then used lentivirus to stably integrate pCMV-DHB-mCherry or pCMV-mCherry-Geminin(1-110)-P2A-mCitrine-Cdt1(30-120) in pLenti-Puro (Addgene: 39481). Cells were screened with puromycin and sorted by FACS to generate monoclonal cell lines.

Primers used in this study were listed in Table 1.1 Plasmids and cell lines constructed in this study were listed in Tables S2 and S3, respectively.

**Microfluidic and cell culture setup for time-lapse microscopy**

Fabrication of the microfluidic device was conducted as described previously [52]. For setting up the microfluidic experiments, HeLa cells were washed with dPBS and detached from the culture dish with 0.25% trypsin EDTA, centrifuged at 200 rcf for 3 minutes and resuspended with the complete imaging medium at a density of 7-10 million cells per mL. The suspension was loaded into the microfluidic device and allow the cells to adhere for at least 36 hours in the standard incubator (37°C, 5% $CO_2$ and 90% humidity). The detail of the loading protocol is described previously [52]. The device was set up in a customized chamber with 5% $CO_2$ and 37°C. The flow of the media was 1 ml/hour and the control of the valves were done with customized Arduino board.

For experiment performed on 24-well tissue culture plate, cells were seeded at 25,000 cells/well for 18 hours before the treatments. Cells were washed with PBS and replaced with new medium before setting with the microscope to acquire images.

**Image acquisition**

Time-lapse images were acquired using a Nikon Ti-E inverted microscope equipped with integrated Perfect-Focus (PFS), Nikon Plan Apochromat Lambda objective lens, and Evolve® 512 EMCCD camera (Teledyne Photometrics). Time-lapse imaging was performed with an on-stage incubator equipped with temperature control and humidified 5% $CO_2$. Images were taken every 5 minutes for phase, Cy5.5 and mCherry channel and every 20 min for YFP and 30 min for CFP using Nikon NES element software.

**Image analysis and single-cell tracking**

Background correction was performed using ImageJ "rolling ball" background subtraction algorithm with 50-pixel radius. Nuclear segmentation was done using the nuclear marker iRFP reporter and then refined by marker-based watershed and the mask was generated. The phase images were used to generate masks for whole-cell segmentation. The masks were applied to other channels to quantify fluorescent intensity. Single-cell segmentation, tracking and quantification were performed using a custom MATLAB code developed in our lab, as described previously [95, 96].

**Cell cycle phase inference**

From the single-cell time traces, we used nuclear and cell morphology changes as markers to identify each cell division, since HeLa cells become rounded and non-adherent when dividing. For CDK2 activity reporter, within one cell cycle G1, S and G2 were identified based on the intensity and dynamics of nuclear DHB-mCherry. Similarly, for the FUCCI reporter, G1 phase was classified as the phase between the end of cell division and the time the YFP-Cdt1 signal reaches maximum. S phase began as YFP-Cdt1 signal starts to decline until it intersects with mCherry-Gem1 signal. The rest of the cell cycle was considered the G2 phase.

**Viral replication assay**

Cells were pretreated with 100 ng/ml IFN-$\alpha$ for 0, 10 or 24 hours and washed with PBS 3 times followed by 8 hours of normal medium. Cells were infected by adding normal medium containing 2500 plaque forming units (PFU) of vesicular stomatitis virus (VSV), which corresponds to a multiplicity of infection (MOI) of ~0.01. Two hours after infection, medium was replaced again with normal medium. Viral supernatant was collected 18 hours post-infection. Viral titer was quantified by plaque assay on BHK cells.

**Immunoblotting**

Immunoblotting was performed as previously described in detail [60].

**Computational modeling**

***Deterministic model:*** The simplified kinetic model of the gene regulatory network consists of two species, IRF9 and USP18, and they impose positive and negative regulation to gene expression, respectively. The positive regulation by IRF9 is represented by the function $pf$:

$$pf = k_1 \cdot \frac{IRF9}{k_2 + IRF9}$$

and the negative regulation by USP18 is represented by the function $nf$:

$$nf = \frac{k_3}{k_3 + USP18}$$

The expression of IRF9 and USP18 are both regulated by interferon (IFN) input and a combination of these two functions, and are governed by the ordinary differential equations (ODEs) below:

$$\frac{d}{dt} IRF9 = I(t) \cdot (k_4 + pf) \cdot nf$$

$$\frac{d}{dt} USP18 = I(t) \cdot S_u \cdot (k_5 + pf) \cdot nf$$

where I(t) is the IFN input, taking either 0 or 1. $S_u$ is a stepwise function that generates a delay in USP18 upregulation:

$$S_u = \begin{cases} 0, \text{when the IFN input time } < \tau \\ 1, \text{when the IFN input time } \geq \tau \end{cases}$$

where $\tau$ is the delay time of USP18 production.

Because the protein decay observed during the time scale of our experiments was very modest, we considered only protein production, but not decay, to keep our model simple. We used the model to quantitatively analyze the USP18 delay time. To this end, we systematically assigned the value of $\tau$ to be from 1 to 20 hours, while keeping all the other parameters free. We fit the model to the data for each assigned value of $\tau$. The ODEs were solved using custom MATLAB code based on the basic Euler's method with dt=0.001. Fitting was done using MATLAB built-in function, *lsqcurvefit*. The time trace data of $P_{IRF9}$-YFP reporter fluorescence under sustained IFN-$\alpha$ stimulation (Fig. 1C) and the data from pretreatment experiments (Fig. 1F) were used for the fitting. We found that the fitting error (between simulations and data) reaches the minimum when $\tau$ is 8 hours (Fig. 3, B and C). The best-fit parameters are summarized in the Table S4.

We further used the model to predict the responses to repetitive versus sustained IFN inputs. In particular, we simulated the responses to a 5 x 8-hour input and a 40-hour sustained input. We found that the 5 x 8-hour input induced a higher expression of IRF9 than that induced by the 40-hour input, and this difference is USP18-dependent (Fig. 3, D and E). This prediction was validated by experiments, as shown in Fig. 3F.

***Incorporation of cell cycle regulation in the model:*** As described in the main text, based on the experimental results in Figs. 4 and 5, we assumed that USP18 expression can be induced immediately if the IFN input starts within an open window of a cell cycle and the delay time would be 0. However, if the input misses the window, the cell will have to

wait until the open window of the next cell cycle and the delay time will equal to the waiting time. The length of a full cell cycle was estimated to be 21.82 hours based on the data (Fig. S4D). The model was fit to the experimentally-determined distribution of USP18 delay times within a cell cycle (Fig. 6B; the data from Fig. 4E) to obtain an estimate of the open window length as 7.3 hours. The stochastic simulation was performed with the stochastic differential equations:

$$\frac{d}{dt}IRF9 = I(t) \cdot (k_4 + pf) \cdot nf + \xi_{IRF9}$$

$$\frac{d}{dt}USP18 = I(t) \cdot S_u(k_5 + pf) \cdot nf + \xi_{USP18}$$

in which, $\xi_{IRF9}$ and $\xi_{USP18}$ are white noise terms, representing expression noise for the two species. Both of the two terms are Gaussian random variables with a mean of zero and the standard deviations set to be 250 and 1000, respectively. The input onset times of single cells within a cell cycle are random numbers uniformly distributed within a cell cycle between 0 to 21.82 hours. $S_u$ is no longer a deterministic stepwise function with a fixed delay $\tau$, instead it is a stochastic stepwise function, where the delay $\tau$ varies depending on the IFN treatment onset within a cell cycle, as described above. Other parameters are the same as those listed in Table S4. We simulated the single-cell responses of the pretreatment experiments with different input durations. For each pretreatment condition, we performed 400 simulations where each simulation represented a single cell exposed to the IFN inputs. Our simulated results were plotted as scatter plots in Figure 1.22C.

**Table 1.1 Primers used in Chapter 1 study**

| Primer names | Sequence |
|---|---|
| ACTB_gRNA5_F | CACCGGCCGCGCTCGTCGTCGACAA |
| ACTB_gRNA5_R | AAACTTGTCGACGACGAGCGCGGCC |
| ACTB_PAM_F | CGCTCGTCGTTGATAACGGCTCCGGCATGTGCAAG |
| ACTB_PAM_R | GCCGTTATCAACGACGAGCGCGGCGATATCATCATCC |
| STAT1_gRNA1_F | CACCGCCTAGAAACACAGGATGTGA |
| STAT1_gRNA1_R | AAACTCACATCCTGTGTTTCTAGGC |
| STAT1_PAM_F | CTCTGTTGCTTCACATCCTGTGTTTCTAGGGAAATGAAAGAAAGGCC |
| STAT1_PAM_R | GGATGTGAAGCAACAGAGTAGCAGGAGGGAATCACAGATGAGAAGG |
| IRF9_gRNA2_F | CACCGCTCAGCTACTTCCGCCTGCG |
| IRF9_gRNA2_R | AAACCGCAGGCGGAAGTAGCTGAGC |
| IRF9_PAM_F | CCTTGGGACAGAGTATCCCCCGCAGGCGCAAGC |
| IRF9_PAM_R | AATTGCTTGCGCCTGCGGGGGATACTCTGTCCCAAGGGTAC |
| USP18_gRNA3_F | CACCGGCAAATCTGTCAGTCCATCC |
| USP18_gRNA3_R | AAACGGATGGACTGACAGATTTGCC |
| USP18 PAM_F | CATCCTCGCTGAGTCCTCGCAGTCCCCGGC |
| USP18 PAM_R | CTCAGCGAGGATGGACTGACAGATTTGCCTCAGGAGCC |
| shRNA_USP18 | TAAAAAAGGAGAAGCATTGTTTTCAAATCTCTTGAATTTGAAAACAATGCTTCTCCTGGG |
| shRNA_neg | TAAAAACAGTCGCGTTTGCGACTGGTCTCTTGAACCAGTCGCAAACGCGACTGGGG |
| shRNA_SOCS1 | CCGGGCACTTCCGCACATTCCGTTCCTCGAGGAACGGAATGTGCGGAAGTGCTTTTTG |

**Table 1.2 Plasmids constructed in Chapter 1 study**

| Plasmid names | Descriptions |
|---|---|
| NHB0234 | *ACTB*-gRNA5 in pSpCas9(BB)-P2A-Puro |
| NHB0250 | Nuclear marker donor: 1kb_UP-NLS-iRFPx2-P2A-1kb_Down in pUC19 |
| NHB0186 | STAT1 gRNA1 in pSpCas9(BB)-P2A-Puro |
| NHB0235 | STAT1 donor: 1.5kb_Up-mCherry-1.5kb_Down in pUC19 |
| NHB0434 | IRF9 gRNA2 in pSpCas9(BB)-P2A-Puro |
| NHB0443 | IRF9 Donor: 1kb_Up-mCitrine-P2A-1kb_Down in pUC19 |
| NHB0503 | shRNA for USP18 in pSuperRetro-puro |
| NHB0504 | shRNA for negative control in pSuperRetro-puro |
| NHB0616 | shRNA for SOCS1 in pLenti-puro |
| NHB0636 | *USP18* gRNA3 in pSpCas9(BB)-P2A-Puro |
| NHB0647 | 1.5kb_Up-NLS-mCerulean-P2A-1.5kb_Down in pUC19 |
| NHB0670 | DHB-mCherry in pLenti-puro |
| NHB0817 | pCMV-mCherry-Gem1-P2A-mCitrine-Cdt1 in pLenti-puro |

**Table 1.3 Cell lines generated in Chapter 1 study**

| Strain Name | Descriptions |
|---|---|
| NHM003 | HeLa *pACTB-NLS-2iRFP-P2A-ACTB* |
| NHM008 | HeLa *pACTB-NLS-2iRFP-P2A-ACTB, pSTAT1-STAT1-mCherry* |
| NHM025 | HeLa *pACTB-NLS-2iRFP-P2A-ACTB, pSTAT1-STAT1-mCherry, pIRF9-IRF9-P2A-mCitrine* |
| NHM026 | HeLa *pACTB-NLS-2iRFP-P2A-ACTB, pSTAT1-STAT1-mCherry, pIRF9-IRF9-P2A-mCitrine, shRNA USP18* |
| NHM027 | HeLa *pACTB-NLS-2iRFP-P2A-ACTB, pSTAT1-STAT1-mCherry, pIRF9-IRF9-P2A-mCitrine, shRNA USP18 negative control* |
| NHM031 | HeLa *pACTB-NLS-2iRFP-P2A-ACTB, pSTAT1-STAT1-mCherry, pIRF9-IRF9-P2A-mCitrine, shRNA SOCS1* |
| NHM032 | HeLa *pACTB-NLS-2iRFP-P2A-ACTB, pSTAT1-STAT1-mCherry, pIRF9-IRF9-P2A-mCitrine, pUSP18-NLS-mCerulean-USP18* |
| NHM035 | HeLa *pACTB-NLS-2iRFP-P2A-ACTB, pUSP18-NLS-mCerulean-USP18, pCMV-DHB-mCherry* |
| NHM036 | HeLa *pACTB-NLS-2iRFP-P2A-ACTB, pUSP18-NLS-mCerulean-USP18, pCMV-mCh-Gem1-P2A-CFP-Cdt1* |

**Table 1.4 Best-fit parameter values of the mathematical models in Chapter 1**

| | | |
|---|---|---|
| $\tau$ | Delay in USP18 upregulation (hr) | 8 |
| $k_1$ | Positive feedback strength ($hr^{-1}$) | 33.33 |
| $k_2$ | Positive feedback saturation constant | 274.29 |
| $k_3$ | Negative feedback saturation constant | 549.99 |
| $k_4$ | IRF9 production rate ($hr^{-1}$) | 1.89 |
| $k_5$ | USP18 production rate ($hr^{-1}$) | 86.87 |
| $IRF9_0$ | IRF9 basal level (a.u.) | 45 |
| $USP18_0$ | USP18 basal level (a.u.) | 0 |

**Acknowledgements**

We thank Dr. Daniel Kaganovich (University Medical Center Gottingen, Germany) for generously providing the plasmids for NLS-iRFPx2 plasmid and Dr. Sabrina Spencer (University of Colorado Boulder) for the DHB-mVenus plasmid. This work was supported by NIH R01 GM111458 (to N.H.). We also thank the Development and Promotion of Science and Technology Talent project (DPST) and the Royal Thai government for the training scholarship.

Chapter 1, in part, has been submitted to *eLife* for publication as it may appear as Anusorn Mudla, Yanfei Jiang, Kei-ichiro Arimoto, Bingxian Xu, Adarsh Rajesh, Andy Ryan, Wei Wang, Matthew D Daugherty, Dong-Er Zhang and Nan Hao. “Cell cycle-gated feedback control mediates desensitization to interferon stimulation.” *eLife* (2020). The dissertation author is the first author of the paper.

## References


1. Purvis, J.E. and G. Lahav, *Encoding and decoding cellular information through signaling dynamics.* Cell, 2013. **152**(5): p. 945-56.

2. Behar, M. and A. Hoffmann, *Understanding the temporal codes of intra-cellular signals.* Curr Opin Genet Dev, 2010. **20**(6): p. 684-93.

3. Mitchell, A., P. Wei, and W.A. Lim, *Oscillatory stress stimulation uncovers an Achilles' heel of the yeast MAPK signaling network.* Science, 2015. **350**(6266): p. 1379-83.

4. Hersen, P., McClean, M. N., Mahadevan, L., & Ramanathan, S., *Signal processing by the HOG MAP kinase pathway.* Proc Natl Acad Sci U S A, 2008. **105**(20): p. 7165-70.

5. Mettetal, J.T., Muzzey, D., Gomez-Uribe, C., and van-Oudenaarden, A., *The frequency dependence of osmo-adaptation in Saccharomyces cerevisiae.* Science, 2008. **319**(5862): p. 482-4.

6. Hao, N. and E.K. O'Shea, *Signal-dependent dynamics of transcription factor translocation controls gene expression.* Nat Struct Mol Biol, 2012. **19**(1): p. 31-9.

7. Hao, N., Gunawardena, J. and O'Shea, E. K., *Tunable signal processing through modular control of transcription factor translocation.* Science, 2013. **339**(6118): p. 460-4.

8. Hansen, A.S. and E.K. O'Shea, *Promoter decoding of transcription factor dynamics involves a trade-off between noise and control of gene expression.* Mol Syst Biol, 2013. **9**: p. 704.

9. AkhavanAghdam, Z., Sinha, J., Tabbaa, O. P. and Hao, N., *Dynamic control of gene regulatory logic by seemingly redundant transcription factors.* Elife, 2016. **5**.

10. Ashall, L., Horton, C. A., Nelson, D. E., Paszek, P., Harper, C.V., Sillitoe, K., Ryan, S., Spiller, D.G., Unitt, J.F., Broomhead, D.S. and Kell, D.B., *Pulsatile stimulation determines timing and specificity of NF-kappaB-dependent transcription.* Science, 2009. **324**(5924): p. 242-6.

11. Tay, S., Jocob J. H., Lee, T.K., Lipniacki, T., Quake, S.R. and Covert, M.W., *Single-cell NF-kappaB dynamics reveal digital activation and analogue information processing.* Nature, 2010.

12. Nelson, D.E., Ihekwaba, A.E.C., Elliott, M., Johnson, J.R., Gibney, C.A., Foreman B.E., Nelson, G., See, V., Horton, C.A. Spiller, D.G. and Edwards, S.W., *Oscillations in NF-kappaB signaling control the dynamics of gene expression.* Science, 2004. **306**(5696): p. 704-8.

13. Harton, M.D., Woo S.K., Amie D.B., Abhyundai, S. and Batchelor, E., *p53 pulse modulation differentially regulates target gene promoters to regulate cell fate decisions.* Mol Syst Biol, 2019. **15**(9): p. e8685.

14. Purvis, J.E., Karhohs, K.W., Caroline M. Batchelor, E., Loewer, A. and Lahav, G., *p53 dynamics control cell fate.* Science, 2012. **336**(6087): p. 1440-4.

15. Batchelor, E., Loewer, A., Mock, C., and Lahav, G., *Stimulus-dependent dynamics of p53 in single cells.* Mol Syst Biol, 2011. **7**: p. 488.

16. Hsu, C.H., S.J. Altschuler, and L.F. Wu, *Patterns of Early p21 Dynamics Determine Proliferation-Senescence Cell Fate after Chemotherapy.* Cell, 2019. **178**(2): p. 361-373 e12.

17. Reyes, J., Chen, J.Y., Steward-Ornstein, J., Karhohs, K. W., Mock, C.S., and Lahav, G., *Fluctuations in p53 Signaling Allow Escape from Cell-Cycle Arrest.* Mol Cell, 2018. **71**(4): p. 581-591 e5.

18. Yang, H.W., Chung, M. Kudo, T. and Meyer, T., *Competing memories of mitogen and p53 signalling control cell-cycle entry.* Nature, 2017. **549**(7672): p. 404-408.

19. Paek, A.L., Liu, J.C. Loewer, A., Forrester, W.C. and Lahav, G., *Cell-to-Cell Variation in p53 Dynamics Leads to Fractional Killing.* Cell, 2016. **165**(3): p. 631-42.

20. Min, M., Rong, Y., Tian, C. and Spencer, S. L., *Temporal integration of mitogen history in mother cells controls proliferation of daughter cells.* Science, 2020.

21. Schneider, W.M., M.D. Chevillotte, and C.M. Rice, *Interferon-stimulated genes: a complex web of host defenses.* Annu Rev Immunol, 2014. **32**: p. 513-45.

22. Barber, G.N., *Host defense, viruses and apoptosis.* Cell Death Differ, 2001. **8**(2): p. 113-26.

23. Watanabe, T., Sugauchi, F. Tanaka, Y., Matsuura, K., Yatsuhashi, H., Murakami, S., Iijima, S., Iio, E. Sugiyama, M., Shimada, T. and Kakuni, M., *Hepatitis C virus kinetics by administration of pegylated interferon-alpha in human and chimeric mice carrying human hepatocytes with variants of the IL28B gene.* Gut, 2013. **62**(9): p. 1340-6.

24. Medrano, R.F.V., Hunger, A., Mendonca, S.A., Bartuto J.A. and Strauss B.E., *Immunomodulatory and antitumor effects of type I interferons and their application in cancer therapy.* Oncotarget, 2017. **8**(41): p. 71249-71284.

25. Schoggins, J.W. and C.M. Rice, *Interferon-stimulated genes and their antiviral effector functions.* Curr Opin Virol, 2011. **1**(6): p. 519-25.

26. Platanias, L.C., *Mechanisms of type-I- and type-II-interferon-mediated signalling.* Nat Rev Immunol, 2005. **5**(5): p. 375-86.

27. Schreiber, G., *The molecular basis for differential type I interferon signaling.* J Biol Chem, 2017. **292**(18): p. 7285-7294.

28. Choubey, D. and K.D. Moudgil, *Interferons in autoimmune and inflammatory diseases: regulation and roles.* J Interferon Cytokine Res, 2011. **31**(12): p. 857-65.

29. Crow, M.K., *Autoimmunity: Interferon alpha or beta: which is the culprit in autoimmune disease?* Nat Rev Rheumatol, 2016. **12**(8): p. 439-40.

30. McNab, F., Mayer-Barber, K., Sher, A., Wack, A. and O'garra, A., *Type I interferons in infectious disease.* Nat Rev Immunol, 2015. **15**(2): p. 87-103.

31. Cameron, M.J., Bermejo-Martin, J.F., Danesh, A., Muller, M.P. and Kelvin, D.J., *Human immunopathogenesis of severe acute respiratory syndrome (SARS).* Virus Res, 2008. **133**(1): p. 13-9.

32. Carrero, J.A., *Confounding roles for type I interferons during bacterial and viral pathogenesis.* Int Immunol, 2013. **25**(12): p. 663-9.

33. Beltra, J.C. and H. Decaluwe, *Cytokines and persistent viral infections.* Cytokine, 2016. **82**: p. 4-15.

34. Landskron, G., De la Fuente, M., Thuwajit, P., Thuwajit, C. and Hermoso, M.A., *Chronic inflammation and cytokines in the tumor microenvironment.* J Immunol Res, 2014. **2014**: p. 149185.

35. Perry, A.K., Gang, C.H.E.N., Zheng, D., Hong, T.A.N.G. and Cheng, G., *The host type I interferon response to viral and bacterial infections.* Cell Res, 2005. **15**(6): p. 407-22.

36. Abreu, S.L., F.C. Bancroft, and W.E. Stewart, 2nd, *Interferon priming. Effects on interferon messenger RNA.* J Biol Chem, 1979. **254**(10): p. 4114-8.

37. Kuri, T., Zhang, X., Habjan, M., Martinez-Sobrido, L., Garcia-Sastre, A., Yuan, Z. and Weber, F., *Interferon priming enables cells to partially overturn the SARS coronavirus-induced block in innate immune activation.* J Gen Virol, 2009. **90**(Pt 11): p. 2686-2694.

38. Rodriguez-Pla, A., Patel, P., Maecker, H.T., Rossello-Urgell, J., Baldwin, N., Bennett, L., Cantrell, V., Punaro, M., Gotte, A. and Nassi, L., *IFN priming is necessary but not sufficient to turn on a migratory dendritic cell program in lupus monocytes.* J Immunol, 2014. **192**(12): p. 5586-98.

39. Phipps-Yonas, H., Seto, J., Sealfon, S.C., Moran, T.M. and Fernandez-Sesma, A., *Interferon-beta pretreatment of conventional and plasmacytoid human dendritic cells enhances their activation by influenza virus.* PLoS Pathog, 2008. **4**(10): p. e1000193.

40. Scagnolari, C. and G. Antonelli, *Type I interferon and HIV: Subtle balance between antiviral activity, immunopathogenesis and the microbiome.* Cytokine Growth Factor Rev, 2018. **40**: p. 19-31.

41. Sarasin-Filipowicz, M., Wang, X., Yan, M., Duong, F.H., Poli, V., Hilton, D.J., Zhang, D.E. and Heim, M.H., *Alpha interferon induces long-lasting refractoriness of JAK-STAT signaling in the mouse liver through induction of USP18/UBP43.* Mol Cell Biol, 2009. **29**(17): p. 4841-51.

42. Makowska, Z., Duong, F.H., Trincucci, G., Tough, D.F. and Heim, M.H., *Interferon-beta and interferon-lambda signaling is not affected by interferon-induced refractoriness to interferon-alpha in vivo.* Hepatology, 2011. **53**(4): p. 1154-63.

43. Lokugamage, K.H., A.; Schindewolf, C.; Rajsbaum, R.; Menachery, V.D., *SARS-CoV-2 is sensitive to type I interferon pretreatment.* BioRxiv, 2020.

44. Blanco-Melo, D.N.-P., B. E.; Liu, W-C.; Uhl, S.; Hoagland, D.; Møller, R.; Jordan, T. X.; Oishi, K.; Panis, M.; Sachs, D.; Wang. T. T.; Schwartz, R. E.; Lim, J. K.; Albrecht, R. A.; tenOever, B. R., *Imbalanced host response to SARS-CoV-2 drives development of COVID-19.* Cell, 2020.

45. Sallard, E., Lescure, F.X., Yazdanpanah, Y., Mentre, F., Peiffer-Smadja, N., Florence, A.D.E.R. and Bouadma, L., *Type 1 interferons as a potential treatment against COVID-19.* Antiviral Res, 2020. **178**: p. 104791.

46. Czerkies, M., Konwek, Z., Prus, W., Kochanczyk, M., Jaruszewicz-Blonska, J., Tudelska, K., Blonski, S., Kimmel, M., Brasier, A.R. and Lipniacki, T., *Cell fate in antiviral response arises in the crosstalk of IRF, NF-kappaB and JAK/STAT pathways.* Nat Commun, 2018. **9**(1): p. 493.

47. Rand, U., Rinas, M., Schwerk, J., Nohren, G., Linnes, M., Kroger, A., Flossdort, M., Kaly-Kullai, K., Hauser, H., Hofer, T. and Koster, M., *Multi-layered stochasticity and paracrine signal propagation shape the type-I interferon response.* Mol Syst Biol, 2012. **8**: p. 584.

48. Patil, S., Fribourg, M., Ge, Y., Batish, M., Tyagi, S., Hayot, F. and Sealfon, S.C., *Single-cell analysis shows that paracrine signaling by first responder cells shapes the interferon-beta response to viral infection.* Sci Signal, 2015. **8**(363): p. ra16.

49. Miao, H., Hollenbaugh, J.A., Zand, M.S., Holden-Wiltse, J., Mosmann, T.R., Perelson, A.S., Wu, H. and Topham, D.J., *Quantifying the early immune response and adaptive immune response kinetics in mice infected with influenza A virus.* J Virol, 2010. **84**(13): p. 6687-98.

50. Stifter, S.A., Bhattacharyya, N., Sawyer, A.J., Cootes, T.A., Stambas, J., Doyle, S.E., Feigenbaum, L., Paul, W.E., Britton, W.J., Sher, A. and Feng, C.G., *Visualizing the Selectivity and Dynamics of Interferon Signaling In Vivo.* Cell Rep, 2019. **29**(11): p. 3539-3550 e4.

51. Tarhini, A.A., H. Gogas, and J.M. Kirkwood, *IFN-alpha in the treatment of melanoma.* J Immunol, 2012. **189**(8): p. 3789-93.

52. Kolnik, M., L.S. Tsimring, and J. Hasty, *Vacuum-assisted cell loading enables shear-free mammalian microfluidic culture.* Lab Chip, 2012. **12**(22): p. 4732-7.

53. Cheon, H., Holvey-Bates, E.G., Schoggins, J.W., Forster, S., Hertzog, P., Imanaka, N., Rice, C.M., Jackson, M.W., Junk, D.J. and Stark, G.R., *IFNbeta-dependent increases in STAT1, STAT2, and IRF9 mediate resistance to viruses and DNA damage.* EMBO J, 2013. **32**(20): p. 2751-63.

54. Kamada, R., Yang, W., Zhang, Y., Patel, M.C., Yang, Y., Ouda, R., Dey, A., Wakabayashi, Y., Sakaguchi, K., Fujita, T. and Tamura, T., *Interferon stimulation creates chromatin marks and establishes transcriptional memory.* Proc Natl Acad Sci U S A, 2018. **115**(39): p. E9162-E9171.

55. Zou, W., Yang, W., Zhang, Y., Patel, M.C., Yang, Y., Ouda, R., Dey, A., Wakabayashi, Y., Sakaguchi, K., Fujita, T. and Tamura, T., *Microarray analysis reveals that Type I interferon strongly increases the expression of immune-response related genes in Ubp43 (Usp18) deficient macrophages.* Biochem Biophys Res Commun, 2007. **356**(1): p. 193-9.

56. Kim, J.H., J.K. Luo, and D.E. Zhang, *The level of hepatitis B virus replication is not affected by protein ISG15 modification but is reduced by inhibition of UBP43 (USP18) expression.* J Immunol, 2008. **181**(9): p. 6467-72.

57. Ritchie, K.J., Hahn, C.S., Kim, K.I., Yan, M., Rosario, D., Li, L., de la Torre, J.C. and Zhang, D.E., *Role of ISG15 protease UBP43 (USP18) in innate immunity to viral infection.* Nat Med, 2004. **10**(12): p. 1374-8.

58. Malakhova, O.A., Yan, M., Malakhov, M.P., Yuan, Y., Ritchie, K.J., Kim, K.I., Peterson, L.F., Shuai, K. and Zhang, D.E., *Protein ISGylation modulates the JAK-STAT signaling pathway.* Genes Dev, 2003. **17**(4): p. 455-60.

59. Francois-Newton, V., de Freitas Almeida, G.M., Payelle-Brogard, B., Monneron, D., Pichard-Garcia, L., Piehler, J., Pellegrini, S. and Uzé, G., *USP18-based negative feedback control is induced by type I and type III interferons and specifically inactivates interferon alpha response.* PLoS One, 2011. **6**(7): p. e22200.

60. Arimoto, K.I., Löchte, S., Stoner, S.A., Burkart, C., Zhang, Y., Miyauchi, S., Wilmes, S., Fan, J.B., Heinisch, J.J., Li, Z. and Yan, M., *STAT2 is an essential adaptor in USP18-mediated suppression of type I interferon signaling.* Nat Struct Mol Biol, 2017. **24**(3): p. 279-289.

61. Malakhova, O.A., Kim, K., Luo, J.K., Zou, W., Kumar, K.S., Fuchs, S.Y., Shuai, K. and Zhang, D.E., *UBP43 is a novel regulator of interferon signaling independent of its ISG15 isopeptidase activity.* EMBO J, 2006. **25**(11): p. 2358-67.

62. Liau, N.P.D., Laktyushin, A., Lucet, I.S., Murphy, J.M., Yao, S., Whitlock, E., Callaghan, K., Nicola, N.A., Kershaw, N.J. and Babon, J.J., *The molecular basis of JAK/STAT inhibition by SOCS1.* Nat Commun, 2018. **9**(1): p. 1558.

63. Liu, Y., Chen, S., Wang, S., Soares, F., Fischer, M., Meng, F., Du, Z., Lin, C., Meyer, C., DeCaprio, J.A. and Brown, M., *Transcriptional landscape of the human cell cycle.* Proc Natl Acad Sci U S A, 2017. **114**(13): p. 3473-3478.

64. Langan, T.J. and R.C. Chou, *Synchronization of mammalian cell cultures by serum deprivation.* Methods Mol Biol, 2011. **761**: p. 75-83.

65. Keyomarsi, K., Sandoval, L., Band, V. and Pardee, A.B., *Synchronization of tumor and normal cells from G1 to multiple cell cycles by lovastatin.* Cancer Res, 1991. **51**(13): p. 3602-9.

66. Javanmoghadam-Kamrani, S. and K. Keyomarsi, *Synchronization of the cell cycle using lovastatin.* Cell Cycle, 2008. **7**(15): p. 2434-40.

67. Kolodziej, M., Goetz, C., Di Fazio, P., Montalbano, R., Ocker, M., Strik, H. and Quint, K., *Roscovitine has anti-proliferative and pro-apoptotic effects on glioblastoma cell lines: A pilot study.* Oncol Rep, 2015. **34**(3): p. 1549-56.

68. Spencer, S.L., Cappell, S.D., Tsai, F.C., Overton, K.W., Wang, C.L. and Meyer, T., *The proliferation-quiescence decision is controlled by a bifurcation in CDK2 activity at mitotic exit.* Cell, 2013. **155**(2): p. 369-83.

69. Bajar, B.T., Lam, A.J., Badiee, R.K., Oh, Y.H., Chu, J., Zhou, X.X., Kim, N., Kim, B.B., Chung, M., Yablonovitch, A.L. and Cruz, B.F., *Fluorescent indicators for simultaneous reporting of all four cell cycle phases.* Nat Methods, 2016. **13**(12): p. 993-996.

70. Brown, S.E., Fraga, M.F., Weaver, I.C., Berdasco, M. and Szyf, M., *Variations in DNA methylation patterns during the cell cycle of HeLa cells.* Epigenetics, 2007. **2**(1): p. 54-65.

71. Woodcock, D.M., Simmons, D.L., Crowther, P.J., Cooper, I.A., Trainor, K.J. and Morley, A.A., *Delayed DNA methylation is an integral feature of DNA replication in mammalian cells.* Exp Cell Res, 1986. **166**(1): p. 103-12.

72. Desjobert, C., El Mai, M., Gérard-Hirne, T., Guianvarc'h, D., Carrier, A., Pottier, C., Arimondo, P.B. and Riond, J., *Combined analysis of DNA methylation and cell cycle in cancer cells.* Epigenetics, 2015. **10**(1): p. 82-91.

73. Komaki, S., Shiwa, Y., Furukawa, R., Hachiya, T., Ohmomo, H., Otomo, R., Satoh, M., Hitomi, J., Sobue, K., Sasaki, M. and Shimizu, A., *iMETHYL: an integrative database of human DNA methylation, gene expression, and genomic variation.* Hum Genome Var, 2018. **5**: p. 18008.

74. Christman, J.K., *5-Azacytidine and 5-aza-2'-deoxycytidine as inhibitors of DNA methylation: mechanistic studies and their implications for cancer therapy.* Oncogene, 2002. **21**(35): p. 5483-95.

75. Momparler, R.L., *Epigenetic therapy of cancer with 5-aza-2'-deoxycytidine (decitabine).* Semin Oncol, 2005. **32**(5): p. 443-51.

76. Tan, Y., Zhou, G., Wang, X., Chen, W. and Gao, H., *USP18 promotes breast cancer growth by upregulating EGFR and activating the AKT/Skp2 pathway.* Int J Oncol, 2018. **53**(1): p. 371-383.

77. Shin, D.Y., Kang, H.S., Kim, G.Y., Kim, W.J., Yoo, Y.H. and Choi, Y.H., *Decitabine, a DNA methyltransferases inhibitor, induces cell cycle arrest at G2/M phase through p53-independent pathway in human cancer cells.* Biomed Pharmacother, 2013. **67**(4): p. 305-11.

78. Danino, T., Kang, H.S., Kim, G.Y., Kim, W.J., Yoo, Y.H. and Choi, Y.H., *A synchronized quorum of genetic clocks.* Nature, 2010. **463**(7279): p. 326-30.

79. Jiang, Y., AkhavanAghdam, Z., Tsimring, L.S. and Hao, N., *Coupled feedback loops control the stimulus-dependent dynamics of the yeast transcription factor Msn2.* J Biol Chem, 2017. **292**(30): p. 12366-12372.

80. Ori, H., E. Marder, and S. Marom, *Cellular function given parametric variation in the Hodgkin and Huxley model of excitability.* Proc Natl Acad Sci U S A, 2018. **115**(35): p. E8211-E8218.

81. Suel, G.M., Garcia-Ojalvo, J., Liberman, L.M. and Elowitz, M.B., *An excitable gene regulatory circuit induces transient cellular differentiation.* Nature, 2006. **440**(7083): p. 545-50.

82. Monke, G., Cristiano, E., Finzel, A., Friedrich, D., Herzel, H., Falcke, M. and Loewer, A., *Excitability in the p53 network mediates robust signaling with tunable activation thresholds in single cells.* Sci Rep, 2017. **7**: p. 46571.

83. Hoffmann, A., Basak, S., Werner, S.L., Huang, C.S. and Hoffmann, A., *The IkappaB-NF-kappaB signaling module: temporal control and selective gene activation.* Science, 2002. **298**(5596): p. 1241-5.

84. Covert, M.W., Leung, T.H., Gaston, J.E. and Baltimore, D., *Achieving stability of lipopolysaccharide-induced NF-kappaB activation.* Science, 2005. **309**(5742): p. 1854-7.

85. Lemmon, M.A., Freed, D.M., Schlessinger, J. and Kiyatkin, A., *The Dark Side of Cell Signaling: Positive Roles for Negative Regulators.* Cell, 2016. **164**(6): p. 1172-1184.

86. Hansen, A.S. and E.K. O'Shea, *cis Determinants of Promoter Threshold and Activation Timescale.* Cell Rep, 2015. **12**(8): p. 1226-33.

87. Sen, S., Cheng, Z., Sheu, K.M., Chen, Y.H. and Hoffmann, A., *Gene Regulatory Strategies that Decode the Duration of NFkappaB Dynamics Contribute to LPS-versus TNF-Specific Gene Expression.* Cell Syst, 2020. **10**(2): p. 169-182 e5.

88. Killip, M.J., Smith, M., Jackson, D. and Randall, R.E., *Activation of the interferon induction cascade by influenza a viruses requires viral RNA synthesis and nuclear export.* J Virol, 2014. **88**(8): p. 3942-52.

89. Doherty, M.R., Cheon, H., Junk, D.J., Vinayak, S., Varadan, V., Telli, M.L., Ford, J.M., Stark, G.R. and Jackson, M.W., *Interferon-beta represses cancer stem cell properties in triple-negative breast cancer.* Proc Natl Acad Sci U S A, 2017. **114**(52): p. 13792-13797.

90. Frank, T., Tuppi, M., Hugle, M., Dötsch, V., van Wijk, S.J. and Fulda, S., *Cell cycle arrest in mitosis promotes interferon-induced necroptosis.* Cell Death Differ, 2019. **26**(10): p. 2046-2060.

91. Tamiya, T., Kashiwagi, I., Takahashi, R., Yasukawa, H. and Yoshimura, A., *Suppressors of cytokine signaling (SOCS) proteins and JAK/STAT pathways: regulation of T-cell inflammation by SOCS1 and SOCS3.* Arterioscler Thromb Vasc Biol, 2011. **31**(5): p. 980-5.

92. Jeknic, S., T. Kudo, and M.W. Covert, *Techniques for Studying Decoding of Single Cell Dynamics.* Front Immunol, 2019. **10**: p. 755.

93. Ran, F.A., Hsu, P.D., Wright, J., Agarwala, V., Scott, D.A. and Zhang, F., *Genome engineering using the CRISPR-Cas9 system.* Nat Protoc, 2013. **8**(11): p. 2281-2308.

94. Ogrodnik, M., Salmonowicz, H., Brown, R., Turkowska, J., Średniawa, W., Pattabiraman, S., Amen, T., Abraham, A.C., Eichler, N., Lyakhovetsky, R. and Kaganovich, D., *Dynamic JUNQ inclusion bodies are asymmetrically inherited in mammalian cell lines through the asymmetric partitioning of vimentin.* Proc Natl Acad Sci U S A, 2014. **111**(22): p. 8049-54.

95. Li, Y., Roberts, J., AkhavanAghdam, Z. and Hao, N., *Mitogen-activated protein kinase (MAPK) dynamics determine cell fate in the yeast mating response.* J Biol Chem, 2017. **292**(50): p. 20354-20361.

96. Li, Y., Jin, M., O'Laughlin, R., Bittihn, P., Tsimring, L.S., Pillus, L., Hasty, J. and Hao, N. *Multigenerational silencing dynamics control cell aging.* Proc Natl Acad Sci U S A, 2017. **114**(42): p. 11253-11258.

## Chapter 2

## The Systematic Study of Synergy in Interferon Signaling


### Abstract

Interferon is an essential cytokine in innate and adaptive immune response against pathogen infection and tumorigenesis. Its effects are primarily through signal transducer and activator of transcription (STAT) 1. Dysregulation of STAT1 results in multiple diseases including chronic inflammation and cancer. The use of interferon alpha (IFN-$\alpha$) in clinical treatment have been unfortunately not effective due to heterogeneity in patient responses, desensitization and hyperactivity of the immune cells. On the other hand, interferon lambda (IFN-$\lambda$) activity is restricted to epithelial cells and shows no desensitization. Nonetheless, IFN-$\lambda$ signal is relatively weaker and slower than IFN-$\alpha$ signal. We engineered a reporter cell line enabled us to monitor STAT1 and transcription of IRF9 and USP18 using CRISPR/Cas9. We employed time-lapse microscopy, single cell analysis and microfluidics to systemically study the dynamics of STAT1 and expression of downstream genes in response to different types of interferon, both individually and in combination. We discovered that interferon gamma (IFN-$\gamma$) has synergy effect with IFN-$\lambda$ in inducing downstream gene expression. Transient pulses of low concentration of IFN-$\gamma$ was sufficient to maintain the synergistic effect while minimizing its adverse side effects. Recently, urgency in development of treatment for COVID-19 has returned attention to IFN treatment. This discovery could guide the way to develop a new interferon delivery method effectively overcome viral infection.


### Introduction

In 1957 Isaacs and Lindenmann used the term “interferon” (IFN) to describe substances that cells produced during viral infection that interfered with viral replication [1].

IFN are involved in both innate and adaptive immunity acting as inducers, regulators and effectors. Three types of IFN has been discovered named IFN-I, -II and -III. All IFN acts through JAK/STAT pathway to induce expression of antiviral factors and several apoptotic proteins. The activity of IFN is not limited to inhibition of virus but also to combat bacterial and parasitic infection, inhibition of cell migration and cell division, disruption of cell differentiation and critical growth stimulatory factors for immune cells. Therefore, IFN has been clinically used not only for virus related diseases such as HBV, HCV, HIV infection but also for cancer treatment. Over the past decades three types of interferon has been discovered based on sequence homology, their receptors and their unique functions.

Human type I IFN consists of 14 subtypes of IFN-$\alpha$, IFN-$\beta$, IFN-$\varepsilon$, IFN-$\kappa$ and IFN-$\omega$. Multiple IFN-I genes are consequence of gene duplication on chromosome 9. Despite shared homology sequence among different IFN-I isoforms, there are subtle differences in functions. IFN-$\alpha$ and IFN-$\beta$ are major IFN-I produced by almost every cell type during infection [2]; however, only IFN-$\beta$ induces IL-10 and PD-L1 causing immune suppression of T-cells [3]. In addition, IFN-$\beta$ binds stronger to IFNAR1 and therefore less desensitized than IFN-$\alpha$ [4]. IFN-$\varepsilon$ is highly expressed in cervio-vaginal tissues [5] and plays significant roles in mucosal immunity such as vaccinia virus (VV) in lung [6], HIV in macrophage [7] and protects female reproductive tract from viral and bacterial infection [8]. At the same concentrations, IFN-$\omega$ shows higher effectiveness than IFN-$\alpha$ and IFN-$\beta$ against influenza virus [9]. In addition, IFN-$\kappa$ is a critical cytokine secreted by keratinocytes to prevent viral infection such as human papillomavirus (HPV-16 or -31) [10].

IFN-I is rapidly produced in almost all cell types upon viral recognition by extracellular pattern recognition receptor such as toll like receptors (TLRs) and intracellular pattern recognition receptors such as RIG-I and the DNA-sensing receptor cyclic GMP-

AMP synthase (cGAS) [11]. There are three main IFN-I inducing pathways. The first pathway is mediated through RIG-I upon RNA viruses [12]. The second pathway is triggered by activation of TLR3 and TLR4 and recruitment of the adapter protein TRIF [13]. The last pathway is activated by TLR7/8 and TLR9 leading to induction of IRF7 [14]. The major producer of IFN-I is plasmacytoid dendritic cells due to their unique ability to sense extracellular nucleic acid molecule [15]. IFN-I controls the spread of virus and pathogen by three major functions. First, they induced ISGs expression to establish antimicrobial state reducing the number of pathogen replication in the infected and neighboring cells. Second, they recruit and activate innate immune cells to promote antigen presentation and enhance natural killer cell functions. Third, IFN-I activates the adaptive immune system leading to the antibody production and clearance of infection [16].

Binding of IFN-I to the heterodimer receptors, IFNAR1 and IFNAR2, caused conformational changes and subsequent auto-phosphorylation of the receptor tyrosine residues. In addition, the receptors associated kinases, TYK2 and JAK1 respectively. IFN-I also induces phosphorylation and dimerization of STAT1 with STAT3, STAT4, STAT5 and STAT6. Phosphorylated STAT1 and STAT2 dimerize, translocate to the nucleus and bind to IRF9 to form ISGF3 complex. ISGF3 activates transcription of promoters containing an ISRE consensus sequence: TTTCNNTTTC [16].

The role of IFN-I can be beneficial to the host but also be deleterious in multiple diseases. IFN-I plays significant role in chronic inflammatory autoimmune disease such as systemic lupus erythematosus (SLE) [17], multiple sclerosis [18] and rheumatoid arthritis [19]. More importantly, IFN-I plays essential role in over production of cytokines and exuberant activation of immune cells termed cytokine storm. Cytokine storm recently becomes a center of attention because it contributes to deaths in a subset of COVID-19

patients [20]. Nonetheless, SARS-CoV-2 has been shown to be sensitive to IFN-β [21][22] and early administration of IFN-I was effective against SARS-CoV infection [23]. It is clear that the clinical usage of IFN-I has to be cautiously studied and adjusted in individual patients to avoid adverse effects and development of potential alternative is necessary.

IFN-γ is the sole member of IFN-II and the gene is located on chromosome 12. Unlike IFN-I, IFN-γ is produced predominantly by natural killer (NK) cells, macrophage and T-cell [24] but not by epithelial cells. IFN-γ plays various protective immune response against infection and cancer [25]. It is induced by receptor-mediated stimulation or in response to other cytokines such as IL-12, IL-15, IL-18, and IFN-I. The production of IFN-γ is negative regulated by IL-4 and IL-10, TGF-β and glucocorticoids. Binding of IFN-γ dimer to IFNGR1 and IFNGR2 causes JAK1 and JAK2 phosphorylation and recruitment of STAT1 of which is also phosphorylated. Phosphorylated STAT1 homodimer forms a complex termed GAF complex, translocates to the nucleus and binds to GAS consensus sequence: TTCNNNGAA [16]. The downstream gene products include antiproliferative, antiangiogenic and pro-apoptotic factors [26]. Dysfunctional IFN-γ signaling leads to bacterial, parasitic and viral infection such as vaccinia virus, Theriler's murine encephalomyelitis virus, *Leishmania major, Toxoplasma gondii, Listeria monocytogenes* , and several poorly virulent mycobacteria species [25]. In addition to antiproliferative effects, several evidences suggest IFN-γ plays complicated role in cancer progression partly due to alterations of tumor cells to redirect IFN-γ effect toward proliferation such as increase DNA stability after radiation [27]. In addition, IFN-γ induced genes such as PD-1 and CTLA-4 reduce ability of T-cell to mediate tumor cell elimination [28].

The discovery of IFN-III is relative very recent compared to IFN-I and II [29] and the genes are clustered on chromosome 17. IFN-III comprises of 4 members: IFN-λ1 (IL-29),

IFN-λ2 (IL-28A), IFN-λ3 (IL-28B), and IFN-λ4. Polymorphism in two single nucleotide variations (SNPs) identified in the GWAS (rs12979860 and rs8099917) linked to IFN-λ3 differentiates the outcome of HCV treatment [27,28]. IFN-III signals through heterodimeric receptors, IFNLR1 (or IL28Rα) and IL10Rβ. The expression of IFNLR1 is restricted to epithelial and some immune cells such as neutrophils [32]. IFN-III is induced similar to IFN-I but difference in the location of TLR results in different types of IFN produced. TLR4 at the plasma membrane of epithelial barriers induced IFN-III production [33]. Additionally, the cytosolic DNA sensor Ku70 can uniquely induce IFN-III but not IFN-I [34]. IFN-III is the main antiviral response in the gut against enteric viruses such as norovirus, reovirus, rotavirus and enteroviruses [35]. Interestingly, IFN-III induces similar ISGs as IFN-I. It was puzzling at first of why cells would maintain the seemingly redundant antiviral defense pathway. Emerging evidences has suggested that the prevalence expression of IFN-III receptors in epithelial provides first-line defense that is less detrimental than IFN-I counterpart [36]. Accordingly, IFN- λ has become an potential alternative for IFN-α because of their receptor distribution and could become a cure for COVID-19 [37].

Even though, IFN-α and IFN-λ share the common signal transduction pathway, the kinetics and magnitude of ISGs induction are different. A study in Huh-7 cells and primary hepatocytes showed hierarchy in ISG induction as IFN-β > IFN-α > IFN-λ3 > IFN-λ1 > IFN-λ2 [38]. In addition, the effects of IFN-α last shorter than IFN-λ [39]. Several differences have been reported between signaling cascade of type I and III. Although, both IFNs activate TYK2 and JAK1, only IFN-I activate STAT3 in addition to STAT1 and STAT2 at larger extend than IFN-III. In some cases, activated STAT3 negatively affect STAT1 phosphorylation but in other cases STAT3 contributes to the induction of antiviral ISGs [40]. In addition, MAPK inhibitors only affect antiviral response induced by IFN-III but not IFN-I,

suggesting different dependency on MAPK pathway to mount antiviral state [41]. Moreover, the unique slow kinetics of ISGs expression induced by IFN-III is not due to the receptor expression level [42]. Interestingly, a subset of ISGs (e.g. CXCL10, CXCL11, IFIT3, IFI30 and TDRD7) are highly induced by IFN- λ1 than by IFN-β in human vaginal epithelial cells. In addition, upper respiratory tract epithelial cells expressed higher IFN-III than IFN-I upon influenza infection [43]. While the CNS parenchyma only expressed IFN-I as antiviral response [44]. Despite many differences between IFN-I and IFN-III, the main antiviral ISGs such as MX1, viperin, and the IFITM, IFIT, and OAS family members are induced higher by both IFN types. It remains an ongoing investigation of how cell regulate these converging signaling pathways of shared component to produce very striking kinetic differences.

There are several studies reporting synergy between different types of cytokines, yet the mechanisms of the synergy remain elusive. It is essential to mention that STAT1 is involved in many of those synergistic mechanisms. Hernadez and the group showed that IFN-λ acted synergistically with IL-22 to induce ISGs and control rotavirus infection through STAT1 activation [45]. Priming the cells with IFN-γ synergistically enhances the IFN-α stimulation through induction of IRF9, which binds to STAT1 and STAT2 and induces ISRE genes[46]. In addition, combination of IFN-γ synergized with IFN-α and IFN-β to inhibit herpes simplex virus type I (HSV-1) infection [47]. Furthermore, IFN-γ cooperates with TNF-α to induce inflammatory genes via the activation of STAT1α and NF-κB [48] Evidently, combination of IFN-γ and LPS boosted iNOS production confirming the synergy and crosstalk between IFN and NF-κB pathways [49]. In addition, IFN-α had been shown to have synergistic interaction with IFN-λ in A549 human lung epithelial cells to induce several antiviral genes [50]. From these examples, synergy exists among cytokines for cells to fight against infection and STAT1 is the key molecule in the process. To our knowledge, there is

not yet a report on synergy between IFN-γ and IFN-λ and more importantly the molecular mechanism of such interaction is largely unknown. We aim to use single cell quantitative analysis to elucidate the mechanism of the synergy between three types of interferon and suggest a potential clinical application in interferon delivery to patients. The techniques used in this study will pave a new way for studying integrative cytokine interaction in real-time which are adaptable to other signaling pathways and other cell types.

**Results**

**Different types of interferon have different STAT1 activation dynamics**

Nuclear translocation of STAT1 can be used to infer STAT1 activation upon IFN treatment. The kinetics of the translocation is similar to the phosphorylation performed by western blot [51]. Using the STAT1-mCherry reporter cell line, we can monitor the dynamic of STAT1 phosphorylation and STAT1 induction in real-time. We first tested whether different types of interferon stimulation would result in different rates of STAT1 activation. We performed the dose response analysis using different concentrations of IFN-α (type I), IFN-γ (type II) and IFN-λ1 (type III). Interestingly, increase concentration of IFN-α leads to faster STAT1 nuclear translocation and the amplitude of nuclear STAT1 signal with a maximum at 100 ng/ml (Figure 2.1B left). We also observed de-translocation of STAT1 after about 2 hours in concentration higher than 100 ng/ml similar to previous studies using western blot and immune-staining techniques [52]. We therefore conclude that the rate of nuclear translocation of STAT1 upon IFN-I is concentration dependent. Longer experiment (60 hours) with 100 ng/ml showed STAT1 induction which contributes to the increase in nuclear STAT1 signal (Figure 2.1D) suggesting a persistent STAT1 activity. Since the previous traditional phosphorylation measurement showed that the level of STAT1 phosphorylation decreased after 4 hours after stimulation, the nuclear STAT1 level here

best represents STAT1 activity. This is consistent with studies showing that prolonged IFN treatment caused persistent induction of ISG due to activity from unphosphorylated STAT1 [53].

Similar to IFN-I, IFN-γ which is the only member of IFN-II also showed dose-dependent of STAT1 nuclear translocation and reached the maximum rate at 25 ng/ml (Figure 2.1B middle). Higher concentration of IFN-γ did not lead to faster nuclear translocation suggesting a limited receptor level. The concentration lower than 25 ng/ml could also reach the same amplitude of nuclear translocation with much slower kinetic. The time-lapse images showed that STAT1 seems to localize only in the nucleus in the IFN-γ treatment (Figure 2.1C). The longer IFN-γ stimulation showed small increase in STAT1 nuclear signal suggesting weak induction of STAT1 by IFN-γ (Figure 2.1D).

Unexpectedly, we did not observe STAT1 nuclear translocation given any concentrations of IFN-λ1 or even after 60 hours (Figure 2.1B right) of incubation. However, we observed slight increase STAT1 in the cytoplasm (Figure 2.1C) suggesting that there might be an undetectable STAT1 activity that contributed to ISG induction. This unanticipated observation highlights the contrast between IFN-I and IFN-III kinetics despite sharing a common downstream signal transduction pathway.

**STAT2 is the limiting factor in STAT1 nuclear translocation in response to IFN-I**

Based on the amplitude of STAT1 activity in response to IFN-α which was only half of IFN-γ response even with very high IFN-α doses, we asked what could limit the full nuclear translocation. It is possible that this limiting factor might be responsible for low STAT1 activity in the case of IFN-λ stimulation. Because STAT1 forms heterodimer with STAT2 prior to nuclear translocation, we hypothesized that STAT2 could be a potential candidate. To test this, we overexpressed YFP-STAT2 by stably integrated a reporter

construct using lentivirus transduction. We observed that YFP-STAT2 localized mostly in the cytoplasm in the absence of IFN (Figure 2.1E) which is consistent with previous studies performed by immunostaining [54]. As expected, upon IFN-$\alpha$ stimulation STAT2 overexpressed cells showed significant increase in STAT1 nuclear translocation similar to the level observed in WT cells in response to IFN-$\gamma$ (Figure 2.1F). In addition, YFP-STAT2 showed clear nuclear translocation. Noteworthily, even though we performed experiment on monoclonal cells, there was heterogeneity in STAT2 expression which contributed to the level of STAT2 nuclear translocation. That's to say, cells with very high STAT2 expression showed less nuclear translocation than cells with modest expression. This suggests the ratio between STAT1 and STAT2 is well maintained in cells and the level of each protein serves as a limiting factor for the other. In addition, it is very interesting to further study how the ratio affects ISG induction or response to infection.

On the other hand, to our surprise STAT2 overexpression prevented STAT1 nuclear translocation in response to IFN-$\gamma$ (Figure 2.1E). Cells with high STAT2 expression showed no STAT1 nuclear translocation. Yet, cells with lower STAT2 expression still showed weak STAT1 nuclear translocation (Figure 2.1F). This is in accordance with a previous study claiming that STAT2 overexpression prevent STAT1 nuclear translocation but not STAT1 phosphorylation [55]. Similarly, overexpression of STAT2 did not increase STAT1 nuclear translocation in IFN-$\lambda$ treatment and no observable STAT2 nuclear translocation. We suspected that STAT1 and STAT2 nuclear translocation in response to IFN-$\lambda$ was undetectable with our current measurement capacity.

Additionally, we also overexpressed CFP-IRF9 and observed that IRF9 is mainly localized in the nucleus (data not shown). However, unlike YFP-STAT2 we did not observe any differences in term of STAT1 nuclear translocation compared to the WT cells. This

indicate that ISGF3 complex is formed inside the nucleus and IRF9 does not limit the nuclear translocation of STAT1. Moreover, expression of C-terminally tagged STAT2 and IRF9 changes the cellular distribution suggesting a presence of important signaling domain at C-terminus [56].

**Heterogeneity in STAT1 induction caused by IFN-λ treatment**

Taking a closer look at time-lapse images of cells treated with IFN-λ, we observed pronounced heterogeneity in STAT1 expression. There were clusters of cells with significantly higher STAT1 induction (Figure 2.2A). The fact that these cells were presence in isolated groups suggesting this bimodal response originated prior to or early in the stimulation. It is likely that a small number of cells process properties allowing them to become a "responder" while the rest of the cells in the population remains as "none-responder". The quantification of nuclear STAT1 signal show only ~11% of cells with expression higher than no treatment (Figure 2.2C). To further investigate the heterogeneity in IFN-λ response, we need to be able to differentiate STAT1 activation from downstream gene induction. Therefore, we developed a triple-colored reporter cell line to monitor two STAT1 downstream genes. Using CRISPR/Cas9 technology we inserted a yellow fluorescent protein (YFP) under the endogenous promoter of a representative ISG *IRF9* ($P_{IRF9}$), with a translational skip spacer (P2A) between the reporter and the *IRF9* coding region (Figure 2.3A). IRF9 is a positive feedback in IFN pathway. In addition, we inserted a cyan fluorescent protein (CFP) with a nuclear localization signal (NLS) under the endogenous *USP18* promoter ($P_{USP18}$) with a P2A spacer between the reporter and the *USP18* coding region (Figure 2.3A). USP18 is a negative feedback in IFN signaling pathway.

We first repeated the IFN-λ dose response experiment. Interestingly, unlike STAT1-mCherry reporter, IRF9 induction showed dose dependent when the concentration was lower than 25 ng/ml. However, the higher concentrations showed similar induction level implying a saturation in the number of cell surface receptors (Figure 2.3B left). We decided to use 100 ng/ml as in further experiments. Even more surprising, unlike IFN-α, IFN-λ barely induced USP18 (Figure 2.3B right). The single cells distribution of nuclear STAT1 signal showed "responder" subpopulation of which had STAT1 activation similar to IFN-α and IFN-γ treated cells while majority showed no STAT1 activation (Figure 2.3C left). Additionally, IFN-λ induced IRF9 better than IFN-γ but less than IFN-α (Figure 2.3C middle). Lastly, it was clear that only subpopulation of cells expresses USP18 upon IFN-λ stimulation and the average induction was much less than in the IFN-α treated cells (Figure 2.3C right).

A more careful analysis of the "responder" population showed that these cells had higher induction of STAT1, IRF9 and USP18 (Figure 2.4A and B). Time lapse images showed that these cells emerged early after IFN-λ stimulation and the kinetics of gene induction were distinct from the "none responder" cells (Figure 2.4C and D). Noticeably, these cells showed delayed USP18 induction compared to IRF9 similar to IFN-α stimulation (Figure 2.4 D). In conclusion, based on our triple colored reporter we found that although IFN-γ had high STAT1 activation but showed no IRF9 and USP18 induction. IFN-α showed strong STAT1 activation and IRF9 induction but came with the high USP18 induction trade-off. Uniquely, for IFN-λ, despite low STAT1 activation, it moderately induced IRF9 but not USP18.

**The synergy between interferon-λ and interferon-γ**

The effectiveness of IFN-α in therapy is limited because of adverse hyperreactivity of immune cells and desensitization due to USP18 induction. Since IFN-λ also induce

similar ISG but weaker amplitude and slower kinetics possibly due to weak STAT1 activation, we asked whether combination with IFN-γ can enhance its activity. Indeed, combination of IFN-λ and IFN-γ significantly increased STAT1 nuclear translocation implying stronger STAT1 activation (Figure 2.5B left). Moreover, IRF9 induction was significantly higher than IFN-λ or IFN-γ alone or the sum of the two IFNs (Figure 2.5B middle). Therefore, we concluded that there was a synergy between IFN-I and IFN-III.

**Differential gene expression between IFN-I and IFN-III**

It is generally accepted that ISG induction is similar between IFN- I and IFN-III [57]. However, recent reports support our observation that there is differential gene expression between these two pathways [58] especially USP18 expression. To confirm our observation, we knock-downed USP18 by stably integrated shRNA in the dual colored reporter cells. We found that USP18-KD showed significant increase in STAT1 nuclear translocation both upon IFN-α and IFN-α + IFN-γ (Figure 2.5 D). This confirms the upregulation of this negative feedback in IFN-I pathway. On the other hand, there was no significant difference between WT and USP18-KD cells in response to IFN-λ or IFN-λ + IFN-γ. We concluded that IFN-I and IFN-III had differential downstream gene expression. We suspected that the different kinetics might be responsible for this disparity. More comprehensive studies are necessary to identify sets of genes activated by different pathway.

**STAT1 activation is responsible for the synergy effect between IFN-II and IFN-III**

Since IFN-λ showed very weak STAT1 activation but IFN-γ showed very strong STAT1 activation, we hypothesized that IFN-γ supplied activated STAT1 for IFN-λ pathway. Because STAT1 activation by IFN-γ is rapid, a short pulse of IFN-γ should be sufficient to create synergy. To test the hypothesis, we used microfluidic device to generate short pulses

of IFN-γ while maintaining the constant flow of IFN-λ. As expected, we observed similar level of IRF9 expression to the sustained stimulation of both IFNs (Figure 2.6A). The time lapse images showed transient STAT1 nuclear translocation caused by IFN-γ and gradual increase in STAT1 and IRF9 expression (Figure 2.6B). However, we performed this experiment on the dual reporter cell line; therefore, we were unable to observe USP18 expression. We expect USP18 level to be lower in the IFN-γ pulses experiment than the sustained because USP18 induction is duration and amplitude dependent.

**Development of synthetic IFN-γ production system to mimic the synergy in vivo**

The main IFN-γ in vivo are natural killer (NK) cells, T-cells and macrophages. To study how epithelial cells respond to IFN-γ produced by these cells, ones need to co-culture them or study them *in vivo*. To simplify the complication of cell culture and multiple cytokines, other than IFN-γ, secreted by the immune cells, we attempted to develop IFN-γ producer cells of which the level of IFN-γ can be tuned. To do this, we integrated a Tet-ON reporter construct in the dual reporter cells (Figure 2.6C). Upon doxycycline addition, the transcription of human IFN-γ will occur along with P2A-nls-CFP which serves as a marker for identifying the producer cells and inferring amount of IFN-γ produced. The initial test showed that the level of IFN-γ and STAT1 activity can be tuned with doses of doxycycline (Figure 2.6C right). In addition, doxycycline could create the synergy effect with IFN-λ as seen with exogenous IFN-γ treatment (Figure 2.6D). Ultimately, we aim to culture the "producer" cells with the "none-producer" cells at different ratio to mimic the in vivo system. This system will allow us to study not only the synergy between two types of IFN but also how the cytokine signal is spread and contained during infection.

## Discussion

IFN pathway is a crucial primary response against virus infection. As the COVID-19 pandemic is threatening health of millions and vastly damaging the world economy, it is clear that understanding how cells regulate IFN pathway is as essential to understanding how virus infect cells. Recent studies suggest the low ISG induction due to dysregulation of IFN-I and IFN-III pathway allows SARS-CoV-2 to replicate stealthily in lung epithelial cells [59]. This insufficient innate immune response coupled with high production of pro-inflammatory cytokines such as IL-6 and chemokines such as CXCLs lead to hyperactivation of immune cells and increase mortality rate in COVID-19 patients [60]. In addition, IFN-I and IFN-III showed promising therapeutic results in number of cases [61,62]. Despite increasing evidences of IFN role in COVID-19, more studies are needed to better understand the timing of administration and how ISG kinetics contribute to success and failure in therapy. This study illustrates unique characteristics and interaction between different type of IFNs. We discovered that IFN-$\gamma$ can synergistically enhance IFN-$\lambda$ while minimize the induction of a negative feedback molecule such as USP18.

IFN-I and IFN-III, even though using different receptors, signal through an identical downstream signaling molecules. Heterodimerization between STAT1 and STAT2 allows nuclear translocation. In the absence of IFN, STAT1 and STAT2 can shuttle between nucleus and cytoplasm [63]. Upon IFN treatment, phosphorylated STAT1 and STAT2 rapidly translocate to the nucleus. However, we observed incomplete nuclear translocation of STAT1. On the other hand, IFN-$\gamma$ stimulation lead to homodimerization of STAT1 and complete nuclear translocation. It is unclear how cells differentiate the dimer formation from the homodimer of phosphorylated STAT1 upon IFN-I stimulation. Nonetheless, we showed that incomplete STAT1 nuclear translocation was caused by lack of sufficient STAT2

partner. Overexpression of STAT2 allowed complete STAT1 nuclear translocation but in turn caused incomplete STAT2 nuclear translocation (Figure 2.1E). It suggests that cells control the strength of IFN-I response via the amount of STAT2 expression. STAT2 acts as a limiting factor in the pathway while acts as an inhibitor in the other pathway. This regulation is vulnerable to zika virus infection because it targets STAT2 for degradation and therefore is able to shut down IFN-I response [64]. Yet, it remains unclear how IFN-λ induced ISG in the absence of detectable STAT1 and STAT2 nuclear translocation. We believe that IFN-λ only weakly activates STAT1 and STAT2, a level that is indistinguishable with our measurement method.

Despite the general weak response to IFN-λ stimulation, a subset of cells showed strong ISG expression. These small percentage of cells emerged early in the treatment and subsequent daughter cells remained “responder” cells. The fact that these cells did not showed strong STAT1 nuclear translocation prompted us to speculate that the ISG promoters in these cells reside in special epigenetic state such as less DNA methylated or highly histone acetylated. This is supported by a study in intestinal epithelial cells which also showed heterogenous response to type III due to cell polarization [65]. To test this possibility, we will treat cells with methyltransferase inhibitor (decitabine) or histone deacetylase inhibitor (valproic acid) and observed changes in ratio of “responders” and “non-responders”. Alternatively, it is possible that these cells express higher level of IFNLR1. To test this possibility, we will perform immunostaining for IFNLR1. In addition, we will sort out these responders and track how sensitivity to IFN-λ change over subsequent culture in order to investigate whether the changes are transient or permanent.

The specificity in IFNLR1 expression limit the response of IFN-λ to epithelial cells. This grants huge advantages over the use of IFN-λ over IFN-α in therapy because it

significantly lowers the risk of cytokine storm caused by overreaction of immune cells to IFN [66]. However, IFN-λ induces weaker ISG expression. In this study we showed that we can enhance IFN-λ activity by increase STAT1 phosphorylation. More importantly, short pulses of IFN-γ is sufficient to create synergy. In addition, the combination of IFN-λ and IFN-γ only slightly induce USP18 expression; therefore, did not cause desensitization. Future experiments need to be performed to characterize more complete sets of genes differentially induced by IFN-α, IFN-λ and IFN-λ+IFN-γ. Our discovery can be applied to develop novel method in IFN-λ delivery in viral infected patients or cancer treatment.

During virus infection cells need to restrain the spread of virus by rapidly upregulate antiviral proteins. However, some of these proteins led to apoptosis and hinder cell growth. Therefore, the response needs to be local to ensure survival of non-infected cells especially in multicellular organisms. In addition to understanding how IFN signaling is regulated within a single cell, we aim to study how IFN secreted by different cells contributed to antiviral response. The synthetic IFN-γ secretion system, we developed, is a proof-of-concept *in vitro* model for researchers to dissect complex interaction of multiple cytokines in a simplified and adjustable set-up. We intended to mimic the interactions between epithelial cells and resident IFN-γ producing cells, such as macrophage and NK cells. It is likely that distribution of these resident immune cells limits the synergy effect within an area of infection and therefore restricts anti-infection response.

Finally, the urgency in understanding basic biology of host innate immune response against SARS-CoV-2 places IFN pathway into the focus of attention. This study provides evidence to support the use of IFN-λ in treatment of COVID-19. The methods used in this study can be easily apply to other signaling pathways to obtain deeper insight on

heterogeneity and temporal responses. Further studies in animal models is needed to validate the proposed strategies and direct clinical application.

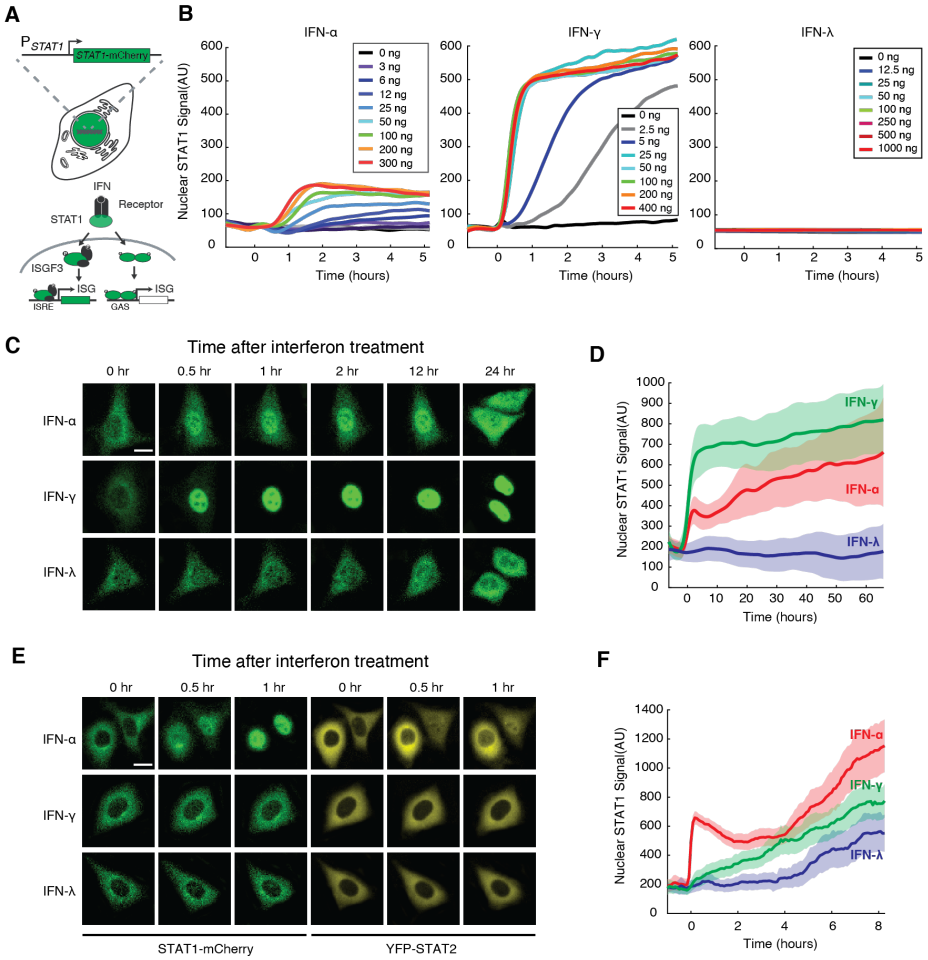


**Figure 2.1 Different types of IFN induce different STAT1 nuclear translocation dynamics.** (A) Schematic of HeLa reporter cell line engineered using CRISPR/Cas9 (top). *STAT1* was tagged with mCherry at C-terminus to monitor the translocation and expression. A simplified diagram of the IFN pathway components that can be monitored using the reporter cell line. Binding of IFN leads to homodimer or heterodimer of STAT1 of which activate different sets of downstream genes. (B) STAT1 nuclear translocation in response to doses of IFN-α, IFN-γ and IFN-λ focusing on the first 6 hours of the stimulation. The stimuli were added at time = 0 hr. Nuclear STAT1 signal was quantified in single cells and the average was shown. (C) Representative time-lapse images of cells showing STAT1 nuclear translocation and STAT1 expression in response to IFN treatment during the first 24 hours. Scale bar is 20μm. (D) Averaged time traces of nuclear STAT1-mCherry. Data are represented as the mean (solid lines) and ± standard deviation (SD) (shaded areas). (E) Representative time-lapse images of cells showing STAT1 nuclear translocation in overexpressed YFP-STAT2 cells in response to IFN treatment. Scale bar is 20μm. (F) Averaged time traces of nuclear STAT1-mCherry fluorescence of experiment shown in (E). Data are represented as the mean (solid lines) and ± standard deviation (shaded areas).

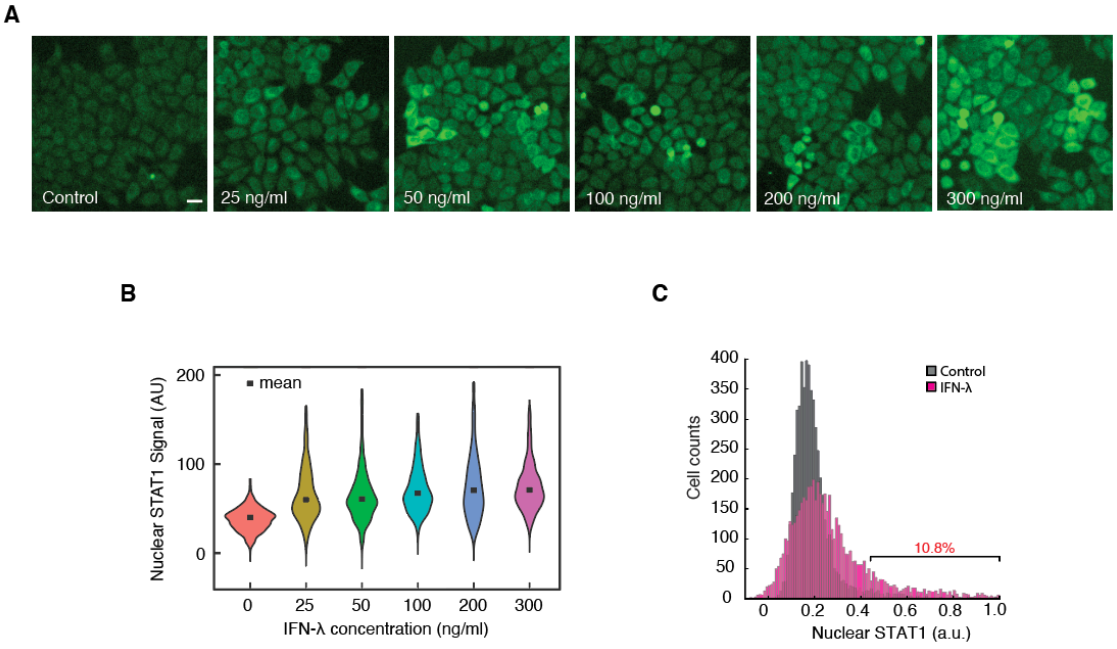


**Figure 2.2 Heterogeneity in STAT1 expression induced by IFN-λ treatment.**
(A) STAT1 expression in cells after treated with different concentrations of IFN-λ for 48 hours. The images show only representative subpopulation of the cells with high STAT1-mCherry expression. (B) Violin plots showing the distribution of STAT1 expression quantified from the full view images shown in (A). (C) Distributions of nuclear STAT1-mCherry fluorescence in single cells without (control) and with 100 ng/ml IFN-λ treatment.

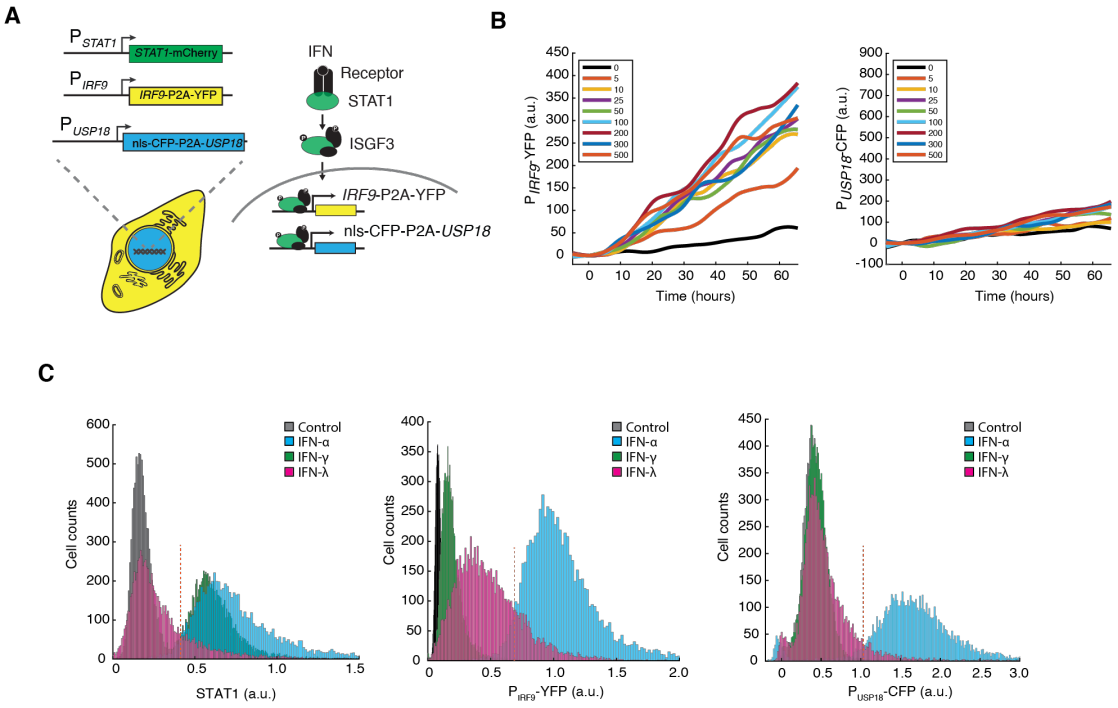


**Figure 2.3 Different type of IFN induced differential downstream gene expression.** (A) Schematic of the triple colored reporter cell line. A coding sequence for P2A-YFP was inserted endogenously into C-terminus of *IRF9* coding sequence. A coding sequence for NLS-CFP-P2A was inserted endogenously into the N-terminus of *USP18* coding sequence of the previous cell line. (B) Average time traces of $P_{IRF9}$-YFP and $P_{USP18}$-CFP quantified from single cells in response to different doses of IFN-λ. (C) Distributions of STAT1-mCherry, $P_{IRF9}$-YFP and $P_{USP18}$-CFP fluorescence in response to no stimuli, 100 ng/ml IFN-α, 25 ng/ml IFN-γ and 100 ng/ml IFN-λ (n = 9241, 7468, 10153 and 9347 cells respectively). The red dashed lines indicate the threshold of cells considered as "responder" cells.

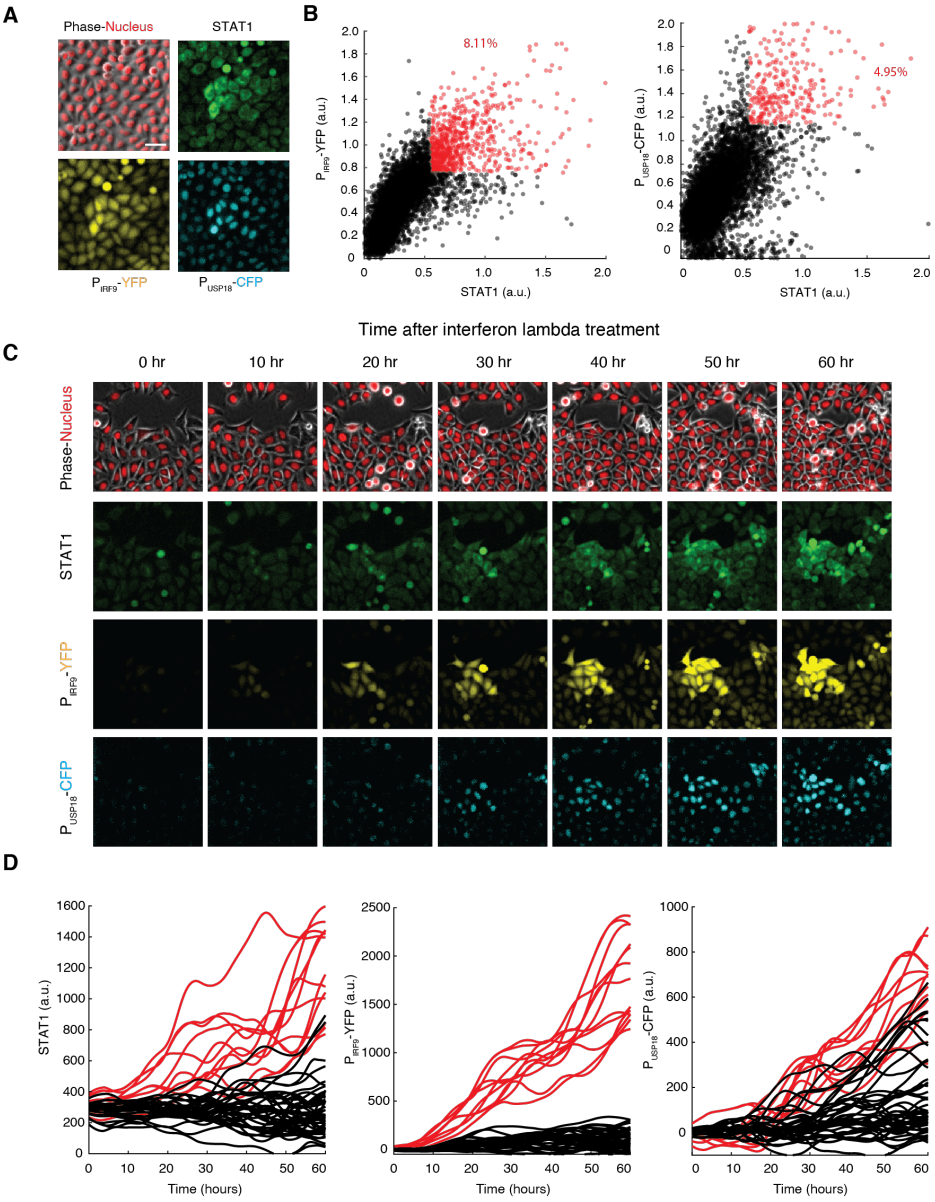


**Figure 2.4 IFN-λ induces strong ISG expression in a subset of population.**
(A) Representative images of a subpopulation of cells with strong IFN-λ response. Cells were treated with 100 ng/ml IFN-λ for 48 hours. (B) Scatterplots showing expression of nuclear STAT1-mCherry, $P_{IRF9}$-YFP and $P_{USP18}$-CFP fluorescence in single cells. The fluorescent signals were normalized to the expression of the nuclear marker. The red data points represent cells with the expression level of both reporters higher than the mean + standard deviation. (C) Time lapse images illustrating the emergence of "responder" cells. Cells were treatment with 100 ng/ml IFN-λ and a subset of the full view image was cropped and analyzed. (D) Time traces of STAT1-mCherry, $P_{IRF9}$-YFP and $P_{USP18}$-CFP fluorescence in single cells from images shown in (C). The red lines indicate cells with strong response classified from the final $P_{IRF9}$-YFP > 500 a.u.

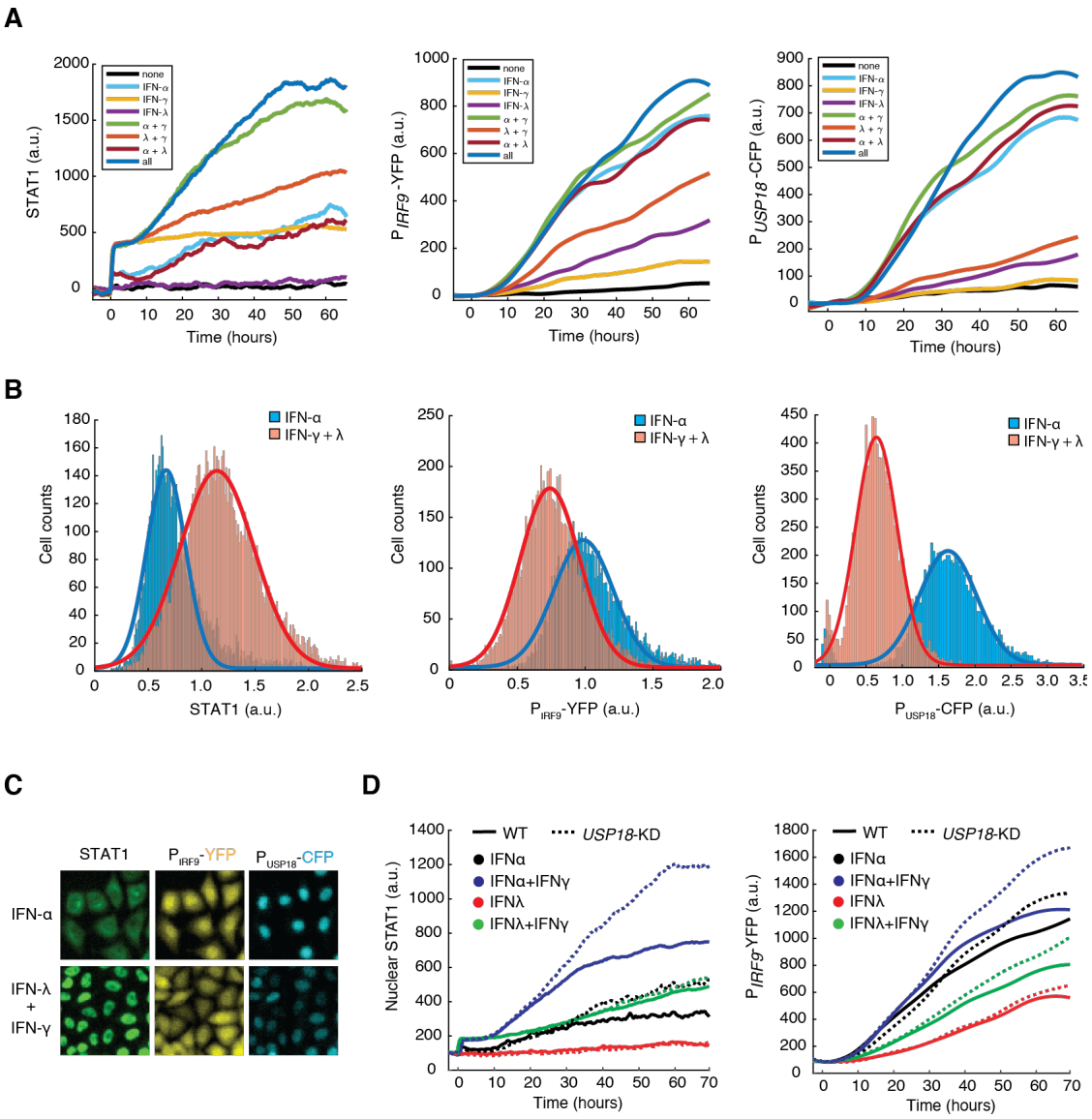


**Figure 2.5 The synergy between IFN-II and IFN-III.** (A) Average time traces of nuclear STAT1-mCherry, $P_{IRF9}$-YFP and $P_{USP18}$-CFP in response to different types of IFN and combination of IFNs. The concentrations of IFN-α, -γ and -λ are 100, 25 and 100 ng/ml respectively. (B) Distributions of nuclear STAT1-mCherry, $P_{IRF9}$-YFP and $P_{USP18}$-CFP fluorescence comparing response to the combination of IFN-γλ to IFN-α. Cells are treated for 72 hours and the images were taken and quantified in single cells. The signals were normalized to nuclear marker signal. Solid lines were fitted as "Gaussian" distribution model. (C) Representative images showing the difference between response to IFN-α and IFN-γλ. (D) Average time traces of nuclear STAT1-mCherry and $P_{IRF9}$-YFP fluorescence in WT cells (solid lines) and USP18-KD cells (dashed lines).

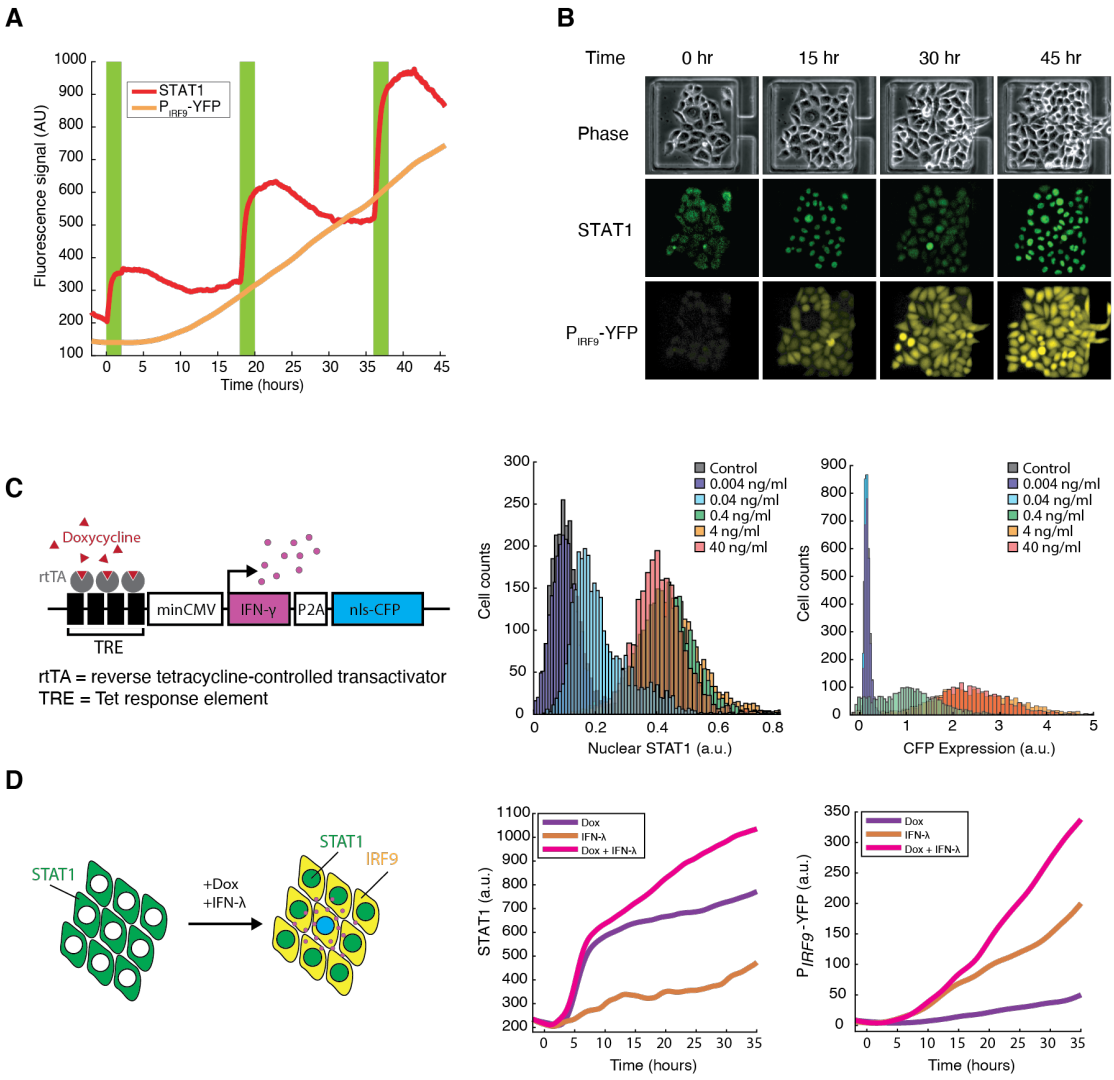


**Figure 2.6: A short pulse of IFN-γ is sufficient to maintain the synergy.**
(A) Average time traces of nuclear STAT1-mCherry and $P_{IRF9}$-YFP fluorescence of cells in microfluidics treated with 2 hour-pulse of 25 ng/ml IFN-γ (green strips) in the presence of sustained 100 ng/ml IFN-λ. (B) Representative time lapse images of cells in one chamber of a microfluidic device in the experiment showed in (A). (C) Schematics of tetracycline-inducible IFN-γ reporter construct. A coding sequence of human *IFN-γ* gene was inserted after a minimum CMV promoter followed by P2A-nls-CFP. Upon addition of doxycycline, rtTA can bind to TREs led to expression and secretion of IFN-γ of which can be inferred from nuclear CFP level. Distributions of nuclear STAT1-mCherry and nuclear CFP fluorescence in response to different doses of doxycycline. (D) Left: schematic showing how doxycycline induces IFN-γ production from the producer cell (blue) causing STAT1 nuclear translocation and the synergy effect seen in IRF9 induction. Right: the average time traces of STAT1-mCherry and $P_{IRF9}$-YFP fluorescence in Tet-inducible reporter cells.

## Materials and Methods

### Cell cultures and Cell line construction

Hela cells were grown in DMEM medium supplemented with 2 mM L-glutamine, 5% fetal bovine serum and 1% penicillin-streptomycin in 5% $CO_2$ in air atmosphere at 37°C. Trypsin-EDTA solution was used for sub-culturing. For time-lapse microscopy, DMEM medium without phenol-red was used to reduce auto-fluorescent background. The sustained interferon signal experiments were performed in 24-well plate. In those cases, the cells were seeded at 5,000 cells/well for 24 hours and fresh medium was replaced before setting the plate with a microscope. We used a microfluidic device to generate pulses of IFN signal. To set up the microfluidic experiment, cells were loaded as described previously [67] and placed in an incubator for 24 hours to allow the cells to adhere. During the experiment the medium was flowed at 1ml/hour.

To generate the nuclear marker cell line, we used CRISPR technique [68] to endogenously insert nuclear localization signal (NLS) sequence followed by 2 copies of infrared fluorescent protein (2iRFP) and a translational skipping sequence (P2A) after actin-β (ACTB) promoter. The cells were screened with antibiotic and sorted by FACS and selected for monoclonal cells. We then performed PCR and sequencing to confirm the correct insertion and integration. The correct clone was then used to generate C-terminus tagged STAT1-mCherry cell line using CRISPR technique[54][69]. The clones were screened in similar manner as the nuclear marker cell line and the correct homozygous clone was used to generate the IRF9-P2A-YFP cell line (named dual colored reporter). Finally, we generated NLS-CFP-P2A-USP18 cell line (named triple colored reporter).

Lentivirus was used to integrate pCMV-YFP-STAT2 reporter construct into the STAT1-mCherry cell line. Cells were screened with puromycin for 5 days and sorted with

FACS for monoclonal cells. The final clone was validated with PCR and sequencing. Similarly, Tet-inducible IFN-γ construct was stably integrated into dual reporter cell line, screened and validated for a single monoclonal and homogenous clone.

The knockdown of *USP18* by shRNA was done using retrovirus transduction. We screened the transfected cells with 1 μg/ml puromycin for 5 days and confirmed the presence of the construct in the cells with PCR and confirmed the knock-down of USP18 with western blotting.

**Chemicals**

The *E. coli*-derived recombinant human IFN-α-1a was obtained from Prospec (CAT# cyt-520). The *E. coli*-derived recombinant human IFN-γ was obtained from R&D Systems (CAT# 285-IF-100). The mouse myeloma cell line, NS0-derived recombinant human IL-29/IFN-λ1 was obtained from R&D Systems (CAT# 1598-IL-025). Throughout this study, type I IFN refers to IFN-α, type II IFN refers to IFN-γ and type III IFN refers to IFN-λ1.

**Time-lapse microscopy**

The time-lapse imaging experiments were performed using a Nikon Ti-E inverted fluorescent microscope with Perfect Focus, coupled with an EMCCD camera (Evolve, Photometrics). The light source is a SOLA system from Lumencor. Images were taken with 10X and 20X objective. During the experiment, the plate or the microfluidic device was taped to a customized holder and placed on the motorized stage of the microscope. For the plate experiment, one position in the middle of the well was chosen while 11 positions were chosen in one microfluidic device. The microscope was programed by NLS Element to acquire phase, cy5.5 and mCherry every 5 min, YFP every 20 min and CFP every 30 min. During the experiments, the cells were maintained in 5% $CO_2$ at 37°C using customized environmental chamber.

**Image Analysis and single-cell tracking**

Background correction was performed using ImageJ “rolling ball” background subtraction algorithm with 50-pixel radius. The images were processed using a custom MATLAB code for single-cell tracking and fluorescence quantification. The nuclear marker (iRFP signal) was used for nuclear segmentation and the phase image was used for cytoplasm segmentation. The single cell trajectories were analyzed, and we performed cell selection to remove incorrect tracking trajectories based on the nuclear size traces. The code was described in detail previously [70,71]

**Table 2.1 Primers used in Chapter 2**

| Primer names | Sequence |
|---|---|
| ACTB_gRNA5_F | CACCGGCCGCGCTCGTCGTCGACAA |
| ACTB_gRNA5_R | AAACTTGTCGACGACGAGCGCGGCC |
| ACTB_PAM_F | CGCTCGTCGTTGATAACGGCTCCGGCATGTGCAAG |
| ACTB_PAM_R | GCCGTTATCAACGACGAGCGCGGCGATATCATCATCC |
| STAT1_gRNA1_F | CACCGCCTAGAAACACAGGATGTGA |
| STAT1_gRNA1_R | AAACTCACATCCTGTGTTTCTAGGC |
| STAT1_PAM_F | CTCTGTTGCTTCACATCCTGTGTTTCTAGGGAAATGAAAGAAAG GCC |
| STAT1_PAM_R | GGATGTGAAGCAACAGAGTAGCAGGAGGGAATCACAGATGAG AAGG |
| IRF9_gRNA2_F | CACCGCTCAGCTACTTCCGCCTGCG |
| IRF9_gRNA2_R | AAACCGCAGGCGGAAGTAGCTGAGC |
| IRF9_PAM_F | CCTTGGGACAGAGTATCCCCCGCAGGCGCAAGC |
| IRF9_PAM_R | AATTGCTTGCGCCTGCGGGGGATACTCTGTCCCAAGGGTAC |
| USP18_gRNA3_F | CACCGGCAAATCTGTCAGTCCATCC |
| USP18_gRNA3_R | AAACGGATGGACTGACAGATTTGCC |
| USP18 PAM_F | CATCCTCGCTGAGTCCTCGCAGTCCCCGGC |
| USP18 PAM_R | CTCAGCGAGGATGGACTGACAGATTTGCCTCAGGAGCC |
| shRNA_USP18 | TAAAAAAGGAGAAGCATTGTTTTCAAATCTCTTGAATTTGAAAA CAATGCTTCTCCTGGG |
| shRNA_neg | TAAAAACAGTCGCGTTTGCGACTGGTCTCTTGAACCAGTCGCA AACGCGACTGGGG |
| BsrGI-STAT2_F | AAAATGTACATGGCGCAGTGGGAAATG |
| NotI-STAT2_R | TTTTGCGGCCGCCTAGAAGTCAGAAGGCATCAAGG |
| BsrGI-IRF9_F | AAAATGTACATGGCATCAGGCAGGGC |
| NotI-IRF9_R | TTTTGCGGCCGCCTACACCAGGGACAGAATGG |
| NheI-hIFNg_F | TTTTGCTAGCATGAAATATACAAGTTATATCTTGGCTTTTCAG |
| SalI-hIFNg_R | TTTTGTCGACTTACTGGGATGCTCTTCGACC |

**Table 2.2 Plasmids constructed in Chapter 2**

| Plasmid names | Descriptions |
|---|---|
| NHB0234 | *ACTB*-gRNA5 in pSpCas9(BB)-P2A-Puro |
| NHB0250 | Nuclear marker donor: 1kb_UP-NLS-iRFPx2-P2A-1kb_Down in pUC19 |
| NHB0186 | STAT1 gRNA1 in pSpCas9(BB)-P2A-Puro |
| NHB0235 | STAT1 donor: 1.5kb_Up-mCherry-1.5kb_Down in pUC19 |
| NHB0434 | IRF9 gRNA2 in pSpCas9(BB)-P2A-Puro |
| NHB0443 | IRF9 Donor: 1kb_Up-mCitrine-P2A-1kb_Down in pUC19 |
| NHB0503 | shRNA for USP18 in pSuperRetro-puro |
| NHB0504 | shRNA for negative control in pSuperRetro-puro |
| NHB0636 | *USP18* gRNA3 in pSpCas9(BB)-P2A-Puro |
| NHB0647 | 1.5kb_Up-NLS-mCerulean-P2A-1.5kb_Down in pUC19 |
| NHB0808 | pCMV-YFP-STAT2 |
| NHB0701 | pCMV-STAT2-YFP |
| NHB0717 | pCMV-CFP-IRF9 |
| NHB0710 | pCMV-IRF9-CFP |
| NHB0664 | TRE-minCMV-IFNg-P2A-NLS-CFP-dDomain |

**Table 2.3 Cell lines generated in Chapter 2**

| Strain Name | Descriptions |
|---|---|
| NHM003 | HeLa *pACTB-NLS-2iRFP-P2A-ACTB* |
| NHM008 | HeLa *pACTB-NLS-2iRFP-P2A-ACTB, pSTAT1-STAT1-mCherry* |
| NHM025 | HeLa *pACTB-NLS-2iRFP-P2A-ACTB, pSTAT1-STAT1-mCherry, pIRF9-IRF9-P2A-mCitrine* |
| NHM026 | HeLa *pACTB-NLS-2iRFP-P2A-ACTB, pSTAT1-STAT1-mCherry, pIRF9-IRF9-P2A-mCitrine, shRNA USP18* |
| NHM027 | HeLa *pACTB-NLS-2iRFP-P2A-ACTB, pSTAT1-STAT1-mCherry, pIRF9-IRF9-P2A-mCitrine, shRNA USP18 negative control* |
| NHM032 | HeLa *pACTB-NLS-2iRFP-P2A-ACTB, pSTAT1-STAT1-mCherry, pIRF9-IRF9-P2A-mCitrine, pUSP18-NLS-mCerulean-USP18* |
| NHM046 | HeLa *pACTB-NLS-2iRFP-P2A-ACTB, pSTAT1-STAT1-mCherry, pIRF9-IRF9-P2A-mCitrine, TRE-minCMV*-P2A-NLS-*mCerulean*-dDomain |

**References:**


[1] A. Isaacs and J. Lindermann, “Virus interference. I. The interferon,” *Proc. R. Soc. London. Ser. B - Biol. Sci.*, 1957.

[2] A. Murira and A. Lamarre, “Type-I interferon responses: From friend to foe in the battle against chronic viral infection,” *Frontiers in Immunology*. 2016.

[3] D. G. Brooks, S. J. Ha, H. Elsaesser, A. H. Sharpe, G. J. Freeman, and M. B. A. Oldstone, “IL-10 and PD-L1 operate through distinct pathways to suppress T-cell activity during persistent viral infection,” *Proc. Natl. Acad. Sci. U. S. A.*, 2008.

[4] G. Schreiber, “The molecular basis for differential type i interferon signaling,” *Journal of Biological Chemistry*. 2017.

[5] D. J. Sharkey, A. M. Macpherson, K. P. Tremellen, and S. A. Robertson, “Seminal plasma differentially regulates inflammatory cytokine gene expression in human cervical and vaginal epithelial cells,” *Mol. Hum. Reprod.*, 2007.

[6] Y. Xi, S. L. Day, R. J. Jackson, and C. Ranasinghe, “Role of novel type i interferon epsilon in viral infection and mucosal immunity,” *Mucosal Immunol.*, 2012.

[7] M. Holmes, F. Zhang, and P. D. Bieniasz, “Single-Cell and Single-Cycle Analysis of HIV-1 Replication,” *PLoS Pathog.*, 2015.

[8] K. Y. Fung, N.E. Cumming, J.C. Horvat, J.R. Mayall, S.A. Stifter, N. De Weerd, L.C. Roisman, J. Rossjohn, S.A. Robertson, and J.E. Schjenken, “Interferon-ε protects the female reproductive tract from viral and bacterial infection,” *Science*. 2013.

[9] S. fang Li, F. rong Zhao, J. jun Shao, Y. li Xie, H. yun Chang, and Y. guang Zhang, “Interferon-omega: Current status in clinical applications,” *International Immunopharmacology*. 2017.

[10] Y. Li, Y. Song, L. Zhu, X. Wang, B. Richers, D.Y. Leung and L. Bin, “Interferon Kappa Is Important for Keratinocyte Host Defense against Herpes Simplex Virus-1,” *J. Immunol. Res.*, 2020.

[11] M. Motwani, S. Pesiridis, and K. A. Fitzgerald, “DNA sensing by the cGAS–STING pathway in health and disease,” *Nature Reviews Genetics*. 2019.

[12] H. Kato, S. Sato, M. Yoneyama, M. Yamamoto, S. Uematsu, K. Matsui, T. Tsujimura, K. Takeda, T. Fujita, O. Takeuchi and S. Akira, “Cell type-specific involvement of RIG-I in antiviral response,” *Immunity*, 2005.

[13] T. Kawasaki and T. Kawai, “Toll-like receptor signaling pathways,” *Frontiers in Immunology*. 2014.

[14] K. Honda, H. Yanai, H. Negishi, M. Asagiri, M. Sato, T. Mizutani, N. Shimada, Y. Ohba, A. Takaoka, N. Yoshida and T. Taniguchi, “IRF-7 is the master regulator of type-I interferon-dependent immune responses,” *Nature*, 2005.

[15] S. Ali, R. Mann-Nüttel, A. Schulze, L. Richter, J. Alferink, and S. Scheu, “Sources of type I interferons in infectious immunity: Plasmacytoid dendritic cells not always in the driver’s seat,” *Frontiers in Immunology*. 2019.

[16] L.B. Ivashkiv and L. T. Donlin, “Regulation of type i interferon responses,” *Nature Reviews Immunology*. 2014.

[17] S. Bezalel, K. M. Guri, D. Elbirt, I. Asher, and Z. M. Sthoeger, “Type I interferon signature in systemic lupus erythematosus,” *Israel Medical Association Journal*. 2014.

[18] A. Hundeshagen, M. Hecker, B.K. Paap, C. Angerstein, O. Kandulski, C. Fatum, C. Hartmann, D. Koczan, H.J. Thiesen and U.K. Zettl, “Elevated type I interferon-like activity in a subset of multiple sclerosis patients: Molecular basis and clinical relevance,” *J. Neuroinflammation*, 2012.

[19] T. L. W. Muskardin and T. B. Niewold, “Type i interferon in rheumatic diseases,” *Nature Reviews Rheumatology*. 2018.

[20] S.H. Nile, A. Nile, J. Qiu, L. Li, X. Jia, and G. Kai, “COVID-19: Pathogenesis, cytokine storm and therapeutic potential of interferons,” *Cytokine and Growth Factor Reviews*. 2020.

[21] E. Sallard, F. X. Lescure, Y. Yazdanpanah, F. Mentre, and N. Peiffer-Smadja, “Type 1 interferons as a potential treatment against COVID-19,” *Antiviral Res.*, 2020.

[22] F. Coperchini, L. Chiovato, L. Croce, F. Magri, and M. Rotondi, “The cytokine storm in COVID-19: An overview of the involvement of the chemokine/chemokine-receptor system,” *Cytokine and Growth Factor Reviews*. 2020.

[23] R. Channappanavar, A.R. Fehr, R. Vijay, M. Mack, J. Zhao, D.K. Meyerholz and S. Perlman, “Dysregulated Type I Interferon and Inflammatory Monocyte-Macrophage Responses Cause Lethal Pneumonia in SARS-CoV-Infected Mice,” *Cell Host Microbe*, vol. 19, no. 2, pp. 181–193, 2016.

[24] E. Alspach, D. M. Lussier, and R. D. Schreiber, “Interferon γ and its important roles in promoting and inhibiting spontaneous and therapeutic cancer immunity,” *Cold Spring Harb. Perspect. Biol.*, 2019.

[25] K. Schroder, P. J. Hertzog, T. Ravasi, and D. A. Hume, “Interferon-γ: an overview of signals, mechanisms and functions,” *J. Leukoc. Biol.*, 2004.

[26] Z. Zha, F. Bucher, A. Nejatfard, T. Zheng, H. Zhang, K. Yea and R.A. Lerner, “Interferon-γ is a master checkpoint regulator of cytokine-induced differentiation,” *Proc. Natl. Acad. Sci. U. S. A.*, 2017.

[27] M.R. Zaidi and G. Merlino, “The two faces of interferon-γ in cancer,” *Clinical Cancer Research*. 2011.

[28] F. Castro, A. P. Cardoso, R. M. Gonçalves, K. Serre, and M. J. Oliveira, “Interferon-gamma at the crossroads of tumor immune surveillance or evasion,” *Frontiers in Immunology*. 2018.

[29] S.V. Kotenko, G. Gallagher, V.V. Baurin, A. Lewis-Antes, M. Shen, N.K. Shah, J.A. Langer, F. Sheikh, H. Dickensheets and R.P. Donnelly, “IFN-λs mediate antiviral protection through a distinct class II cytokine receptor complex,” *Nature Immunology*. 2003.

[30] R. Firdaus*,* A. Biswas, K. Saha, A. Mukherjee, S. Chaudhuri, A. Chandra, A. Konar and P.C. Sadhukhan, “Impact of host IL28B rs12979860, rs8099917 in interferon responsiveness and advanced liver disease in chronic genotype 3 hepatitis C patients,” *PLoS One*, 2014.

[31] S.J. Griffiths, C. M. Dunnigan, C. D. Russell, and J. G. Haas, “The role of interferon-λ locus polymorphisms in Hepatitis C and other infectious diseases,” *Journal of Innate Immunity*. 2015.

[32] M.T. Baldridge, S. Lee, J.J. Brown, N. McAllister, K. Urbanek, T.S. Dermody, T.J. Nice and H.W. Virgin, “Expression of Ifnlr1 on Intestinal Epithelial Cells Is Critical to the Antiviral Effects of Interferon Lambda against Norovirus and Reovirus,” *J. Virol.*, 2017.

[33] C. Odendall, A. A. Voak, and J. C. Kagan, “Type III IFNs Are Commonly Induced by Bacteria-Sensing TLRs and Reinforce Epithelial Barriers during Infection,” *J. Immunol.*, 2017.

[34] X. Zhang, T.W. Brann, M. Zhou, J. Yang, R.M. Oguariri, K.B. Lidie, H. Imamichi, D.W. Huang, R.A. Lempicki, M.W. Baseler and T.D. Veenstra, “Cutting Edge: Ku70 Is a Novel Cytosolic DNA Sensor That Induces Type III Rather Than Type I IFN,” *J. Immunol.*, 2011.

[35] H.M. Lazear, J. W. Schoggins, and M. S. Diamond, “Shared and Distinct Functions of Type I and Type III Interferons,” *Immunity*. 2019.

[36] E.V. Mesev, R. A. LeDesma, and A. Ploss, “Decoding type I and III interferon signalling during viral infection,” *Nature Microbiology*. 2019.

[37] L. Prokunina-Olsson, N. Alphonse, R.E. Dickenson, J.E. Durbin, J.S. Glenn, R. Hartmann, S.V. Kotenko, H.M. Lazear, T.R. O'Brien, C. Odendall and O.O. Onabajo, “COVID-19 and emerging viral infections: The case for interferon lambda,” *J. Exp. Med.*, 2020.

[38] C.R. Bolen, S. Ding, M. D. Robek, and S. H. Kleinstein, “Dynamic expression profiling of type I and type III interferon-stimulated hepatocytes reveals a stable hierarchy of gene expression,” *Hepatology*, 2014.

[39] S.M. Laidlaw and L.B. Dustin, “Interferon lambda: Opportunities, risks, and uncertainties in the fight against HCV,” *Front. Immunol.*, 2014.

[40] M. H. Tsai, L. M. Pai, and C. K. Lee, “Fine-tuning of type I interferon response by STAT3,” *Frontiers in Immunology*. 2019.

[41] K. Pervolaraki, M.L. Stanifer, S. Munchau, L.A. Renn, D. Albrecht, S. Kurzhals, E. Senis, D. Grimm, J. Schroder-Braunstein, R.L. Rabin and S. Boulant, “Type I and type III interferons display different dependency on mitogen-activated protein kinases to mount an antiviral state in the human gut,” *Front. Immunol.*, 2017.

[42] K. Pervolaraki, S.R. Talemi, D. Albrecht, F. Bormann, C. Bamford, J.L. Mendoza, K.C. Garcia, J. McLauchlan, T. Hofer, M.L. Stanifer and S. Boulant, “Differential induction of interferon stimulated genes between type I and type III interferons is independent of interferon receptor abundance,” *PLoS Pathog.*, 2018.

[43] J. Klinkhammer, D. Schnepf, L. ye, M. Schwaderlapp, H.H. Gad, R. Hartmann, D. Garcin, T. Mahlakoiv and P. Staeheli, “IFN-λ prevents influenza virus spread from the upper airways to the lungs and limits virus transmission,” *Elife*, 2018.

[44] F. Sorgeloos, M. Kreit, P. Hermant, C. Lardinois, and T. Michiels, “Antiviral type I and type III interferon responses in the central nervous system,” *Viruses*. 2013.

[45] P.P. Hernandez, T. Mahlakoiv, I. Yang, V. Schwierzech, N. Nguyen, F. Guendel, K. Gronke, B., Ryffel, C. Holscher, L. Dumoutier and J.C. Renauld, “Interferon-lambda and interleukin 22 act synergistically for the induction of interferonstimulated genes and control of rotavirus infection,” *Nat. Immunol.*, 2015.

[46] D.E. Levy, D. J. Lew, T. Decker, D. S. Kessler, and J. E. Darnell, “Synergistic interaction between interferon-alpha and interferon-gamma through induced synthesis of one subunit of the transcription factor ISGF3.,” *EMBO J.*, 1990.

[47] B. Sainz and W. P. Halford, “Alpha/Beta Interferon and Gamma Interferon Synergize To Inhibit the Replication of Herpes Simplex Virus Type 1,” *J. Virol.*, vol. 76, no. 22, pp. 11541–11550, 2002.

[48] Y. Ohmori, R. D. Schreiber, and T. A. Hamilton, “Synergy between interferon-γ and tumor necrosis factor-α in transcriptional activation is mediated by cooperation between signal transducer and activator of transcription 1 and nuclear factor κB,” *J. Biol. Chem.*, 1997.

[49] E. D. Chan and D. W. H. Riches, “IFN-γ + LPS induction of iNOS is modulated by ERK, JNK/SAPK, and p38mapk in a mouse macrophage cell line,” *Am. J. Physiol. - Cell Physiol.*, 2001.

[50] E.A. Voigt and J. Yin, “Kinetic Differences and Synergistic Antiviral Effects Between Type I and Type III Interferon Signaling Indicate Pathway Independence,” *J. Interf. Cytokine Res.*, 2015.

[51] J. Dempoya, T. Matsumiya, T. Imaizumi, R. Hayakari, F. Xing, H. Yoshida, K. Okamura and K. Satoh, “Double-Stranded RNA Induces Biphasic STAT1 Phosphorylation by both Type I Interferon (IFN)-Dependent and Type I IFN-Independent Pathways,” *J. Virol.*, 2012.

[52] O.H. Krämer, S.K. Knauer, G. Greiner, E. Jandt, S. Reichardt, K.H. Gührs, R.H. Stauber, F.D. Böhmer and T. Heinzel, “A phosphorylation-acetylation switch regulates STAT1 signaling,” *Genes Dev.*, 2009.

[53] H. Cheon and G.R. Stark, “Unphosphorylated STAT1 prolongs the expression of interferon-induced immune regulatory genes,” *Proc. Natl. Acad. Sci.*, 2009.

[54] M. Köster and H. Hauser, “Dynamic redistribution of STAT1 protein in IFN signaling visualized by GFP fusion proteins,” *Eur. J. Biochem.*, 1999.

[55] J. Ho, C. Pelzel, A. Begitt, M. Mee, H.M. Elsheikha, D.J. Scott and U. Vinkemeier, “STAT2 Is a Pervasive Cytokine Regulator due to Its Inhibition of STAT1 in Multiple Signaling Pathways,” *PLoS Biol.*, 2016.

[56] G. Banningeri and N. C. Reich, “STAT2 nuclear trafficking,” *J. Biol. Chem.*, 2004.

[57] D.E. Levy, I. J. Marié, and J. E. Durbin, “Induction and function of type i and III interferon in response to viral infection,” *Current Opinion in Virology*. 2011.

[58] M. L. Stanifer, K. Pervolaraki, and S. Boulant, “Differential regulation of type I and type III interferon signaling,” *International Journal of Molecular Sciences*. 2019.

[59] D. Blanco-Melo, B.E. Nilsson-Payant, W.C. Liu, S. Uhl, D. Hoagland, R. Møller, T.X. Jordan, K. Oishi, M. Panis, D. Sachs and T.T. Wang, “Imbalanced Host Response to SARS-CoV-2 Drives Development of COVID-19,” *Cell*, 2020.

[60] D. Acharya, G. Q. Liu, and M. U. Gack, “Dysregulation of type I interferon responses in COVID-19,” *Nature Reviews Immunology*. 2020.

[61] Q. Zhou, V. Chen, C.P. Shannon, X.S. Wei, X. Xiang, X. Wang, Z.H. Wang, S.J. Tebbutt, T.R. Kollmann and E.N. Fish, “Interferon-α2b Treatment for COVID-19,” *Front. Immunol.*, 2020.

[62] A. Park and A. Iwasaki, “Type I and Type III Interferons – Induction, Signaling, Evasion, and Application to Combat COVID-19,” *Cell Host and Microbe*. 2020.

[63] N. Au-Yeung, R. Mandhana, and C. M. Horvath, “Transcriptional regulation by STAT1 and STAT2 in the interferon JAK-STAT pathway,” *JAK-STAT*, 2013.

[64] A. Grant, S.S. Ponia, S. Tripathi, V. Balasubramaniam, L. Miorin, M. Sourisseau, M.C. Schwarz, Sánchez-Seco, M.P. M.J. Evans, S.M. Best and A. García-Sastre, “Zika Virus Targets Human STAT2 to Inhibit Type i Interferon Signaling,” *Cell Host Microbe*, 2016.

[65] S. Bhushal, M. Wolfsmüller, T.A. Selvakumar, L. Kemper, D. Wirth, M.W. Hornef, H. Hauser and M. Köster, “Cell polarization and epigenetic status shape the heterogeneous response to type III interferons in intestinal epithelial cells,” *Front. Immunol.*, vol. 8, no. JUN, 2017.

[66] C. Savarin and C.C. Bergmann, “Fine Tuning the Cytokine Storm by IFN and IL-10 Following Neurotropic Coronavirus Encephalomyelitis,” *Frontiers in immunology*. 2018.

[67] K. Kolnik, L.S. Tsimring and J. Hasty, “Vacuum-assisted cell loading enables shear-free mammalian microfluidic culture,” *Lab Chip*, 2012.

[68] F.A. Ran, P.D. Hsu, J. Wright, V. Agarwala, D. A. Scott, and F. Zhang, “Genome engineering using the CRISPR-Cas9 system,” *Nat. Protoc.*, 2013.

[69] A. Samsonov, N. Zenser, F. Zhang, H. Zhang, J. Fetter, and D. Malkov, “Tagging of Genomic STAT3 and STAT1 with Fluorescent Proteins and Insertion of a Luciferase Reporter in the Cyclin D1 Gene Provides a Modified A549 Cell Line to Screen for Selective STAT3 Inhibitors,” *PLoS One*, 2013.

[70] Y. Li, J. Roberts, Z.A. AkhavanAghdam, and N. Hao, “Mitogen-activated protein kinase (MAPK) dynamics determine cell fate in the yeast mating response,” *J. Biol. Chem.*, 2017.

[71] Y. Li, M. Jin, R. O’Laughlin, P. Bittihn, L.S. Tsimring, L. Pillus, J. Hasty and N. Hao, “Multigenerational silencing dynamics control cell aging,” *Proc. Natl. Acad. Sci. U. S. A.*, 2017.